



Cardiff Catalysis Institute  
Sefydliad Catalyddu Caerdydd

---

# **The Preparation of Heterogeneous Catalysts for the Selective Transformation of Green Chemicals and Bio-Renewables**

---

Thesis submitted in accordance with the requirements of the University of Cardiff for the degree of doctor in philosophy by:

**Gavin Morgan King**

School of Chemistry  
Cardiff University

2016

## Acknowledgements

I would like to express my gratitude to Professor Graham Hutchings, who not only provided me with the opportunity to undertake this PhD, but also gave me invaluable advice, support, and encouragement throughout. I could not have asked for a kinder, more generous supervisor.

I am forever indebted to Dr. Gemma Brett, Dr. Peter Miedziak, and Dr. Simon Kondrat. Their help, support, advice, and friendship over the past 3 years has been invaluable. I wish to thank them as deeply, and sincerely as possible for their succour when I needed it most.

I would like to thank Dr. Jennifer Edwards, Dr. Sarwat Iqbal, Dr. David Morgan, and Professor David Knight, all of whom have provided extensive assistance and guidance at various points during my PhD.

I gratefully acknowledge all the staff within the chemistry department, especially Steve Morris for the indispensable technical support throughout.

Last but not least, I would like to thank Mum, Dad, Lloyd, and Louise. Words cannot express how grateful I am to all of you, without your love and support this would not have been possible. Thank you.

# Contents

1. Introduction.....	1
1.1 Catalysis: A historical perspective .....	1
1.2 Principles of Catalysis .....	2
1.3 Catalyst Classifications .....	4
1.4 Green Chemistry .....	5
1.5 Renewable Energy: Energy Challenges of the 21 <sup>st</sup> Century.....	6
1.6 Discovery of Furfural .....	8
1.7 References .....	25
2. Experimental .....	30
2.1 Introduction .....	30
2.2 Chemicals Used .....	30
2.3. Definitions .....	31
2.4 Catalyst Preparation .....	31
Physical Grinding.....	31
Impregnation .....	32
2.5 Catalyst testing .....	32
Benzyl alcohol oxidation .....	32
Hydrogen peroxide hydrogenation .....	33
Glycerol Oxidation .....	34
Furfuryl alcohol hydrogenation.....	34
Furfural Hydrogenation .....	35
2.6 Catalyst Characterisation .....	35
X-Ray Diffraction (XRD) .....	35
X-Ray Photoelectron Spectroscopy (XPS) .....	38
Microwave plasma atomic emission spectroscopy (MP-AES).....	40
Transmission Electron Microscopy (TEM) .....	41
Gas Chromatography (GC).....	43
2.7 References.....	46
3. Physical mixing of metal acetates: Optimisation of catalyst parameters to produce highly active bimetallic catalysts.....	47
3.1 Introduction .....	47
3.2 Results and Discussion.....	50
3.2.1 Effect of Au:Pd ratio.....	50
3.2.2 X-Ray Photoelectron Spectroscopy (XPS) .....	58
3.2.3 X-Ray Diffraction (XRD) .....	60

3.2.4	Glycerol Oxidation .....	61
3.2.5	Hydrogen Peroxide Synthesis.....	63
3.2.6	Oxidation of other alcohols .....	65
3.3	Conclusions .....	66
3.4	References.....	67
4.	An investigation of the effect of the addition of tin to 5wt% Pd/TiO <sub>2</sub> for the hydrogenation of furfuryl alcohol.....	69
4.1	Introduction .....	69
4.2	Results and Discussion.....	71
4.2.1	The Effect of Reaction Time on the Catalytic Hydrogenolysis of FA .....	73
4.2.2	X-Ray Diffraction (XRD) .....	76
4.2.3	Transmission Electron Microscopy .....	78
4.2.4	X-Ray Photoelectron Spectroscopy (XPS) .....	79
4.2.5	Sn-Pd bimetallic catalysts .....	81
4.2.5.1	Sn-Pd bimetallic catalysts - The effect of Temperature.....	82
4.2.5.2	Sn-Pd bimetallic catalysts - The effect of Pressure.....	83
4.2.5.3	Sn-Pd bimetallic catalysts - The effect of Solvent .....	83
4.2.5.4	Sn-Pd bimetallic catalysts - The effect of Sn:Pd ratio .....	84
4.2.5.5	X-ray photoelectron spectroscopy .....	86
4.2.5.6	X-ray diffraction .....	89
4.2.5.7	Transmission electron microscopy.....	89
4.3	Conclusions .....	91
4.4	References.....	92
5.	Palladium and Ruthenium heterogeneous catalysts for the hydrogenation of furfural.....	94
5.1.	Introduction .....	94
5.2	Results and Discussion.....	95
5.2.1	Ru-Pd/TiO <sub>2</sub> catalysts for furfural hydrogenation.....	99
5.2.2	XRD Analysis.....	101
5.2.3	TEM Analysis.....	101
5.2.4	TPR Analysis .....	101
5.2.5	XPS analysis.....	102
5.3	Discussion.....	120
5.4	Conclusions .....	124
5.5	References.....	125
6.	Conclusions and Future Work .....	128



# Chapter 1

## 1. Introduction

This chapter introduces the historical discovery of the catalytic effect; the principles that underlie our understanding of catalysis today; and the application of catalytic systems for the production of value-added chemicals from renewable, lignocellulosic-derived furfural.

### 1.1 Catalysis: A historical perspective

In the early part of the 19<sup>th</sup> century the scientific study of chemistry was beginning in earnest. It was possible, at this time, for just one scientist to produce an annual report that documented the progress achieved throughout the whole of chemistry over the course of the previous year. One hundred and eighty years ago, the responsibility of undertaking this task for the Stockholm Academy of Sciences lay with the noted chemist Jöns Jakob Berzelius (1779-1848), as indeed it had done for a number of preceding years.<sup>1</sup> In his treatise Berzelius systematically reviewed a number of experimental observations, in both homogeneous and heterogeneous systems, which reported on the occurrence of chemical reactions taking place only when in the presence of trace amounts of substances that weren't themselves taking part in the reaction.<sup>2</sup> He went on to propose that these observations could be rationally interrelated to the existence of an inherent new force which he called the 'catalytic force', with 'catalysis' being the term used to describe the decomposition of bodies by this force.

*“Many bodies have the property of exerting on other bodies an action which is very different from chemical affinity. By means of this action they produce decomposition in bodies, and form new compounds into the composition of which they do not enter. This new power, hitherto unknown, I shall call it catalytic power. I shall also call catalysis the decomposition of bodies by this force.”<sup>3</sup>*

In the years that followed Berzelius' discovery many other examples of catalytic action were reported, and as science progressed theoretical and experimental techniques were proposed that could enable accurate determination of the rates of chemical reactions.<sup>2</sup> These discoveries allowed for F.W. Ostwald to define a catalyst as:

*“A substance that increases the rate at which a chemical system approaches equilibrium, without being consumed in the process.”<sup>2</sup>*

## 1.2 Principles of Catalysis

Ostwald's definition contains within it a number of important implications, the position of chemical equilibrium within a catalysed reaction being one such example. The equilibrium position in a catalysed reaction will be at the same point as a reaction ultimately occurring in the absence of catalyst.<sup>2</sup> This is because the equilibrium constant  $K$  is dependent on the Gibbs free energy of the reaction:

$$K = \exp(-\Delta G / RT)$$

Which is itself determined by the enthalpy and entropy changes of the process:

$$\Delta G = \Delta H - T\Delta S$$

A catalyst can only increase the rate of a reaction that is thermodynamically allowed under a given set of conditions i.e. where there is a negative change in Gibbs free energy.<sup>2</sup>

In order to understand how a catalyst is able to influence the rate of a chemical reaction it is useful to revisit Svante Arrhenius' hypothesis on how temperature can effect a non-catalysed gas-phase reaction: Arrhenius stated that the rate of reaction  $r$  was dependent on the number of molecular collisions occurring with an energy greater than a critical level called the *activation energy*  $E$ .<sup>2</sup> The number of collisions occurring above this level,  $Z$ , was found to increase exponentially with increasing temperature in line with the Boltzmann distribution fraction so that:

$$r = Z \exp(-E / RT)$$

Practically, the rate of reaction may be lower than that described by the equation above if the collisions between molecules need to occur in a specific orientation, and as such a *steric factor*  $P$  is often added to the right-hand side.<sup>2</sup>

There are, however, difficulties in attempting to compare a heterogeneous reaction taking place on the surface of solid in a small volume of space, with the homogeneous gas-phase reaction presented above. If the heterogeneous reaction were dependent on the frequency of collisions between a reactant and the surface, this number (expressed per cm<sup>2</sup>) would typically be expected to be in the region of 10<sup>12</sup> smaller than the collision frequency  $Z$  occurring in the gas-phase.<sup>2</sup> As a result, in order to account for this huge discrepancy in collision frequency between the two systems it has been concluded that the activation energy of a catalysed reaction has to theoretically be *at least* 65 kJ mol<sup>-1</sup> lower than activation energy of the homogeneous gas-phase reaction, and realistically it has be around 100 kJ mol<sup>-1</sup> less.<sup>2</sup> Consequently, it is proposed that *catalysts act by lowering the activation energy of a reaction*.<sup>2</sup> The catalyst achieves this by providing new and energetically more

favourable routes to overcoming the potential energy barrier that exists between reactants and products.<sup>2</sup>

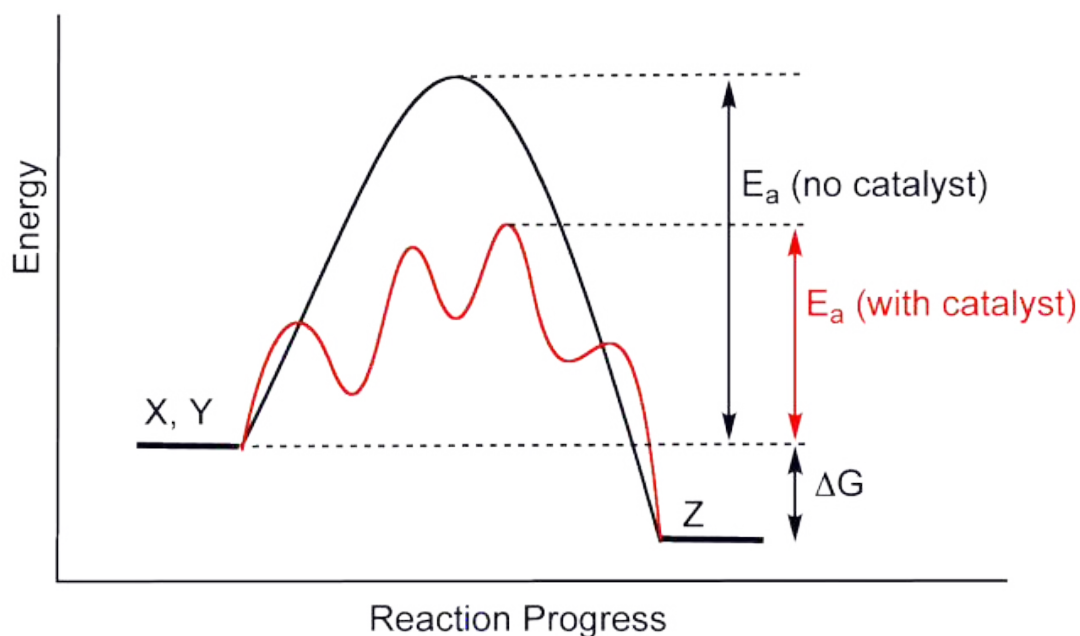


**Figure 1: Potential energy diagram of an exothermic reaction of the reactants X and Y to the product Z. The black line describes the potential energy barrier existing for a non-catalysed reaction; the red line represents an analogous catalysed reaction, with formation of lower energy transition states that result in lowering the overall activation energy of the reaction.<sup>4</sup>**

### 1.3 Catalyst Classifications

Catalysts are defined as being either heterogeneous or homogenous depending on whether the catalyst and the substrate exist in the same phase or not. Whilst enzymes are biocatalysts, they are usually considered as being part of separate group. In homogeneous catalysis the reactants and the catalyst exist in the same phase, an example being the atmospheric catalytic destruction of ozone by Cl

radicals.<sup>5</sup> In heterogeneous catalysis the catalyst and the reactants are in a different phase, with the catalyst typically being a solid, with gaseous or liquid reactants - an example of which being the synthesis of ammonia from gaseous molecular  $N_2$  and  $H_2$  over a solid Fe catalyst.<sup>5</sup> Heterogeneous catalysts most commonly take the form of a dispersed metal supported on a secondary material such as carbon, or mixed metal oxides, with the support acting to maintain and contribute to the overall activity of the catalyst.

Heterogeneous catalysis is of immeasurable importance to the global economy, with an estimated 90% of all chemical manufacturing processes currently employed throughout the world utilising some form of catalyst.

All catalytic systems discussed, produced and investigated in this body of work will be heterogeneous in nature.

## 1.4 Green Chemistry

Green chemistry, or sustainable chemistry as it also known, is the design, development, and application of chemical processes that are aimed to eliminate or reduce the use or production of chemical substances that are hazardous to the environment. As a philosophy it originated in the early 1990's, with the passing of the Pollution Prevention Act in the USA at a similar time, it helped generate significant awareness of the issues surrounding sustainability and the environment.<sup>6</sup> There exists 12 key principles of green chemistry, criteria that chemical scientists use today to guide them in the sustainable development of chemical processes:<sup>6</sup>

1. Waste prevention is more desirable than to treat or clean waste formed.
2. Synthesis methods should be designed in order to maximise the incorporation of materials used into the desired final product.

3. If and whenever practicable, synthesis techniques and methods should be designed to utilise and generate substances with little or no toxicity to human life and the environment.
4. Design of chemical products should be centred around maintaining efficacy whilst reducing toxicity
5. Solvents, separating agents and other auxiliary substances should be removed from processes wherever possible
6. Energy requirements should be minimised, with syntheses performed under ambient conditions wherever possible.
7. Feedstocks should ideally be renewable whenever practicable.
8. Derivatization should be avoided if possible.
9. Catalytic reagents should be used in preference to stoichiometric reagents.
10. Chemical products should be designed in such a way that they degrade innocuously without persisting and polluting the environment
11. Methods of analysis should be developed that allow for monitoring of processes in real time so that the potential for chemical accidents can be reduced as low as possible
12. Substances within a chemical process should be chosen to minimise the potential for chemical accidents.

## **1.5 Renewable Energy: Energy Challenges of the 21<sup>st</sup> Century**

The world's population currently exceeds 7 billion people with this number expected to rise to 9 billion by the year 2050. The rapid upsurge of development in economies such as India and China has inevitably arisen in tandem with an increased demand for oil - a commodity essential for industrialisation; providing the energy and

raw chemicals needed for manufacturing, as well as bitumen for the construction of transport infrastructures required for import and export. As the expanding population of developing countries become wealthier many individuals will go on to purchase automobiles, refrigerators, and televisions etc., all of which require energy ultimately derived from oil for their production. The supply of oil is however finite and diminishing, and this growing demand in concert with the concomitant increase in CO<sub>2</sub> emissions and their adverse environmental effects is of major concern politically, economically and academically. In light of this, there has been increased interest in the development of a green, sustainable and cost-effective alternative to petroleum fuels and platform chemicals derived from oil. Renewable resources of energy, such as hydroelectric, wind, and solar power have the potential to meet some of these energy requirements; however replacement of chemicals derived from petroleum need to contain carbon atoms and biomass provides both a viable and attractive solution to all of these problems.

Currently, first generation biofuels are produced from vegetable oils, starches and sugars. However, a potentially more sustainable, more abundant and cheaper alternative would be biofuels derived from lignocellulose. Lignocellulose is comprised of lignin and the carbohydrate polymers cellulose and hemicellulose (figure 2).

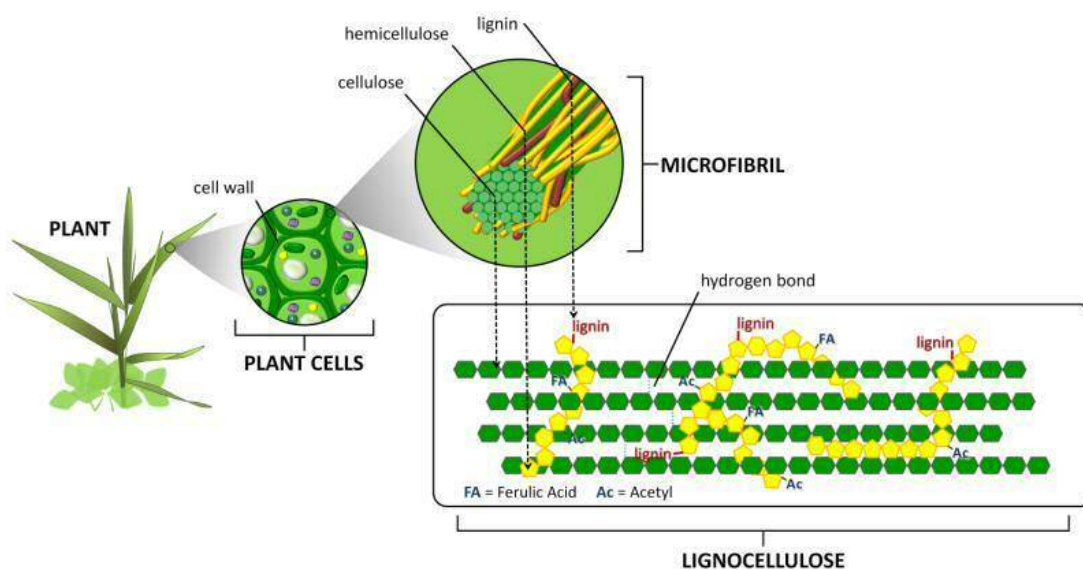


**Figure 2. Lignocellulose structure, showing lignin, cellulose, and hemicellulose components.<sup>7</sup>**

It is the C<sub>5</sub> sugars, mainly xylose and arabinose, contained within the hemicellulose component of lignocellulosic biomass that furfural is derived from (figure 3).<sup>8</sup>

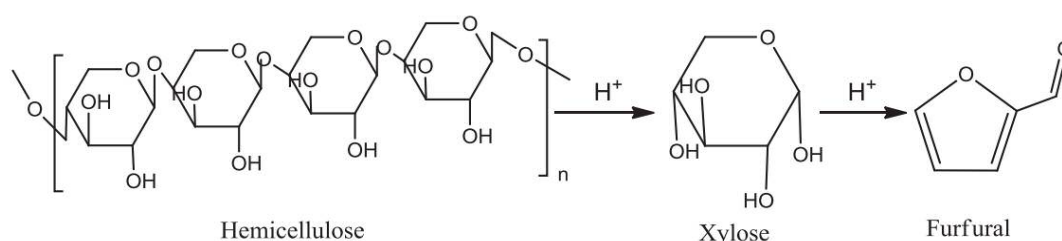


**Figure 3. Furfural production from hemicellulose biomass.<sup>9</sup>**

## 1.6 Discovery of Furfural

Furfural, otherwise known as furfuraldehyde, or Furan-2-carbaldehyde by IUPAC nomenclature, was first isolated in 1832 (some accounts say 1821) by the German Chemist Johann Wolfgang Döbereiner. It was observed as a by-product of formic acid synthesis from sugar, sulfuric acid, and manganese dioxide, co-evaporating with water as a water soluble oily substance.<sup>ref</sup> In 1840 John Stenhouse, a Scottish

Chemist, discovered that the same substance could be produced by reacting sulfuric acid with a variety of vegetative plant substances. Stenhouse went on to recognise the resin forming tendencies of furfural, and assigned the empirical formula as  $C_5H_4O_2$ . In 1845 George Fownes confirmed that Stenhouse had correctly determined the empirical formula, and proposed the name “furfurol”, derived from the Latin *furfor*, meaning bran, referring to its common source of origin; and *oleum*, meaning oil. The “ol” suffix was later replaced with “al”, due to the presence of the aldehyde functionality.

### Physical Properties of Furfural

Furfural has, as already mentioned, a chemical formula of  $C_5H_4O_2$  and a concomitant molecular weight of  $96.08 \text{ g mol}^{-1}$ . A colourless to red-brown oily liquid at room temperature, with an almond-like odour, furfural is a heterocyclic aldehyde, the furan ring structure having been determined by the combined efforts of Harries, Marckwald, and Baeyer.

**Table 1. Physical properties of furfural.<sup>9</sup>**

Molecular weight	96.08	$\text{g mol}^{-1}$
Boiling point	161.7	$^{\circ}\text{C}$
Freezing point	-36.5	$^{\circ}\text{C}$
Density, ( $25^{\circ}\text{C}$ )	1.16	$\text{g/mL}$
Critical pressure	5.502	Mpa
Critical temperature	397	$^{\circ}\text{C}$
Solubility in water, ( $25^{\circ}\text{C}$ )	8.3	wt%
Dielectric constant, ( $20^{\circ}\text{C}$ )	41.9	
Heat of vaporisation (liquid)	42.8	$\text{kJ mol}$
Heat of combustion, ( $25^{\circ}\text{C}$ )	234.4	$\text{kJ mol}$
Enthalpy of formation	-151	$\text{kJ mol}$
Explosion limits (in air)	2.1- 19.3	vol %
Flash point	61.7	$^{\circ}\text{C}$
Autoignition temperature	315	$^{\circ}\text{C}$

Furfural provides a comprehensive platform from which a large number of potential biofuel components can be derived (figure.4).

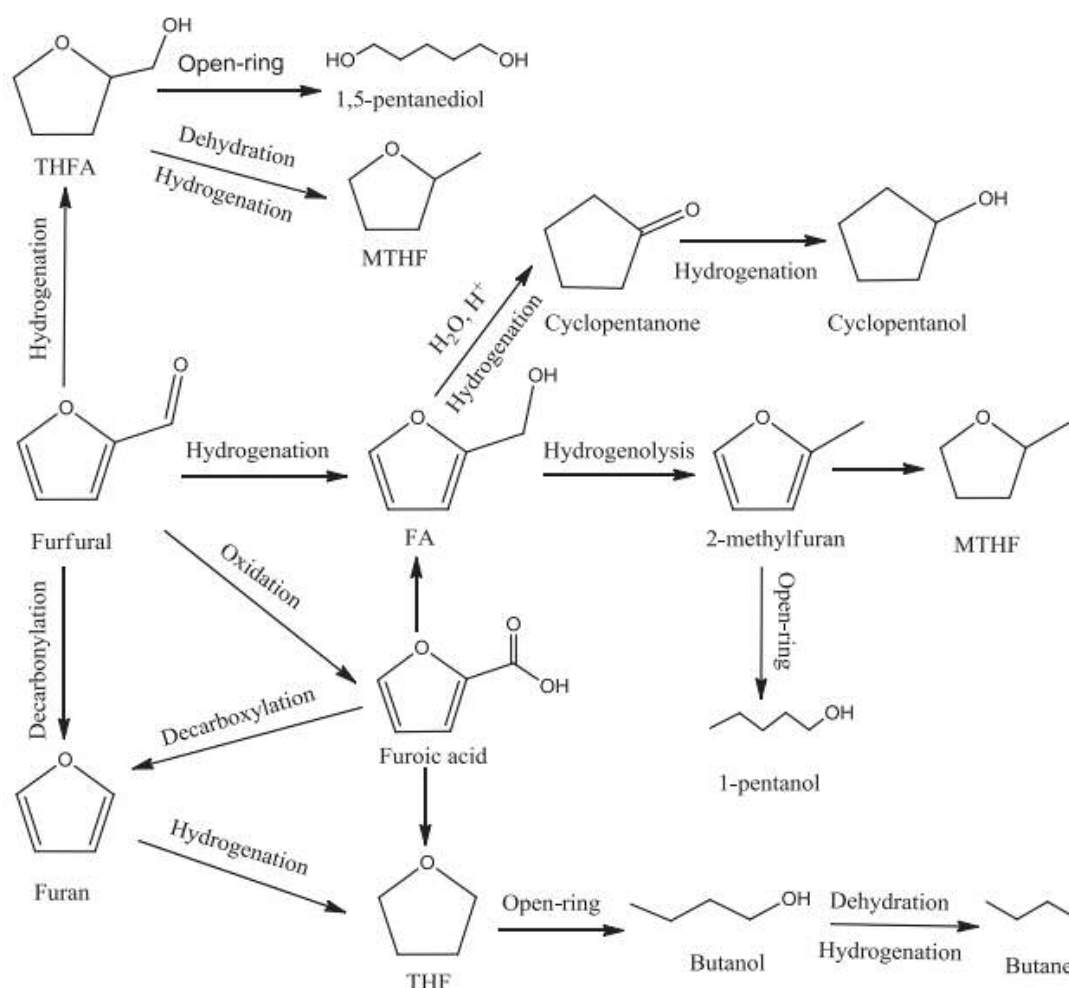


**Figure 4. Potential pathways for the conversion of furfural to valorised chemicals .<sup>9</sup>**

The upgrade strategies employed aim to increase the energy density and miscibility in hydrocarbon fuels through deoxygenation, and the potential to increase the carbon chain length to yield high boiling point diesel additives. The industrial and commercial applicability of a furfural platform for lignocellulosic biofuels is heavily dependent on

(a). The cost competitive manufacture of furfural; (b). The fuel properties of upgraded furanic derivatives, and it is to these that we now turn our attention.

### **Economics and Manufacturing of Furfural**

If furfural is to provide a viable platform for the production of biofuels it is essential that its manufacture be both affordable and sustainable. The current feedstock is predominantly dependent on agriculturally produced, hemicellulose-rich, lignocellulosic materials such as sugarcane bagasse and corncobs. Lignocellulose is an attractive raw material in that it is inexpensive, abundant, and potentially more sustainable than the vegetable oils and plant derived carbohydrates from which first generation biofuels are derived. It is however, notoriously recalcitrant, the upgrading of which is both complex and expensive.

**Table 2. Global production of Furfural<sup>10</sup>**

<b>Country</b>	<b>Feedstock</b>	<b>Production (t per annum)</b>
China	Corn cob	200,00
Dominican Republic	Bagasse	32,000
South Africa	Bagasse	20,000
Thailand	Corn cob	8,500
Spain	Corn cob	6,000
Others (India + S.America)	Corn cob/Bagasse	< 15,000
Russia (Internal use)	Corn cob	-
<b>Total</b>	-	<b>&gt; 280,000</b>

**Table 3. Global Consumption of Furfural<sup>10</sup>**

<b>Geographical Location</b>	<b>Consumption (t per annum)</b>
Europe	12,000
United States	8,000
Middle East	7,000
Japan	6,000
Taiwan	5,000
S. America	5,000
China	5,000
Australia + S.Africa	2,000
Others	< 50,000
<b>Total</b>	<b>50,000 - 100,000</b>

**Table 4. Global price of furfural between 1995-2002.<sup>10</sup>**

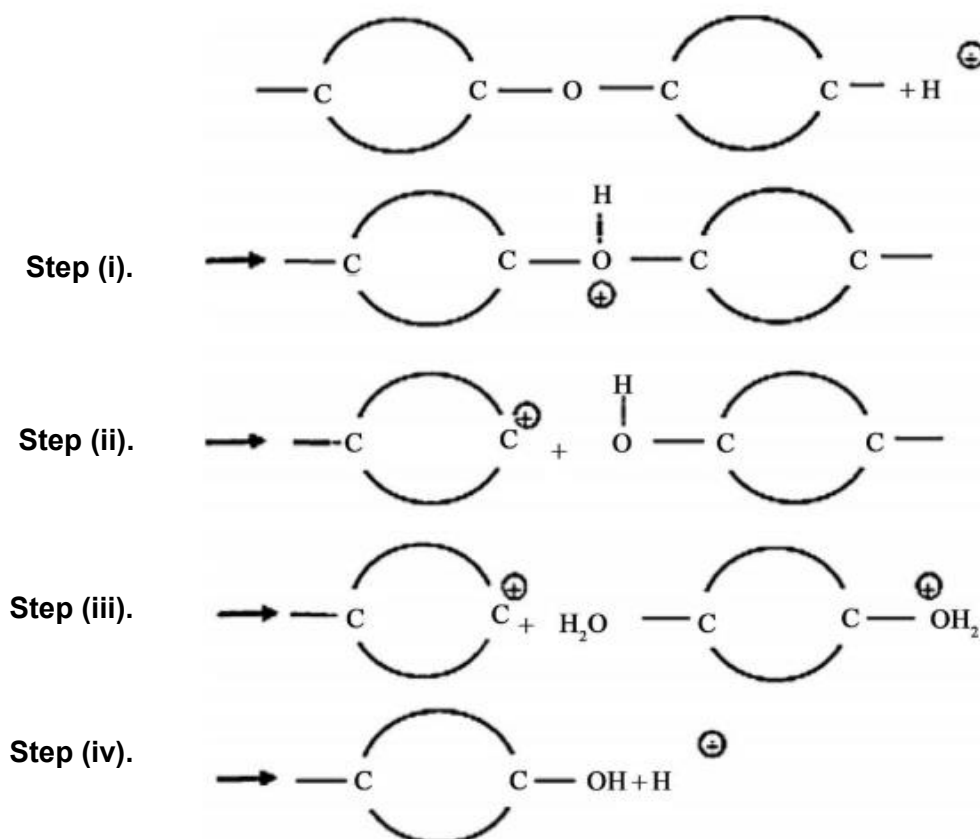
<b>Year</b>	<b>Price Range (\$/t)</b>	<b>Comments</b>
1995	675 - 1250	Chinese Production affected by drought
1996	840 - 1845	Chinese Production affected by drought
1997	860 - 1225	Chinese Production affected by drought
1998	830 - 990	-
1999	690 - 865	-
2000	630 - 705	-
2001	> 650	-
2002	500 - 1100	-

The current global production of furfural is approximately 400 kt per annum, the majority of which is upgraded to furfuryl alcohol from which furan resins are subsequently produced.<sup>7</sup> China is the world's largest manufacturer of furfural, with the Dominican Republic's Central Roma Corporation Ltd. and Illovo Sugar Ltd. of South Africa also being significant producers. The processes employed by these companies, typically operating in batch at capacities of only several kt annum<sup>-1</sup>, all originate from the first commercial process developed by Quaker Oats in 1922. In this

process, oat hulls are subjected to liquid acid catalysis to facilitate the hydrolysis and dehydration of hemicellulose-derived pentosan to yield furfural (figure 5) which is subsequently stripped from the reactor with high volumes of steam.<sup>8</sup>

### Figure 5. Furfural production from pentosan

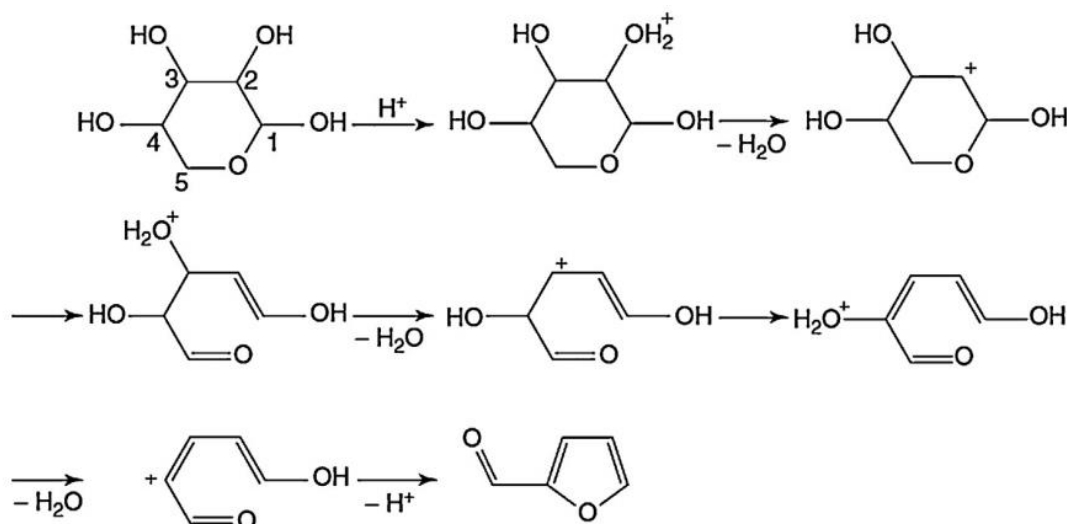
**Step 1:** Acid hydrolysis of pentosan to yield pentose.<sup>11,12</sup>



- (i). The initial step involves protonation of an ether (oxygen) linkage within the pentosan polymer resulting in a positively charged trivalent oxygen.
- (ii). Subsequent cleavage of the C-O bond generates a hydroxyl group on one side of the cleaved ether bridge with concomitant generation of a carbocation on the other side.
- (iii). Uptake of water by the carbocation leads to the formation of  $\text{H}_2\text{O}^+$

- (iv). Formation of a hydroxyl group occurs due to liberation of hydrogen from  $\text{H}_2\text{O}^+$ . This sequence is repeated until all ether bridges have been hydrolysed and individual pentose molecules have been liberated.

**Step 2:** Dehydration of pentose to furfural.<sup>11,12</sup>



- (i). A proton attacks the lone electron pair of a hydroxyl oxygen bound to a C atom generating a transition state containing a positively charged trivalent oxygen.
- (ii). Due to the increased electronegativity of O over C, the positive charge relocates to a neighbouring C prior to splitting of the C-O bond, followed by liberation of  $\text{H}_2\text{O}$ .
- (iii). Formation of a double bond occurs as 2 electrons from a neighbouring C-O bond are drawn into the space between the 2 C atoms causing the concomitant fission of the C-O bond.
- (iv). A liberated  $\text{H}^+$  attacks another OH lone pair to free another  $\text{H}_2\text{O}$ .

- (v). Due to the trivalency of the C atom, the last 1,4-elimination does not result in the formation of a ring because the 2 C atoms involved in the double bond duly adopt planar structures maintaining bond angles of  $120^\circ$ .
- (vi). Elimination of a hydrogen ion accompanies furfural generation.

These processes only tend to yield approximately 10wt% furfural, comprising only 50-60% of the theoretical yield.<sup>8</sup> This low product yield, in combination with the high energy requirement for downstream separation, means that cost competitive production of furfural for utilisation as a progenitor to biofuels is not possible with current conventional technology.<sup>8</sup>

### **Fuel Properties of Furanic Derivatives**

Jean-Paul Lange and colleagues at Shell Global Solutions carried out a comprehensive screening process of the fuel properties possessed by furanic derivatives.<sup>8</sup> A preliminary evaluation involved characterising the components in line with four criteria which assessed: (a). the energy density; (b). polarity; (c). ignition characteristics; and (d). boiling point.<sup>8</sup> This approach allowed for identification of derivatives that were compatible with existing fuel distribution systems and currently available vehicles.<sup>8</sup>

Initial results discovered that the aldehyde and alcohol functionalities that are present in furfural and furfuryl alcohol molecules respectively are undesirable due to the existence of a polarity mismatch for blending with hydrocarbon fuels.<sup>8</sup> Whilst this is to a degree manageable, as is the case for ethanol, it is an unattractive proposition as it reduces the concentrations required for blending with existing fuels, and may cause unwanted side effects, such as incompatibility with contemporary fuel distribution

networks and vehicles, or an increase in volatility.<sup>8</sup> Upgrade strategies that result in removal of the aldehyde or alcohol group are desirable as the components produced have higher energy densities and reduced polarities which improve their solvency. As figure 4 illustrates, a large number of potential pathways exist for the upgrading of the furfural platform to biofuels, but perhaps the most versatile reaction route is that of hydrogenation. Hydrogenation of furfural can result in 2-Methylfuran (2-MF) and Methyltetrahydrofuran (MTHF), compounds that have excellent fuel blending properties (figure 5).

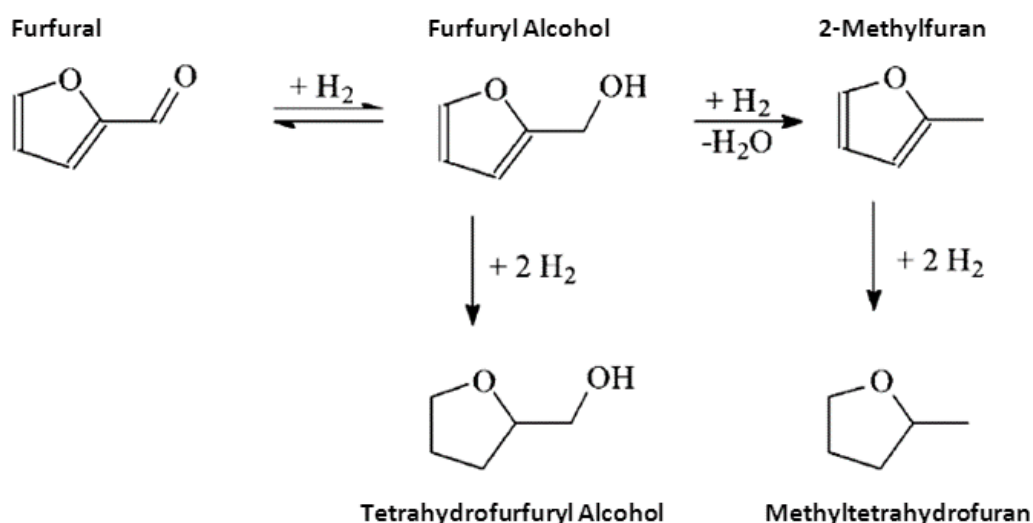


**Figure 6. Reaction scheme showing furfural hydrogenation production to the value added products furfuryl alcohol, and tetrahydrofurfuryl alcohol; and the biofuel components 2-methylfuran and methyltetrahydrofuran.<sup>8</sup>**

### Catalytic Hydrogenation of Furfural

The reactant structure itself and the manner in which it adsorbs on the metal surface is also important as this can affect the selectivity to intermediates and desired products. A number of theoretical studies have been conducted in order to ascertain

the probable adsorption geometry of furfural. A multifunctional molecule, furfural can potentially bind to a catalytic surface through the carbonyl moiety or through its aromatic furan ring depending on how strongly binding the catalyst is.<sup>23</sup> On Palladium, a strong-binding catalyst, furfural is anticipated to be orientated parallel to the plane of the surface, this “flat” adsorption conformer being thermodynamically favourable to facilitate the decarbonylation of furfural.

The Generalised Gradient Approximation (GGA) within the Density Functional Theory (DFT) has been employed by numerous groups to further ascertain the nature of the interaction between furfural and a catalytic surface. GGA does, however, have a shortcoming in that it fails to account for Van der Waals interactions. Consequently an inaccuracy exists due to an inherent inability to delineate the interactions between an aromatic molecule and the metal surface. This is especially pertinent in regards to catalysts determined as being weakly-binding, where a combination of both Van der Waals and electrostatic interactions are predicted.<sup>23</sup>

In order to further investigate the manner in which furfural orientates itself on a catalytic surface Vorotnikov *et al.* employed dispersion-corrected DFT to calculate the energetics associated with the conversion of furfural to furan, furfuryl alcohol and 2-methylfuran on Pd(III). The author's considered three main surface arrangements: (i). *Flat*, whereby the furan ring is orientated parallel to the plane of the surface, with all carbon atoms of the furan ring bound to the surface; (ii). *Bent*, with the furan ring positioned such that only two furanic carbons interact with the metal with the molecular plane of the molecule tilted with respect to the Pd (III), or with the furan ring tilted in such a manner that the surface interacts with the carbonyl carbon or the carbon oxygen bond; (iii). *Upright*, where the molecular plane is angled perpendicular to the surface. Of these adsorption conformers, the authors report a clear preference for furfural adsorption in a flat conformation over the hollow site. The bent conformations were discovered to display a significant degree of interaction with the surface through

the carbonyl group however they were also considerably less stable than the flat conformers. Upright adsorption conformations were found to be significantly less favourable than the flat and bent geometries.<sup>23</sup>

### **Catalytic Hydrogenation of Furfural to Furfuryl Alcohol.**

Of the possible furfural hydrogenation products, furfuryl alcohol [FA] is the most common with an estimated 62% of all annual global furfural production being converted to FA.<sup>9</sup> With the chemical formula  $C_5H_6O_2$  and a molar mass of  $98.10 \text{ g mol}^{-1}$ , this colourless-to-amber liquid is used predominantly in the production of foundry resins, the manufacture of which typically requiring the polymers generated from the cross-linking of FA with itself and other compounds, such as urea, formaldehyde, furfural, phenolic molecules etc.<sup>9</sup> These FA derived resins are inherently chemically, thermally, and mechanically robust. Such properties render these resins resistant to corrosion, and largely insoluble in most common solvents.<sup>9</sup> Due to its ability to withstand erosion, FA has also found application in production of speciality plastics reinforced with furan fibres for piping uses, as well as in high performance chemical processes that use oxygenated organic solvents, and chlorinated aromatics.<sup>9</sup>

Over the course of the past few decades, a number of different methods and a variety of catalysts have been studied for the production of FA from furfural (table 5) One of the most regularly used catalysts in the past has been copper chromite,<sup>9</sup> with commercial hydrogenation of furfural to FA occurring over a 1-2% copper chromite catalyst operating in the region of 69-103 bar  $H_2$ , at  $175^\circ\text{C}$ , in 110 gallon autoclave reactors.<sup>9</sup> Raney Nickel and copper-chromium oxide catalysts have also been demonstrated as being active for the hydrogenation of furanic compound, with Wojcik reporting FA production at 96-99% of the theoretical yield over a copper-chromium oxide catalyst at  $175^\circ\text{C}$ , with effective suppression of side reactions that could disrupt

the integrity of the furanic ring.<sup>9</sup> Increasing the temperature to 250 °C over the same catalyst facilitated further hydrogenation of FA, whilst a marginal increase in pressure would result in the production of 2-methylfuran (36%); pentanol (36%); 1,5-pentanediol (15%); and 1,2-pentanediol (14%).

**Table 5. Catalytic hydrogenation of Furfural to Furfuryl alcohol.<sup>9</sup>**

Catalyst	Temp (°C)	P (bar H <sub>2</sub> )	t (h)	Solvent	Conv. (%)	Yield (%)
5% Pt/C	175	80	0.5	n-butanol	99.3	47.9 <sup>14</sup>
5% Pt/C	175	80	0.5	n-decanol	94.5	26.3 <sup>14</sup>
5% Pd/C	150	20	4	HOAc assisted	41.2	14.4 <sup>15</sup>
5% Pd/Al <sub>2</sub> (SiO <sub>3</sub> ) <sub>3</sub>	150	20	4	HOAc assisted	56.9	30 <sup>15</sup>
5% Cu/Al <sub>2</sub> (SiO <sub>3</sub> ) <sub>3</sub>	150	20	4	HOAc assisted	26.1	7.8 <sup>15</sup>
5% Ni/Al <sub>2</sub> (SiO <sub>3</sub> ) <sub>3</sub>	150	20	4	HOAc assisted	23.9	6.2 <sup>15</sup>
Ni-Ce-B	180	10	3	EtOH	96.8	N.D. <sup>16</sup>
Ni-Fe-B	200	10	4	EtOH	100	100 <sup>17</sup>
Cu <sub>11.2</sub> Ni <sub>2.4</sub> -MgAlO	300	10	-	EtOH	89.9	87 <sup>18</sup>
5% Pt/C	175	30	1	-	100	27 <sup>19</sup>
2% Ir/TiO <sub>2</sub>	90	6.2	-	heptane/EtOH	30	30 <sup>20</sup>
PtSn/SiO <sub>2</sub>	100	10	8	2-propanol	85	83.5 <sup>21</sup>
1% Pd/SiO <sub>2</sub>	250	-	-	-	69	10 <sup>22</sup>
10% Cu/SiO <sub>2</sub>	230	-	-	-	69	67.6 <sup>22</sup>
2% Pt/TiO <sub>2</sub> /MgO	200	-	-	-	33.6	22.8 <sup>23</sup>
MoNiB/γ-Al <sub>2</sub> O <sub>3</sub>	80	50	3	methanol	99.1	90.2 <sup>24</sup>
Cu-MgO-Cr	200	-	6	-	71.6	71.6 <sup>25</sup>
Cu-Cr	300	-	-	-	60	21-42 <sup>26</sup>
Ni <sub>74.5</sub> P <sub>12.1</sub> B <sub>13.4</sub>	80	-	-	furfural/EtOH	95	77.9 <sup>27</sup>
PtSn <sub>0.2</sub> /SiO <sub>2</sub>	100	-	8	propan-2-ol	100	96 <sup>28</sup>
1% Pt/SiO <sub>2</sub>	100	-	8	propan-2-ol	46	45.5 <sup>28</sup>
2% Ni/SiO <sub>2</sub>	100	-	8	propan-2-ol	31	23.6 <sup>28</sup>
Cu-Fe	160	90	5	-	91	89.5 <sup>29</sup>
Cu-Cr	260	1	-	-	53	51.9 <sup>30</sup>
Cu/MgO	180	1	-	-	98	96 <sup>31</sup>
Cu-Ca/SiO <sub>2</sub>	130	1	-	-	100	99 <sup>32</sup>
CuLa/MCM-41	140	1	-	-	98	> 97 <sup>33</sup>

**Table 5 (Continued). Catalytic hydrogenation of Furfural to Furfuryl alcohol.<sup>9</sup>**

Catalyst	Temp (°C)	P (bar H <sub>2</sub> )	t (h)	Solvent	Conv. (%)	Yield (%)
Cu-MgO	180	1	-	-	98	96 <sup>34</sup>
Cu-Cr/TiO <sub>2</sub>	140	1	-	-	90	79.2 <sup>35</sup>
Pt/TiO <sub>2</sub> -V <sub>2</sub> O <sub>5</sub> -SiO <sub>2</sub>	150	1	-	-	87	79.2 <sup>23</sup>
Ir-ReOx/SiO <sub>2</sub>	30	8	6	water	> 99	> 99 <sup>36</sup>
Cu-Zn-Cr-Zr oxide	170	20	3.5	isopropanol	> 99	> 95 <sup>37</sup>
Raney Ni-CuPMo12	80	20	1	EtOH	98	97 <sup>38</sup>
Co-Mo-B alloy	100	10	3	EtOH	> 99	> 99 <sup>39</sup>
Pt-Sn/SiO <sub>2</sub>	100	10	8	isopropanol	90	88.2 <sup>16</sup>
Ni-Ce alloy	80	10	3	EtOH	97	97 <sup>40</sup>
Ru/C	165	25	-	MTHF	91	42.4 <sup>41</sup>
Cu/Zn/Cr/Zr (3:2:1:4)	170	20	3.5	isopropyl alcohol	100	96 <sup>42</sup>
Ni-Sn	110	30	1.25	isopropanol	72	70 <sup>43</sup>
Ni-Sn/TiO <sub>2</sub>	110	30	1.25	isopropanol	> 99	> 99 <sup>43</sup>

### Tetrahydrofurfuryl alcohol

Tetrahydrofurfuryl alcohol (THFA), chemical formula C<sub>5</sub>H<sub>10</sub>O<sub>2</sub> with a molar mass of 102 g mol<sup>-1</sup>, is a water miscible, transparent liquid, with a high boiling point and a mild odour.<sup>9</sup> THFA is commercially manufactured at an annual volume of approximately 30 t by the Japanese company Koatsu Chemical Industries, and as a green solvent it has found application across a number of different industries, including use within the agricultural sector, in printing inks, and in electronic and industrial cleaners.<sup>9</sup> THFA can either be produced from furfural or directly from FA, with conventional production involving a separate two-step process that initially catalytically hydrogenates furfural to the FA intermediate over a copper-chromite catalyst, before undergoing a subsequent noble metal catalysed hydrogenation step to remove aromaticity from the furan ring and generate the desired THFA product.<sup>9</sup> Resasco et al. recently published a comparative study of silica supported Cu, Ni, and Pd catalysts for the

hydrodeoxygenation of furfural, and reported 5% selectivity to THFA over a 5% Ni/SiO<sub>2</sub> catalyst at 230 °C.<sup>9</sup> Homogeneous catalysts have also been successfully applied to furfural hydrogenolysis and FA hydrogenation, with Gowda et al. reporting 26% selectivity to THFA was using a Ru(II)bis(diimine) complex.<sup>9</sup>

**Table 6. Catalytic hydrogenation of Furfural to Tetrahydrofurfuryl alcohol.<sup>9</sup>**

Catalyst	T (°C)	P (bar H <sub>2</sub> )	t (h)	Solvent/Flow Conditions	Conv. (%)	Yield (%)
NiO/SiO <sub>2</sub>	200	1	-	-	15	> 14.9 <sup>39</sup>
Ni/SiO <sub>2</sub>	140	1	-	GHSV = 1.1 mol h <sup>-1</sup> g catalyst <sup>-1</sup>	> 99	> 93.1 <sup>44</sup>
Raney			1.2			
Ni/Al(OH) <sub>3</sub>	110	30	5	isopropanol	> 99	> 99 <sup>43</sup>
Ni-Pd/SiO <sub>2</sub>	40	80	8	water	99	95 <sup>45</sup>
RuO <sub>2</sub>	120	50	2.5	methanol	100	76 <sup>46</sup>
Ni 5132P + Cu						
V1283	130	40	3	methanol	100	97 <sup>46</sup>
Ni 473P + Cu						
V1283	130	40	3	methanol	99	95 <sup>46</sup>
RuO <sub>2</sub> + Cu						
V1283	120	50	1.5	methanol	100	86 <sup>46</sup>
Pd/C + Cu						
V1283	120	50	3.5	methanol	99	28 <sup>46</sup>
5% Ru/C	120	50	3	methanol	99	59 <sup>46</sup>
Ni 5132P	130	40	4.8	methanol	66	4 <sup>46</sup>
Ru/C	165	25	-	1-butanol-water	100	16.6 <sup>41</sup>
Ru/C	165	25	-	MTHF	91	11.2 <sup>41</sup>
Ni-Sn	110	30	5	isopropyl alcohol	16	4 <sup>43</sup>
1.4% Pt + 1.4%						
Ru/C	160	80	0.5	water	100	9.7 <sup>19</sup>
3% Pd/C	160	80	0.5	water	98.4	62.1 <sup>19</sup>
Pd-Ir-ReOx/SiO <sub>2</sub>	50	60	2	water	> 99.9	78 <sup>47</sup>
Pd-Rh-						
ReOx/SiO <sub>2</sub>	50	60	2	water	> 99.9	18.8 <sup>47</sup>
Pt-Li/Co <sub>2</sub> AlO <sub>4</sub>	140	15	24	ethanol	> 99.9	31.3 <sup>48</sup>

## Methylfuran and Methyltetrahydrofuran

As already mentioned Furfural provides a platform from which a number of lignocellulosic biofuels can be derived, including C<sub>10</sub>-C<sub>15</sub> coupling products, valerate esters, ethylfurfuryl ethers, and ethyltetrahydrofurfuryl ethers.<sup>8</sup> Of the various production routes that exist for upgrading of furanic compounds hydrogenation remains the most versatile, allowing for the production of the biofuel components 2-methylfuran (MF), and methyltetrahydrofuran (MTHF).

Under ambient conditions both MF and MTHF exist as colourless, mobile liquids that display chemical properties that make them comparable to the widely used solvents furan, and tetrahydrofuran (THF).<sup>9</sup> Besides its application potential as a solvent and as a component of biofuels, MF has also found use as a feedstock source for the production of functionally substituted aliphatic molecules, sulfur and nitrogen heterocycles, methylfurfural, and the antimalarial drug chloroquine.<sup>9</sup>

**Table 7. Catalytic hydrogenation of Furfural to 2-Methylfuran.<sup>9</sup>**

Catalyst	T (°C)	P(bar H <sub>2</sub> )	t (h)	Solvent/Flow Conditions	Conv. (%)	Yield (%)
5% Pt/C	175	80	0.5	n-butanol	99.3	40.4 <sup>14</sup>
5% Pt/C	175	80	0.5	n-decanol	94.5	23.2 <sup>14</sup>
5% Pt/C	175	80	0.5	n-butanol/H <sub>2</sub> O (1:1 vol)	99.7	30.8 <sup>14</sup>
5% Pt/C	190	30	0.5	H <sub>2</sub> O	100	3.7 <sup>14</sup>
5%Pd/C + Al <sub>2</sub> (SiO <sub>3</sub> ) <sub>3</sub>	150	20	4	acetic acid-assisted	69.4	17.9 <sup>15</sup>
5% Pd/C	150	20	4	acetic acid-assisted	41.2	8.9 <sup>15</sup>
5% Pt/C	160	30	1	H <sub>2</sub> O	96.5	4.9 <sup>19</sup>
5% Pt/C	175	30	1	H <sub>2</sub> O H <sub>3</sub> PO <sub>4</sub> (85%)	100	36.6 <sup>19</sup>
Cu-Zn-Al	225	-	6	LHSV = 0.7 h <sup>-1</sup>	99.9	93 <sup>49</sup>
2%Pt/TiO <sub>2</sub> /SiO <sub>2</sub>	150	-	-	LHSV = 2 h <sup>-1</sup> (H <sub>2</sub> /Fur = 2/1)	69.4	18.9 <sup>23</sup>
2%Pt/TiO <sub>2</sub> /MgO	250	-	-	LHSV = 2 h <sup>-1</sup> (H <sub>2</sub> /Fur = 2/1)	50.4	5.9 <sup>23</sup>
2%Pt/TiO <sub>2</sub> /γ-Al <sub>2</sub> O <sub>3</sub>	200	-	-	LHSV = 2 h <sup>-1</sup> (H <sub>2</sub> /Fur = 2/1)	33.2	4.7 <sup>23</sup>

**Table 7 (Continued). Catalytic hydrogenation of Furfural to 2-Methylfuran.<sup>9</sup>**

Catalyst	T (°C)	P(bar H <sub>2</sub> )	t (h)	Solvent/Flow	Conv. (%)	Yield (%)
Cu-Mn-Si	279	1	-	LHSV = 0.49 h <sup>-1</sup>	99.8	93.5 <sup>50</sup>
Cu/Zn/Al/Ca/Na (59:33:6:1:1)	250	-	-	LHSV = 0.3 h <sup>-1</sup> (H <sub>2</sub> /Fur = 25)	99.7	87 <sup>51</sup>
Cu/Zn/Al/Ca/Na (59:33:6:1:1)	300	-	-	LHSV = 0.3 h <sup>-1</sup> (H <sub>2</sub> /Fur = 25)	99.7	77.6 <sup>51</sup>
Cu/Cr/Ni/Zn/Fe (43:45:8:3:1)	200	-	-	LHSV = 0.3 h <sup>-1</sup> (H <sub>2</sub> /Fur = 25)	99.6	67 <sup>51</sup>
CuO/CuFe <sub>2</sub> O <sub>4</sub>	220	90	14	-	99.4	51.1 <sup>52</sup>
CuLa-β zeolite	180	1	-	GHSV = 0.087 mol h <sup>-1</sup> g <sup>-1</sup> catalyst	9.5	7.8 <sup>35</sup>
Cu-Zn-Al oxide	150	1	-	LHSV=0.3 g h <sup>-1</sup> g <sup>-1</sup> catalyst	99	86.1 <sup>53</sup>

MTHF exhibits the rare property of being inversely soluble in water, that is, its solubility decreases with increasing temperature.<sup>9</sup> MTHF has found application as a speciality solvent, providing a higher boiling point alternative to THF.<sup>9</sup> In addition to its use as a biofuel component, MTHF is also used in formulation of electrolytes for secondary lithium electrodes.<sup>9</sup>

**Table 8. Catalytic hydrogenation of Furfural to 2-Methyltetrahydrofuran.<sup>9</sup>**

Catalyst	Temp (°C)	P(bar H <sub>2</sub> )	t (h)	Solvent	Conv. (%)	Yield (%)
NiCu/SBA-15	160	40	4	water	> 99	> 16.8 <sup>54</sup>
NiCu/SBA-15	160	40	4	water	> 99	> 35.6 <sup>54</sup>
NiCu/SBA-15	160	40	4	water Na <sub>2</sub> HPO <sub>4</sub>	> 99	> 27.7 <sup>54</sup>
3% Pd/C	160	80	0.5	water Na <sub>2</sub> CO <sub>3</sub>	99.8	16.7 <sup>19</sup>
5% Pt/C	175	80	0.5	water	100	9.4 <sup>55</sup>
Rh-ReOx/SiO <sub>2</sub>	120	60	24	water	> 99.9	26.9 <sup>47</sup>
Pd-Ir-ReOx/SiO <sub>2</sub>	120	60	24	water	> 99.9	11.9 <sup>47</sup>
Pd-Ir-ReOx/SiO <sub>2</sub>	40		2			
5% Pd/C	175	80	1	water	100	35.6 <sup>14</sup>
5% Ru/C	175	80	1	water	100	6.1 <sup>14</sup>
CoMnCr	175	80	0.5	water	100	16.5 <sup>14</sup>
Raney Ni						
Actimet C	160	30	1	water	100	23.4 <sup>14</sup>

Copper-based catalysts operating in the region of 200-300 °C and at low pressure have been reported for the selective (95%) conversion of furfural to 2-MF, with Cu-chromite, Raney-Cu, and Cu/Al<sub>2</sub>O<sub>3</sub> all displaying similar activity, with Cu-chromite exhibiting the greatest stability.<sup>8</sup> Rapid deactivation was reported, however regeneration was achieved through the burning off of coke at 400°C. The observed deactivation during vapour-phase production prompted the question as to whether milder conditions, such as in the liquid phase, could also be employed for the successful production of 2-MF. A number of papers have claimed hydrogenolysis of furfural to 2-MF over palladium supported catalysts under mild conditions with Nudelman and colleagues reporting success with Pd/C under 2 bar H<sub>2</sub> at room temperature. Sun et al., achieved 100% yield of 2-MF in only 1 hour under 1 bar H<sub>2</sub> at 18°C using a polymer supported Pd<sup>II</sup> complex. 2-MF has also been produced under stripping conditions through reactive distillation, allowing for the continuous removal of 2-MF and avoiding consecutive hydrogenation of 2-MF which is thought to limit the selectivity.<sup>8</sup> MTHF has been produced via a two-step process in which a primary reactor achieves hydrogenolysis of furfural to 2-MF over a Ba/Mn-promoted Cu-chromite catalyst operating under 1 bar H<sub>2</sub> at 175°C, before subsequent ring hydrogenation of 2-MF to MTHF in a second reactor utilising Ni-based catalysts at 130°C. A two-stage process has also been reported in which supercritical CO<sub>2</sub> is used in conjunction with Cu-chromite and Pd/C catalysts, although the commercial benefit of operating under supercritical CO<sub>2</sub> as opposed to a pure substrate feed is unclear.<sup>8</sup>

The processes described above for the production of MTHF are undesirable in their employment of toxic chromite or dependence on supercritical CO<sub>2</sub>. There are no reports in the literature of a heterogeneously catalysed process for the production of MTHF from furfural operating under low H<sub>2</sub> pressure at ambient temperature, and considering the excellent gasoline blending properties of MTHF, the development of

a catalyst able to actively and selectively produce MTHF under the mild conditions described would be industrially attractive.

Catalysts and conditions currently employed for the hydrogenation of furfural to furfuryl alcohol, furfural to tetrahydrofurfuryl alcohol, and the hydrogenation of furfural to 2-MF and MTHF, are presented in tables 5-8. An understanding of the catalysts and conditions illustrated in these tables is valuable as the conceptual designing of a heterogeneous metal supported catalyst that is both active and selective for the conversion of furfural to MTHF is not an easy task. A number of factors, such as the chosen metal and the respective support will affect both activity and selectivity, as will the method of catalyst preparation and activation, the metal precursor, the reaction conditions and the operation mode. Consequently it is necessary to develop an understanding of the catalyst structure through characterisation techniques, and relate catalytic activity to the observed morphology. This is in itself demanding, as our current understanding of hydrogenation over heterogeneous catalysts describes a reaction proceeding through a number of surface reaction steps, such as adsorption, reaction and desorption. In addition the true reaction mechanism has further considerations that need to be elucidated; whether adsorption is dissociative or non-dissociative for example, the possibility of coke formation and subsequent catalyst deactivation, adsorption of the solvent etc.

## 1.7 References

1. Robertson, A.J.B. *Platinum Metals Rev.*, 1975, 19 (2)
2. Bond, G.C., Louis, C., Thompson, D.T. 2006. *Catalysis by Gold*. London: Imperial College Press.
3. Berzelius J.J, *Edinburgh New Philosophical Journal*, 21 (1836), 223.
4. <http://chemistry.about.com/od/chemicalreactions/a/catalysts-catalysis.htm>
5. M. Bowker, *The Basis and Applications of Heterogeneous Catalysis*, Oxford University Press, Oxford, 1998.
6. P. T. Anastas and J. C. Warner, *Green Chemistry: Theory and Practice*, Oxford University Press, New York, 1998.
7. G.O. Ribeiro, R.J. Gruninger, A. Badhan, T.A. McAllister. *Animal Frontiers*, 2016, 6, 20-26.
8. J.-P. Lange, E. Van der Heide, J. Van Buijtenen, R.Price, *ChemSusChem* **2012**, 5, 150-166.
9. Yan K, Wu G, Lafleur T, Jarvis C. *Renew Sust Energ Rev* 2014; 38: 663-676.
10. Win, D.T. *AU Journal of Technology*, 2005, 8, 185-190
11. K.J. Zeitsch, *The Chemistry and Technology of Furfural and its many By-Products*, Elsevier, Amsterdam, 2000.
12. I. Agirrezabal-Telleria, I. Gandarias, P.L. Arias. *Catalysis Today*, 2014, 234, 42-58
13. V. Vorochnikov, G. Mpourmpakis, D. Vlachos, *ACS catal*, 2012, 2, 2496-2504.
14. Hronec M, Fulajtarová K. *Catal Commun* 2012;24:100-4.

15. Yu WJ, Tang Y, Mo LY, Chen P, Lou H, Zheng XM. *Bioresour Technol* 2011;102:8241–6.
16. Li H, Zhang S, Luo H. *Mater Lett*. 2004;58:2741–6.
17. Li H, Luo H, Zhuang L, Dai W, Qiao M. *J Mol Catal A* 2003;203:267–75
18. Xu CH, Zheng LK, Liu JY, Huang ZY. *Chin J Chem* 2011;29:691–7.
19. Hronec M, Fulajtarová K, Liptaj T. *Appl Catal A* 2012;437–438:104–11.
20. Reyes P, Salinas D, Oportus CM, Murcia J, Borda HG, Fierro JG. *Quim Nova* 2010;33:77–80.
21. Merlo AB, Vetere V, Ruggera JF, Casella ML.. *Catal Commun* 2009;10:1665–9.
22. Sitthisa S, Resasco DE. *Catal Lett* 2011;141:784–91.
23. Kijenski J, Winiarek P, Paryjczak T, Lewicki A, Miko łajska. *Appl Catal A* 2002;233:171–82.
24. Wei SQ, Cui HY, Wang JH, Zhuo SP, Yi WM, Wang LH, et al. *Particuology* 2011;9:69–74.
25. Nagaraja BM, Padmasri AH, Raju BD, Rao KSR. *Int J Hydrogen Energy* 2011;36:3417–25.
26. Rao R, Dandekar A, Baker RTK, Vannice MA.. *J Catal* 1997;171:406–19.
27. Lee SP, Chen YW. *Ind Eng Chem Res* 1999;38:2548–56.
28. Vetere V, Merlo AB, Ruggera JF, Casella ML.. *J Braz Chem Soc* 2010;21:914–20
29. Yan K, Chen AC. *Energy* 2013;58:357–63.
30. Seo G, *J Catal* 1981;67:424–9.

31. Nagaraja BM, Siva Kumar V, Shasikala V, Padmasri AH, Sreedhar B, Raju BD, et al. *Catal Commun* 2003;4:287–93.
32. Wu J, Shen Y, Liu C, Wang H, Geng C, Zhang Z. *Catal Commun* 2005;6:633–7
33. Hao XY, Zhou W, Wang JW, Zhang YQ, Liu S. *Chem Lett* 2005;34:1000–1.
34. Nagaraja BM, Padmasri AH, Raju BD, Rao KSR. *J Mol Catal A* 2007;265:90–7.
35. Huang W, Li H, Zhu B, Feng Y, Wang S, Zhang S. *Ultrason Sonochem* 2007;14:67–74.
36. Tamura M, Tokonami K, Nakagawa Y, Tomishige K. *Chem Commun* 2013;49:7034–6.
37. Baijun L, Lianhai L, Bingchun W, Tianxi C, Iwatani K. *Appl Catal A* 1998;171:117–22.
38. Chen X, Li H, Luo H, Qiao M. *Appl Catal A* 2002;233:13–20.
39. Seo G, Chon H. *J Catal* 1981;67:424–9.
40. Li H, Luo H, Zhuang L, Dai W, Qiao M. *J Mol Catal A* 2003;203:267–75.
41. Ordonsky VV, Schouten JC, van der Schaaf J, Nijhuis TA. *Appl Catal A* 2013;451:6–13.
42. Sharma RV, Das U, Sammynaiken R, Dalai AK. *Appl Catal A* 2013;454:127–36.
43. Rodiansono Khairi S, Hara T, Ichikuni N, Shimazu S. *Catal Sci Technol* 2012;2:2139–45.

44. Nakagawa Y, Nakazawa H, Watanabe H, Tomishige K. *ChemCatChem* 2012;4:1791–7.
45. Nakagawa Y, Tomishige K. *Catal Commun* 2010;12:154–6.
46. Merat N, Godawa C, Gaset A. *J Chem Technol Biotechnol* 1990;48:145–59.
47. Liu S, Amada Y, Tamura M, Nakagawa Y, Tomishige K. *Green Chem* 2014;16(2):617–26.
48. Xu WJ, Wang HF, Liu XH, Ren JW, Wang YQ, Lu GZ. *Chem Commun* 2011;47:3924–6
49. Yang J, Zheng HY, Zhu YL, Zhao GW, Zhang CH, Teng BT, et al. *Catal Commun* 2004;5:505–10.
50. Zheng HY, Zhu YL, Huang L, Zeng ZY, Wan HJ, Li YW. *Catal Commun* 2008;9:342–8
51. Zheng HY, Zhu YL, Teng BT, Bai ZQ, Zhang CH, Xiang HW, et al. *J Mol Catal A* 2006;246:18–23.
52. Yan K, Chen AC. *Fuel* 2014;115:101–8.
53. Zheng HY, Zhu YL, Bai ZQ, Huang L, Xiang HW, Li YW. *Green Chem* 2006;8:107–9.
54. Yang Y, Du Z, Huang Y, Lu F, Wang F, Gao J, et al. *Green Chem* 2013;15:1932–40
55. Hronec M, Fulajtárova K, Micusik M. *Appl Catal A* 2013;468:426–31.

# Chapter 2

## 2. Experimental

### 2.1 Introduction

This chapter lists and describes the materials and methods used in performing the reactions presented in this thesis. The initial section of this chapter provides information on the chemicals and experimental reactors utilised, as well as the methodologies used for the preparation and testing of heterogeneous catalysts. The second section of this chapter describes the equipment used for the quantitative analysis of experimental results.

### 2.2 Chemicals Used

The Chemicals listed below were used as received.

Gold (III) acetate, 99.9% Alfa Aesar

Palladium (II) acetate, 99.9% Sigma Aldrich

Hydrogen tetrachloroaurate trihydrate, Johnson Matthey

Palladium chloride, Johnson Matthey

Titania, P25 Degussa

Benzyl alcohol, 98% Sigma Aldrich

Glycerol,  $\geq 99\%$ , Sigma Aldrich

50% Hydrogen peroxide (stabilised), Sigma Aldrich

Cinnamyl alcohol, 98% Sigma Aldrich

Furfuryl Alcohol, 98% Sigma Aldrich

Furfural, 98% Sigma Aldrich

Tin (IV) chloride hydrate, 98% Sigma Aldrich

1,2-dichloroethane, 98% Sigma Aldrich

Methanol, 99.8% Sigma Aldrich

Ethanol, 99.8% Sigma Aldrich

1-propanol, 99.8% Sigma Aldrich

Water HPLC, Sigma Aldrich

## 2.3. Definitions

---

---

---

## 2.4 Catalyst Preparation

### Physical Grinding

TiO<sub>2</sub> supported Monometallic Pd, monometallic Au, and Au-Pd bimetallic catalysts were prepared by physical grinding of the precursor metal acetates with preformed titania (TiO<sub>2</sub>, P25, Degussa). As an example, the 2.5wt%Au-2.5wt%Pd/TiO<sub>2</sub> catalyst (1.0 g) was prepared according to the following procedure: Palladium acetate (0.0474 g) and gold acetate (0.0526 g) were added to the preformed TiO<sub>2</sub> support (0.95 g) in a pestle and mortar before being physically ground for 5 mins. The resulting material was subsequently heat treated at 350 °C for 2 hours, with a ramp rate of 20 °C min<sup>-1</sup> under flowing Helium.

## Impregnation

TiO<sub>2</sub> supported Monometallic Pd, monometallic Au, monometallic Ru, bimetallic Au-Pd bimetallic, bimetallic Sn-Pd, and bimetallic Ru-Pd catalysts were prepared by impregnation of titania (TiO<sub>2</sub>, P25, Degussa). For example, a bimetallic 2.5wt%Au-2.5wt%Pd/TiO<sub>2</sub> catalyst (1.0 g) was prepared according to the following methodology: Initial preparation of an aqueous H<sub>2</sub>AuCl<sub>4</sub>.6H<sub>2</sub>O stock solution (12.25 g Au in 1000 ml H<sub>2</sub>O) allowed for the extraction of 2.04 ml stock solution, to which 0.0417 g PdCl<sub>2</sub> was added. The resulting solution was heated at 80 °C and agitated at 400 rpm until the PdCl<sub>2</sub> had homogeneously dissolved in solution. 0.95 g TiO<sub>2</sub> was added to the solution and agitated at 400 rpm until a paste with a toothpaste-like consistency was formed. The resulting material was heated in an oven at 110 °C for 16 hours, before being calcined in static air at 400 °C with a ramp rate of 20 °C min<sup>-1</sup>, for 3 hours.

## 2.5 Catalyst testing

### Benzyl alcohol oxidation

Catalyst testing was carried out using a stainless steel autoclave (Autoclave Engineers In-line MagneDrive III). The autoclave had a nominal volume of 100 mL and a maximum operating pressure of 140 bar. Benzyl alcohol testing involved charging the vessel with 40 mL benzyl alcohol and 25 mg catalyst, before purging the reactor three times with nitrogen, followed by three times with oxygen, before leaving the vessel at the desired oxygen pressure of 10 bar. This pressure was maintained throughout the course of the reaction, with any oxygen consumed in the reaction being replenished. The oxidation reaction had a fixed temperature of 140 °C, and an agitation speed of 1500 rpm. Reaction sampling was carried out periodically by

means of a sampling pipe, and analysed using a GC (Varian 3800) equipped with a CP-wax column.

### **Direct synthesis of Hydrogen peroxide**

Direct hydrogen peroxide synthesis was performed using reaction parameters that have previously been established by the Hutchings group as being optimal. Hydrogen peroxide synthesis and hydrogenation reactions were carried out using a Parr Instruments stainless steel autoclave with a specified maximum operating pressure of 140 bar, and a nominal volume of 100 mL. Catalytic testing required charging the autoclave with 0.01 g catalyst, and 8.5 g solvent (5.6 g methanol and 2.9 g water), before purging with 7 bar 5% H<sub>2</sub>/CO<sub>2</sub>. The autoclave was subsequently charged with 29 bar 5% H<sub>2</sub>/CO<sub>2</sub> at a temperature of 20 °C. A pressure drop to 26 bar was observed as the gasses dissolved in the solvent, which was followed by addition of 11 bar 25% O<sub>2</sub>/CO<sub>2</sub>. A subsequent decrease in temperature to 2 °C was followed by agitation of the reaction mixture at 1200 rpm for 30 mins. Determination of hydrogen peroxide productivity was achieved by titrating aliquots of the final reaction mixture with acidified Ce(SO<sub>4</sub>)<sub>2</sub> [0.01 M] in the presence of ferroin indicator.

### **Hydrogen peroxide hydrogenation**

Hydrogen peroxide hydrogenation was evaluated using a Parr Instruments stainless steel autoclave with a specified maximum operating pressure of 140 bar, and a nominal volume of 100 mL. Catalytic testing required charging the autoclave with 0.01 g catalyst, and a 4 wt% hydrogen peroxide solution (5.6 g methanol, 2.22 g water and 0.68 g hydrogen peroxide 50% w/w), before purging with 7 bar 5% H<sub>2</sub>/CO<sub>2</sub>. The autoclave was subsequently charged with 29 bar 5% H<sub>2</sub>/CO<sub>2</sub> at a temperature of 20 °C. A subsequent decrease in temperature to 2 °C was followed by agitation of the reaction mixture at 1200 rpm for 30 mins. Determination of hydrogen peroxide

conversion was achieved by titrating aliquots of the final reaction mixture with acidified  $\text{Ce}(\text{SO}_4)_2$  [0.0288 M] in the presence of ferroin indicator.

### **Glycerol Oxidation**

Glycerol oxidation reactions were evaluated by charging a 50 mL glass reactors with 0.3 mol L<sup>-1</sup> glycerol solution, base solution (NaOH, substrate:base = 2), and catalyst (glycerol:metal mole fraction = 500), before being charged three times with oxygen and left at a final pressure of 3 bar. This pressure was maintained throughout the course of the reaction, with any oxygen consumed in the reaction being replenished. The reaction mixture was heated to a fixed temperature of 60 °C, and was agitated throughout the course of the reaction (0.5-4.0 h). Post-reaction, the glass reactor was cooled to room temperature before sampling of the reaction mixture prior to analysis. Analysis of the reaction mixture was performed using high-pressure liquid chromatography (HPLC) fitted with ultraviolet and refractive index detectors. Separation of reactants and products was achieved using a Metacarb 67H column eluted with 0.01 mol L<sup>-1</sup> aqueous H<sub>3</sub>PO<sub>4</sub> at a flow rate of 0.3 mL min<sup>-1</sup>. The eluent was used to dilute reaction mixture samples (0.5 mL) to a volume of 5.0 mL. Product identification was achieved by comparison against known standards. Quantification was accomplished by use of an external calibration method.

### **Furfuryl alcohol hydrogenation.**

Furfuryl alcohol hydrogenation reactions were performed in a Colaver glass reactor charged with 1.0 g furfuryl alcohol, 15 mL of chosen solvent, and 0.1 g of catalyst. The reactor was sealed and purged with 3 bar nitrogen before being pressurised with the chosen hydrogen pressure (1–3 bar constant pressure), and agitated at 1000 rpm for 60 minutes unless specified otherwise. Post-reaction, the reaction mixture was centrifuged before being analysed by GC (Bruker Sion 456-GC fitted with a Br-1ms capillary column). Product identification was achieved by comparison against known

standards. Quantification was accomplished by use of an external calibration method, with 1-propanol being used as the external standard.

## **Furfural Hydrogenation**

Furfural hydrogenation was performed using a stainless steel stirred autoclave (50 ml, Parr Instruments, Model 5500HP). A Teflon liner was charged with 0.1 g catalyst 1.0 g furfural, 15 mL of and solvent, before being added to the autoclave. The sealed autoclave was then purged with nitrogen three times, followed by purging with hydrogen three times prior to being pressurized to the required hydrogen pressure. The reaction mixture in the autoclave was agitated at 1000 rpm at the chosen reaction temperature. When the reaction was completed, the mixture was cooled, filtered and centrifuged prior to being analysed by GC (Bruker Sion 456-GC fitted with a Br-1 ms capillary column). Product identification was achieved by comparison against known standards. Quantification was accomplished by use of an external calibration method, with 1-propanol being used as the external standard.

## **2.6 Catalyst Characterisation**

### **X-Ray Diffraction (XRD)**

#### **Introduction**

X-ray diffraction (XRD) is a non-destructive technique that can be used to determine the average bulk structure of crystalline materials. XRD has a detection limit of approximately 5wt% and be used to identify crystallite phases above *ca.* 5 nm<sup>1</sup>.

## Background

X-rays for diffraction techniques are generated by bombarding a metal target, usually Cu or Mo, with a beam of high energy electrons emitted from a heated filament. This electron beam causes ionisation of K-shell (1s) electrons in the target atoms, creating vacancies that are subsequently filled by electrons from the L (2p) or M (3p) levels, resulting in the emission of  $K_{\alpha}$  and  $K_{\beta}$  X-rays.

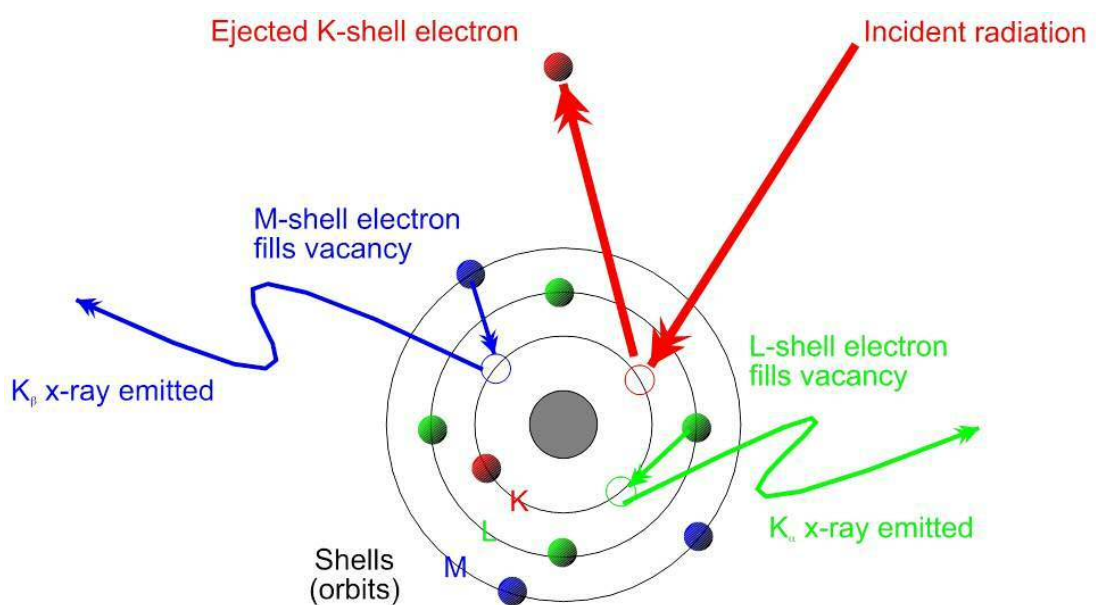


**Figure 2.1. Diagram demonstrating the emission of X-rays caused by outer shell electrons filling inner electron holes.<sup>2</sup>**

The X-rays produced are filtered in order to provide a monochromatic source, and as they hit the target crystalline sample they are scattered via interaction with atomic electrons within the atomic planes of the crystallite material, with X-rays scattered from different parts of the electron undergoing interference.

The conditions for constructive interference are described by Bragg's law.

Where,  $n$  = an integer;  $\lambda$  = X-ray wavelength,  $d$  = lattice spacing <sub>$hkl$</sub> ,  $\theta$  = angle between incident and normal to the lattice plane.

Bragg's law describes a scenario whereby, if an X-ray of wavelength  $\lambda$  is to enter a crystal lattice at angle  $\theta$  (with respect to the lattice planes  $hkl$ , spaced out equidistantly with an interplanar distance of  $d$ ), constructive interference will occur only for X-rays that are reflected from the  $hkl$  planes at the specular angle, providing the path length difference between the scattered X-rays is a whole integer multiple of the wavelength.<sup>3</sup>

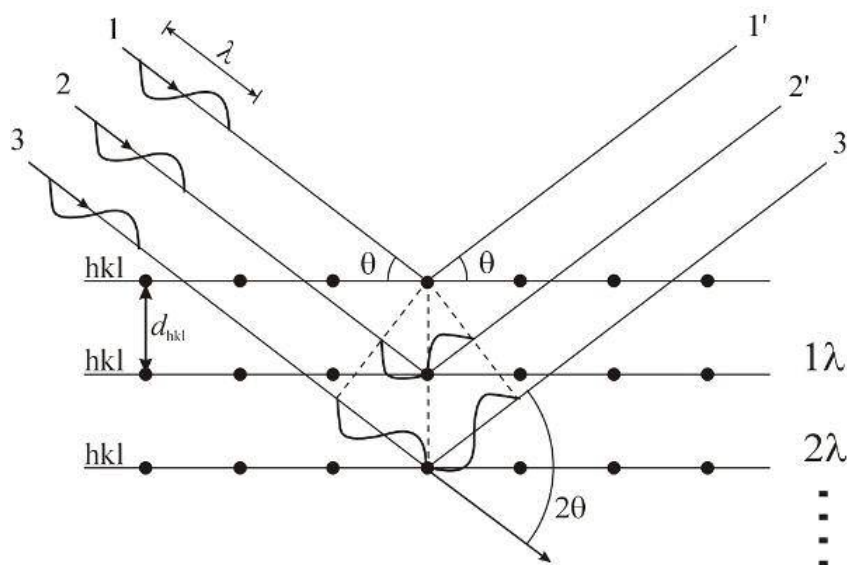


**Figure 2.2. Diffraction of X-rays from the lattice planes  $hkl$  at an angle to satisfy Bragg's law for constructive interference.<sup>3</sup>**

In the case of supported metal nanoparticles, as can be produced in the preparation of heterogeneous catalysts, the small crystallite structures can cause incomplete destructive interference which results in line broadening. This allows for the

determination of crystallite size from the shape of the peaks generated. Broader peaks will be generated from smaller crystallites, as they contain fewer lattice planes; with larger crystallites, being comprised of greater numbers of lattice planes, producing narrower, more defined peaks. Through application of the Scherrer equation below, the crystallite size of a supported metal particle can be estimated.

---

Where,  $n$  = crystallite size;  $K$  = form factor;  $\lambda$  = wavelength;  $\Delta 2\theta$  = full-width half-maximum of peak;  $\theta$  = angle of diffraction.

### **Procedure**

Characterisation of bulk materials was performed using powder X-ray diffraction (XRD) on a ( $\theta$ - $\theta$ ) PANalytical X'pert Pro powder diffractometer with a Cu  $K_{\alpha}$  radiation source with a working voltage of 40 KeV at 40 mA. Analysis was conducted using a 40 min scan with a back filled sample. The ICDD data base was used to identify the diffraction pattern of phases.

## **X-Ray Photoelectron Spectroscopy (XPS)**

### **Introduction**

X-Ray photoelectron spectroscopy (XPS) is a surface analysis technique that allows for the gathering of information pertaining to the elemental composition, and electronic state of elements present at the surface of a material to a depth of around 10 nm.<sup>4</sup>

### **Background**

XPS is based on the principles of the photoelectric effect, whereby a high energy X-ray source (typically Mg  $K_{\alpha}$ , 1253.6 eV; or Al  $K_{\alpha}$ , 1486.3 eV) is directed at a sample

resulting in the ejection of a core electron with a given kinetic energy.<sup>4</sup> The kinetic energy is a function of the energy of the incident X-rays; the binding energy of the ejected core electron; and of the spectrometer work function. The binding energy of the core electron is specific to both the element in question, and its corresponding oxidation state, with higher elemental oxidation states having concomitantly higher core electron binding energies. In order for the core electron to be ejected on irradiation, the energy of the incident X-rays must necessarily be higher than that of electron's binding energy. The work function of the spectrometer must also be taken into account, as this is the energy required to eject a given electron from the Fermi level into a vacuum.<sup>5</sup> Consequently, in order for an electron to be detected the incident X-rays must have a higher energy than the electron binding energy and work function combined, with the excess energy difference being measured as the kinetic energy of the electron.

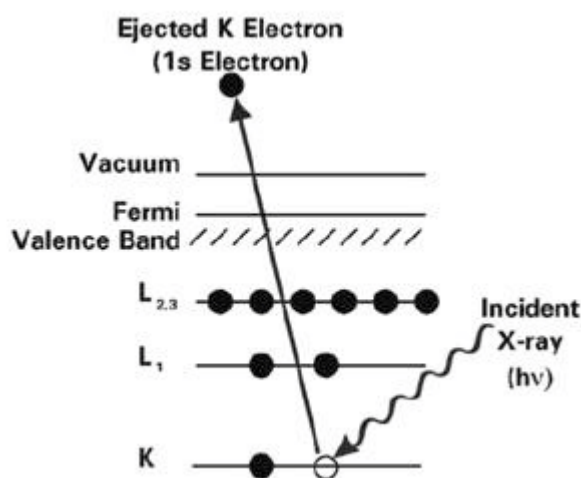


**Figure 2.3** Diagram showing high energy X-ray radiation ejecting an electron from the Fermi level into the vacuum.<sup>5</sup>

The equation below describes the photoemission process.

$$E_k = h\nu - E_b - \phi$$

Where,  $E_k$  = photoelectron kinetic energy;  $h$  = Planck's constant;  $\nu$  = frequency of incident radiation;  $E_b$  = binding energy of electron with respect to sample Fermi level;  $\phi$  = spectrometer work function.

As the electron binding energy and work function is specific to each element, by maintaining the energy of the incident X-ray photons at a constant level, the XPS spectral data can be generated in a form describing either intensity of detected photoelectrons as a function of kinetic energy, or intensity of detected photoelectrons as a function of binding energy.

### **Procedure**

XPS measurements were conducted using a Kratos Axis Ultra DLD spectrometer with an Al  $K_{\alpha}$  radiation power source (120 W). For survey scans, an analyser pass energy of 160 eV was used, with 40 eV of energy used for detailed regional scans. Powder samples were mounted using double-sided adhesive tape, with binding energies being referenced as described in the relevant research chapters.

## **Microwave plasma atomic emission spectroscopy (MP-AES)**

### **Introduction**

MP-AES is an analytical technique that relies upon the basic principles of atomic emission. It is used for the simultaneous determination of multiple elements within a given analytical sample.

## **Background**

Microwave energy is used to generate a nitrogen plasma which is subsequently heated to around 4725 °C by a quartz torch. Acid digested samples are sprayed into the torch flame, resulting in sample atomisation and electron excitation. As the excited electrons fall from their excited states into lower quantised energy levels, photons of characteristic wavelength and energy are released which can in turn be detected. Through application of a mirror grating and monochromatic detector, individual wavelengths can be detected. This enables analysis with enhanced sensitivity for elements with which interfering wavelengths can be issue. Because of the high temperatures employed in MP-AES, this technique can be seen as more favourable than associated analytical methods such as spectrometers based on flame atomic absorption, as greater accuracy can be afforded at increased temperatures.

## **Procedure**

A known quantity of catalyst is submerged in 5 mL Aqua Regia and allowed to dissolve over a 24 hour period before being diluted with 50 mL deionised water. PTFE syringe filters are then used to filter off any remaining undigested particulate matter before being subjected to MP-AES analysis (Agilent MP-AES 4100 series), with calibrations of multiple wavelengths used for each element analysed

## **Transmission Electron Microscopy (TEM)**

### **Introduction**

Electron microscopy allows the generation of high resolution images that can be used for the characterisation of nanostructures. Electron microscopy can afford resolutions high enough for the detection of single atoms.<sup>6,7</sup> Interpretation of images obtained

from electron microscopy can provide information on material topology, and particle size distribution.

## Background

Typically, a tungsten electrode is used to generate a beam of high energy electrons by thermionic emission. This electron beam is directed at a sample, with which it can interact with the surface in a number of ways, inducing a variety of different physical phenomena which can subsequently be detected.

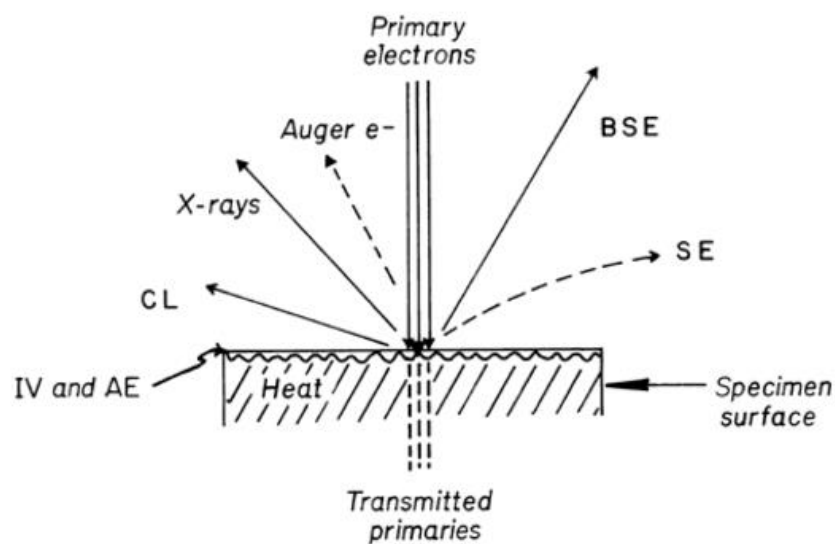


**Figure 2.4 demonstrates a number of possible ways with which the primary electron source can interact with the sample surface.<sup>8</sup> BSE = back scattered electrons; CL = cathodoluminescence; SE = emitted secondary electrons; IV = charging from induced voltages; AE = charging via adsorbed electrons.<sup>8</sup>**

The atomic potentials of the electrons in the sample cause scattering of the incident electron beam, with the extent to which the electrons are scattered being roughly proportional to atomic number. The electron scattering effect is strong enough that it can even be applied for the diffraction of electrons in a gaseous sample. The scattered electrons are gathered by a detector and are used to generate an image

based on the intensity of scattered electrons detected, with heavier elements scattering the electrons more efficiently than light elements, thereby providing brighter images.

### Procedure

TEM was performed using a JEOL 2100 fitted with a LaB6 filament operating at 200 kV. Powdered catalyst samples were prepared by dispersion in ethanol with the subsequent suspension being dropped onto a lacey carbon film over a 300 mesh copper grid. TEM analysis was not carried out by the author.

## Gas Chromatography (GC).

### Background

Gas Chromatography is a technique utilised for the separation and quantitative detection of the components comprising a mixture of liquids or solution. The analyte is heated such that the constituent compounds enter the gas phase in an injector port, prior to being mixed with a transport gas that carries the compounds across a column that serves to separate the substances, before analysis by a detector.

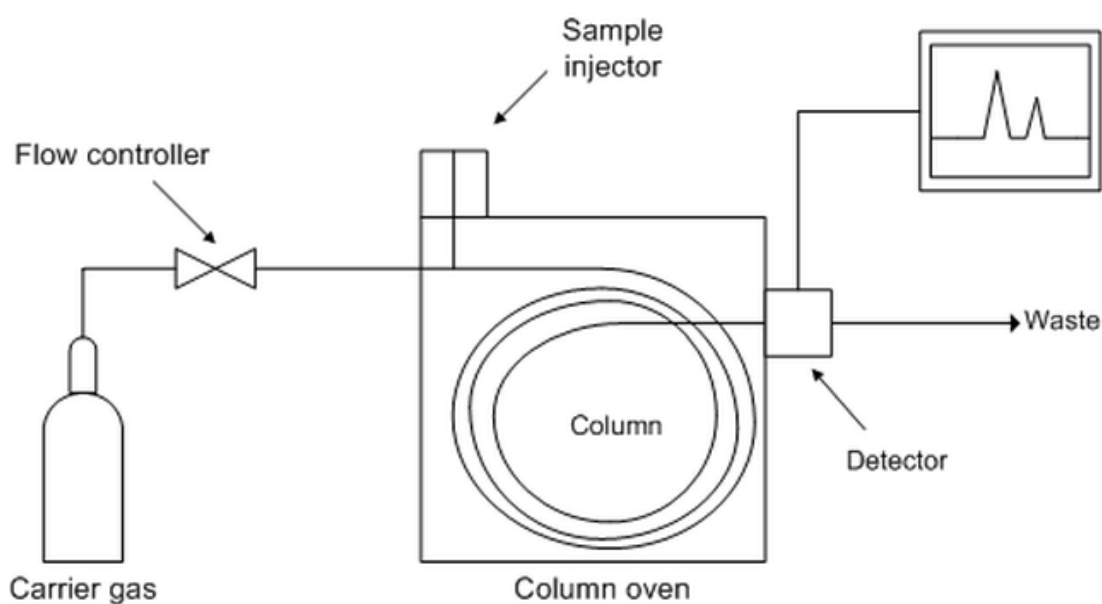
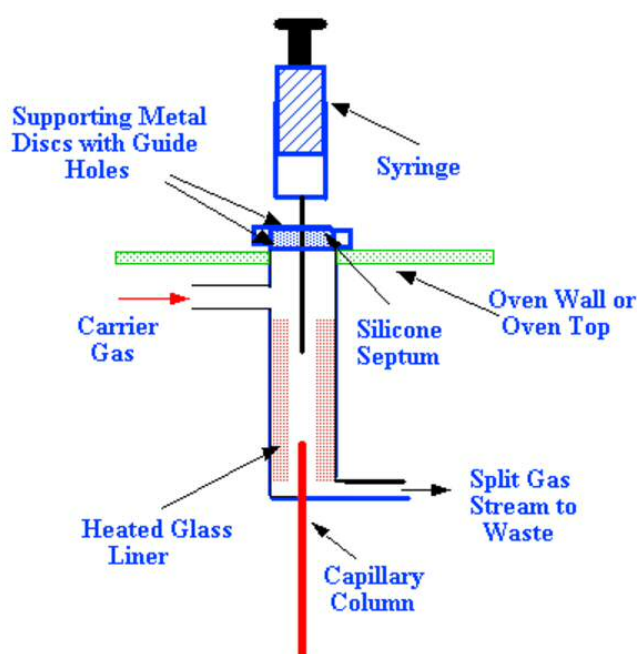


Figure 2.5 Generalised diagram of gas chromatography set-up.<sup>9</sup>

The vast majority of Gas Chromatographs now use capillary columns packed with an inert substance to separate the components of the injected sample. These columns can be increased in length in order to achieve more facile separation without the risk of a concomitant drop in pressure. One drawback of this sample however is that these columns can only process low sample volumes, therefore requiring the use of a split injector. In a split injector, a syringe containing the sample is introduced through a septum so that the sample can be injected into the injector port. Here, it is subsequently heated and mixed with a carrier gas before being separated into two component parts dictated by the split ratio and the carrier gas rate of flow.



**Figure 2.6 Diagram to show basic set up of GC injector port.<sup>10</sup>**

Separation of a samples constituent components in the capillary column is followed by quantified detection by means of a flame ionisation detector (FID). The capillary column is situated such within the GC that it feeds directly into the FID detector. As the sample enters the detector it is immediately mixed with hydrogen and air before undergoing pyrolysis through exposure to a flame. The combustion of the sample results in the production of carbocations which can subsequently be detected by the

anode detector. The resulting gaseous products, most of which is water, is removed from the GC via an exhaust vent.

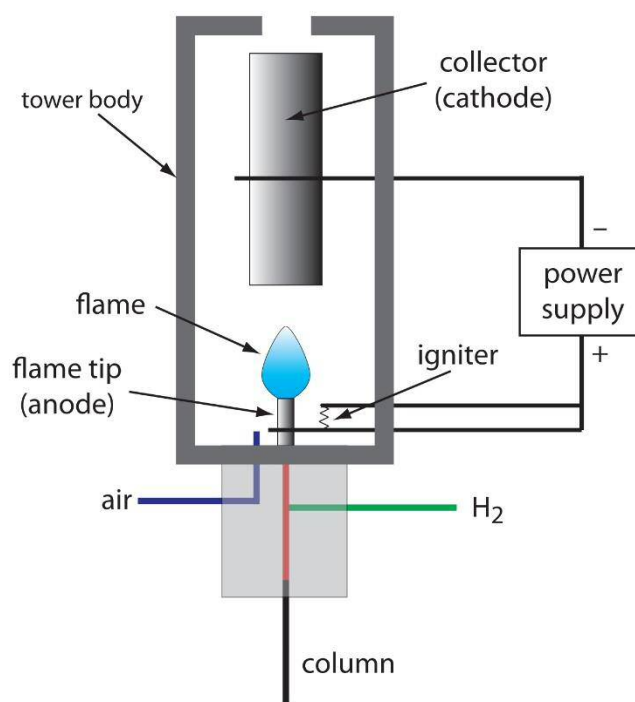


**Figure 2.7** Diagram to show the components of a flame ionisation detector (FID).

## 2.7 References

1. J. W. Niemantsverdriet, *Spectroscopy in Catalysis 3rd Edition*, Wiley, **2007**, 148-154.
2. <https://www.bruker.com/products/x-ray-diffraction-and-elemental-analysis/handheld-xrf/how-xrf-works.html>
3. <https://fys.kuleuven.be/iks/nvsf/experimental-facilities/x-ray-diffraction-2013-bruker-d8-discover>
4. J. W. Niemantsverdriet, *Spectroscopy in Catalysis 3rd Edition*, Wiley, **2007**, 39-80.
5. <http://xpssimplified.com/whatisxps.php>
6. P. M. Voyles, J. L. Grazul and D. A. Muller, in *Ultramicroscopy*, Netherlands, Editon edn., 2003, vol. 96, pp. 251-273.  
Y. Zhu, H. Inada, K. Nakamura and J. Wall, in *Nat Mater*, England, Editon edn., 2009, vol. 8, pp. 808-812
7. [http://www.pharmacopeia.cn/v29240/usp29nf24s0\\_c1181.html](http://www.pharmacopeia.cn/v29240/usp29nf24s0_c1181.html)
8. <http://chemistry.about.com/od/imagesclipartstructures/ig/Lab-Equipment---Instruments/Gas-Chromatograph-Diagram.htm>
9. [http://www.chromatography-online.org/Injection-Devices/Open-Tubular-Column/rs\\_2\\_15.php](http://www.chromatography-online.org/Injection-Devices/Open-Tubular-Column/rs_2_15.php)
10. [http://chemwiki.ucdavis.edu/Core/Analytical\\_Chemistry/Analytical\\_Chemistry\\_2.0/12\\_Chromatographic\\_and\\_Electrophoretic\\_Methods/12.4%3AGas\\_Chromatography](http://chemwiki.ucdavis.edu/Core/Analytical_Chemistry/Analytical_Chemistry_2.0/12_Chromatographic_and_Electrophoretic_Methods/12.4%3AGas_Chromatography)

# Chapter 3

## 3. Physical mixing of metal acetates: Optimisation of catalyst parameters to produce highly active bimetallic catalysts

### 3.1 Introduction

Heterogeneous catalysis is of fundamental importance in the manufacture of fine and bulk chemicals, and has a central role in ensuring green chemistry processes are as environmentally sound, and non-hazardous as possible. The application of catalysts to select oxidation reactions can potentially lead to greener industrial routes to manufacture than non-catalytic alternative production processes. Within the field of heterogeneous catalysis gold nanoparticles have been shown to be efficacious for the direct synthesis of hydrogen peroxide,<sup>1</sup> for CO oxidation,<sup>2,3</sup> and for the oxidation of alcohols,<sup>4,5</sup> and alkenes.<sup>6-8</sup> In addition, the alloying of gold with palladium has been demonstrated to elicit a synergistic effect that results in a significant enhancement in catalytic activity for alcohol activity,<sup>9,10</sup> and has also been shown to substantially increase the yield of hydrogen peroxide formed in the direct synthesis reaction.<sup>10,11</sup>

Typically, the catalysts utilised for the oxidation reactions above are produced by one of the three most common catalyst preparation techniques, that is to say by either the wet impregnation, deposition precipitation, or sol-immobilisation methodology. Regardless of the chosen method of catalyst preparation however, all three techniques require  $\text{HAuCl}_4$  as the gold metal precursor, making it very difficult to remove all residual chloride from the final catalyst. This chloride contamination can be extremely detrimental to catalyst activity, having been shown to result in the blocking of active sites,<sup>12</sup> and formation of Au-Cl-Au bridges causing particle

agglomeration.<sup>13</sup> One well documented example of chloride presence affecting catalytic activity is that of CO oxidation over monometallic gold catalysts, where a Cl:Au atom ratio of only 0.1 was shown to reduce the catalytic activity by ~50%, even though the majority of the Cl<sup>-</sup> present was found to be associated exclusively with the Al<sub>2</sub>O<sub>3</sub> support.<sup>14,15</sup> Phosphate blocking of Al<sub>2</sub>O<sub>3</sub> support sites demonstrated that a Cl:Au atom ratio of as little as 0.0006 could impinge catalytic activity.

A number of methods by which to reduce the level of chloride contamination exist, however they often result in a concomitant lowering of catalyst activity by alternative means, or are considered impractical from a green chemistry perspective. One such method involves careful tuning of the deposition pH to facilitate HAuCl<sub>4</sub> hydrolysis, whilst reducing the concentration of chloride deposited onto the support.<sup>15</sup> However, in order to ensure complete HAuCl<sub>4</sub> hydrolysis the deposition pH needs to be adjusted to around pH 10; an unfavourable level of basicity that negatively impacts Au loading.<sup>15,16</sup> Heat treatment of the final catalyst has also been shown to reduce Cl<sup>-</sup> contamination, however this can result in sintering causing particle agglomeration.<sup>15</sup> Other studies have focused on adjusting the deposition and impregnation catalyst preparation methodologies to allow for the addition of ammonia, as ammonia has been reported as being effective in lowering the catalyst chloride concentration to below 200 ppm.<sup>17-19</sup> Unfortunately, from a green and process chemistry perspective scale-up of a preparation methodology that involves ammonia addition is unfavourable due to inherent toxic and corrosive properties.

Connell et al. have previously shown that supported metal nanoparticles can be prepared through the physical mixing of metal acetates followed by a heat treatment step under an inert atmosphere.<sup>20</sup> The Hutchings group went on to demonstrate the potential of this methodology for the production of supported chloride-free monometallic Au, and bimetallic Au-Pd alloy catalysts prepared by the physical mixing of Au and Pd acetates with a support followed by subsequent heat

treatment.<sup>21</sup> As this catalyst preparation technique does not generate a source of aqueous chloride ions there is a significant reduction in waste, which ultimately means that catalysts prepared by this physical mixing methodology can be considered greener than analogous catalysts prepared by the alternative production techniques discussed previously. When tested for benzyl alcohol oxidation, and direct synthesis of hydrogen peroxide, supported bimetallic Au-Pd alloy catalysts prepared by the physical mixing method displayed extremely high activity compared to the activities of analogous catalysts prepared by wet impregnation, and deposition-precipitation methods. Catalysts prepared by the physical mixing technique were found to be comprised of large particles ( $\mu\text{m}$ ) of Au and Pd, with significant quantities of well-dispersed  $< 10$  nm particles also present. It is the sub 10 nm particles that the high catalytic activity is attributed to.

Previous work conducted within the Hutchings group showed that catalysts prepared by the physical mixing methodology exhibited greater activity for both hydrogen peroxide synthesis and benzyl alcohol oxidation than optimised catalysts prepared by the wet impregnation and deposition-precipitation techniques analogous with regard to weight loadings and metal ratio.<sup>9</sup> This body of work is centred on further investigation into the parameters affecting the preparation of catalysts by the physical mixing and thermal treatment of metal acetate precursors with a support, and the optimization of catalysts produced through this methodology for a variety of reactions. More specifically, the research has been directed at attempting to improve metal dispersion, with results demonstrating that through carefully controlling the metal loading and Au:Pd ratio the catalytic activities for the oxidation of select alcohols can be varied considerably, and significantly enhanced TOFs (turn over frequency) can be achieved.

## 3.2 Results and Discussion

All Au and Pd monometallic and bimetallic catalysts discussed herein were prepared supported on titania as previous work conducted within the Hutchings group has demonstrated that titania is an extremely efficacious support for both oxidation and reduction reactions.<sup>10,11</sup> Titania supported 2.5 wt% Au- 2.5 wt% Pd catalysts prepared by the impregnation route and by the deposition-precipitation method are well known as being effective catalysts for the oxidation of benzyl alcohol, however it has previously been shown that equivalent catalysts prepared by the physical grinding methodology are more active still for benzyl alcohol oxidation and other redox processes.<sup>21</sup>

### 3.2.1 Effect of Au:Pd ratio

With regard to Au:Pd bimetallic catalysts prepared by the impregnation method, a study has shown that the highest initial activity for benzyl alcohol oxidation was achieved with an Au:Pd metal ratio of 1:1 by weight (~1:1.85 molar ratio).<sup>22</sup> The same metal ratio was reported to have afforded the highest initial activity for the direct synthesis of hydrogen peroxide also.<sup>23</sup> However, when analogous catalysts were prepared by the sol-immobilisation methodology and tested for glycerol oxidation, the optimal Au:Pd weight ratio was found to be ~1:1.6 (1:3 molar ratio).<sup>24</sup> These reports clearly indicate that the optimum Au:Pd metal ratio differs according to both catalyst preparation method, and choice of substrate.

In order to further investigate the relationship between catalytic activity and AuPd metal ratio, a series of titania supported bimetallic catalysts with a total AuPd metal loading of 5 wt% were prepared with varying Au:Pd ratios, and tested for benzyl alcohol oxidation. The results of these experiments are presented in Fig. 1 and Fig. 2, with Fig. 1 showing how benzyl alcohol conversion varies as a function of time with

varying Au:Pd ratios; and Fig. 2 showing the corresponding selectivities to the products benzaldehyde and toluene.

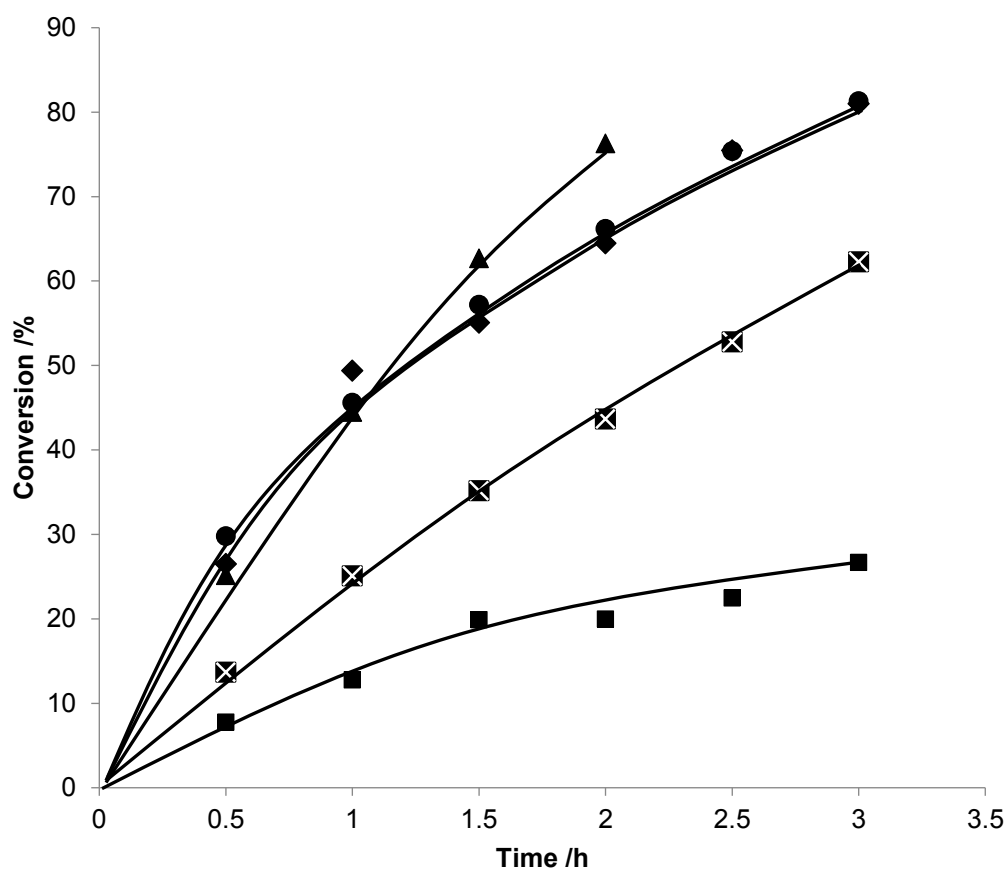


**Figure 1: Benzyl alcohol conversion over 5wt% AuPd/TiO<sub>2</sub> catalysts prepared by the physical grinding methodology with varying gold:palladium (weight) ratios. ◆ 5%Pd, ● 4%Pd-1%Au, ▲ 2.5%Pd-2.5%Au, ⊠ 1%Pd-4%Au, ■ 5%Au.**

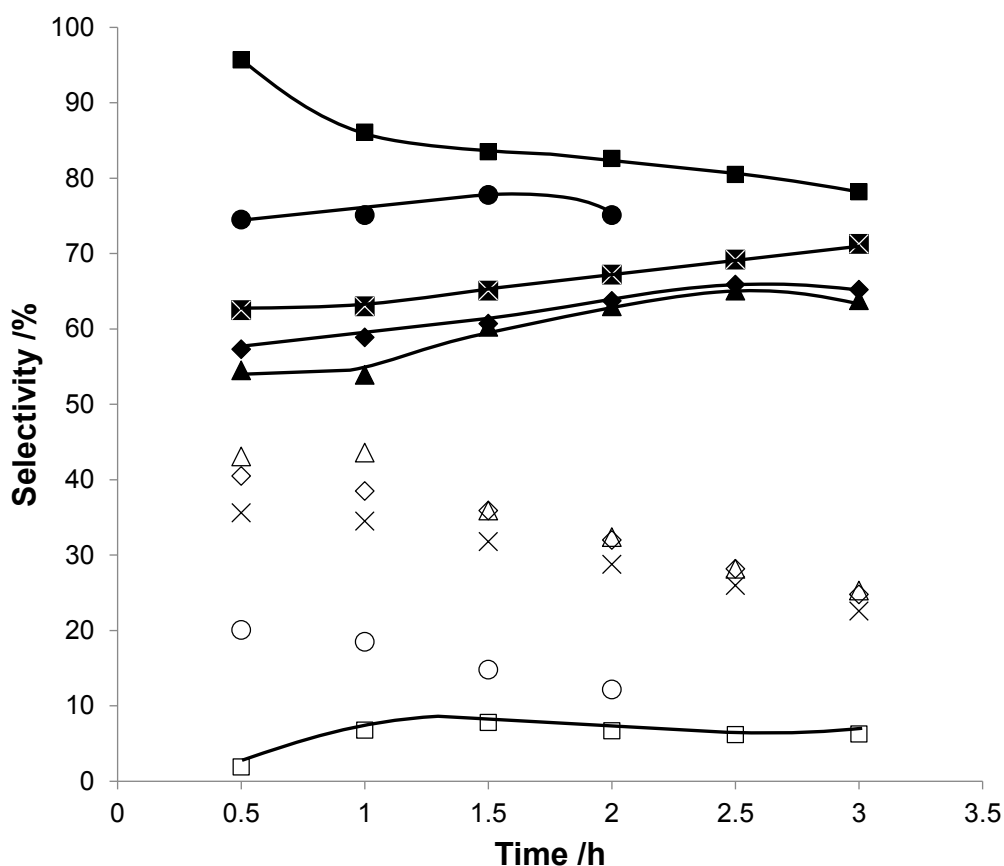


**Figure 2: The selectivity towards benzaldehyde and toluene during the oxidation of benzyl alcohol by 5wt% AuPd/TiO<sub>2</sub> catalysts prepared by the physical grinding methodology with various gold:palladium (weight) ratios. ▲ 5%Pd, ◆ 4%Pd-1%Au, ● 2.5%Pd-2.5%Au, ◻ 1%Pd-4%Au, ■ 5%Au. Filled symbols = benzaldehyde, open symbols = toluene.**

From figure 1 above it can be seen that the monometallic 5 wt% Pd/TiO<sub>2</sub> catalyst and the 1 wt% Au – 4 wt% Pd/TiO<sub>2</sub> catalysts exhibited very similar activities for benzyl alcohol conversion. The catalyst achieving the highest rate of substrate conversion was the 1:1 ratio, 2.5 wt% Au-2.5 wt% Pd/TiO<sub>2</sub> catalyst. An equivalent catalyst prepared by the impregnation method has displayed highest benzyl alcohol conversion at this Au:Pd ratio.<sup>22</sup> Substantially lower levels of conversion were observed with the 4 wt% Au-1 wt% Pd/TiO<sub>2</sub> catalyst; with the monometallic 5

wt%Au/TiO<sub>2</sub> catalyst performing worst, displaying yet significantly lower rates of benzyl alcohol conversion.

It is worth noting however, that with regard to the 4 wt% Au-1 wt% Pd/TiO<sub>2</sub> catalyst synergism effects are clearly evident, with the time-on-line data showing that after 3 hours, the catalyst had converted almost twice the amount of benzyl alcohol substrate, than the 5 wt% Au catalyst achieved in the same time.

It is important to note that as the aforementioned catalysts were all prepared by the physical grinding method to have a total metal loading of 5 wt% with varying Au:Pd metal ratios, the catalysts comprising of a higher gold content would necessarily have the least number of moles of metal due to gold having an atomic mass almost twice that of palladium. Consequently, it is imperative that the initial activities of each catalyst be quantitatively standardised, the simplest means of standardising catalytic activity being by turn over frequency (TOF). The TOFs (mol substrate converted per mol of metal per hour) calculated at 0.5 h for each of the 5 catalysts tested for benzyl alcohol oxidation are presented in table 1.

**Table 1. Variation of TOF's with differing gold:palladium (weight) ratios for 5 wt% (metal) catalysts prepared by the physical grinding methodology for the conversion of benzyl alcohol.**

Au:Pd ratio (wt)	TOF (calculated at 0.5h) (h <sup>-1</sup> )
0:1	34164
1:4	30892
1:1	42156
4:1	27958
1:0	18752

The table clearly shows that when AuPd catalysts were prepared by the physical grinding method a synergistic effect between the 2 metals can be observed. As has previously been reported, monometallic Pd catalysts display significantly higher levels

of activity (TOF at 0.5 h = 34164 h<sup>-1</sup>) than a corresponding monometallic Au counterpart (TOF at 0.5 h = 18752 h<sup>-1</sup>), regardless of whether the catalyst has been prepared by the physical grinding technique, or by other common catalyst preparation methods, namely the impregnation, and deposition-precipitation methodologies.<sup>21</sup>

The increased activity observed with the monometallic Pd catalysts can however be partially attributed to the disproportionation of benzyl alcohol to the products benzaldehyde and toluene, with low selectivity to the former, and significant selectivity to the latter.<sup>25</sup>

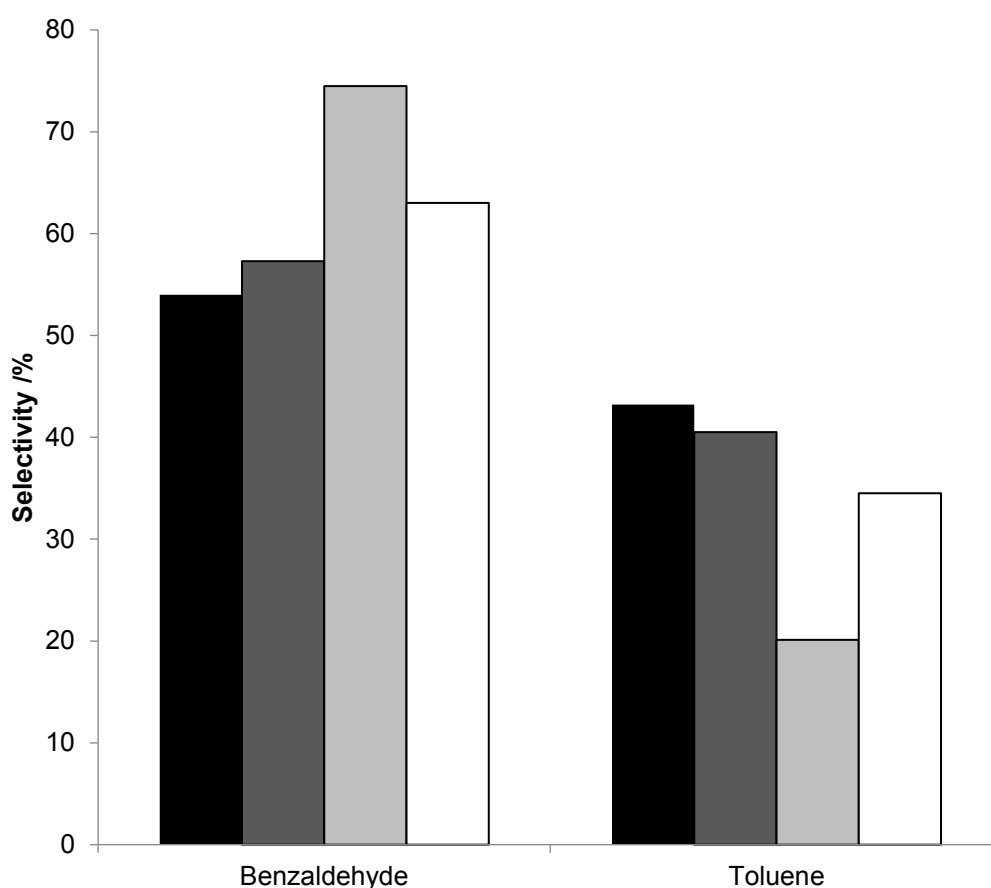
The 1.0 wt% Au-4.0 wt% Pd catalyst exhibited a TOF at 0.5 h of 30892 h<sup>-1</sup>, a TOF only marginally lower than that achieved over the monometallic Pd catalyst. By comparing this observed TOF with the relatively high selectivity towards toluene, it follows that the predominant active metal species in this catalyst is monometallic Pd, however the small concentration of Au present is acting by modulating activity. This deduction is based on the understanding that alloying between Au and Pd is known to elicit a synergistic effect on catalytic activity, whilst acting concomitantly to limit disproportionation of benzyl alcohol – both effects of which were observed to some degree in this instance.

The 2.5wt%Au-2.5wt%Pd catalyst displayed the highest activity, with a TOF at 0.5h of 42156 h<sup>-1</sup>, and was also observed to display the lowest selectivity towards toluene of all the catalysts containing Pd. This display of synergism is a characteristic effect attributed to the alloying of Au and Pd, the formation of these alloys having previously been confirmed by STEM analysis of a 2.5wt%Au-2.5wt%Pd catalyst also prepared by the physical grinding methodology.<sup>21</sup>

The 4.0wt%Au-1.0wt%Pd catalyst displayed lower activity than the 2.5wt%Au-2.5wt%Pd catalyst, however this activity was also associated with a notable increase in the selectivity towards toluene, suggesting that the observed lack of synergism is

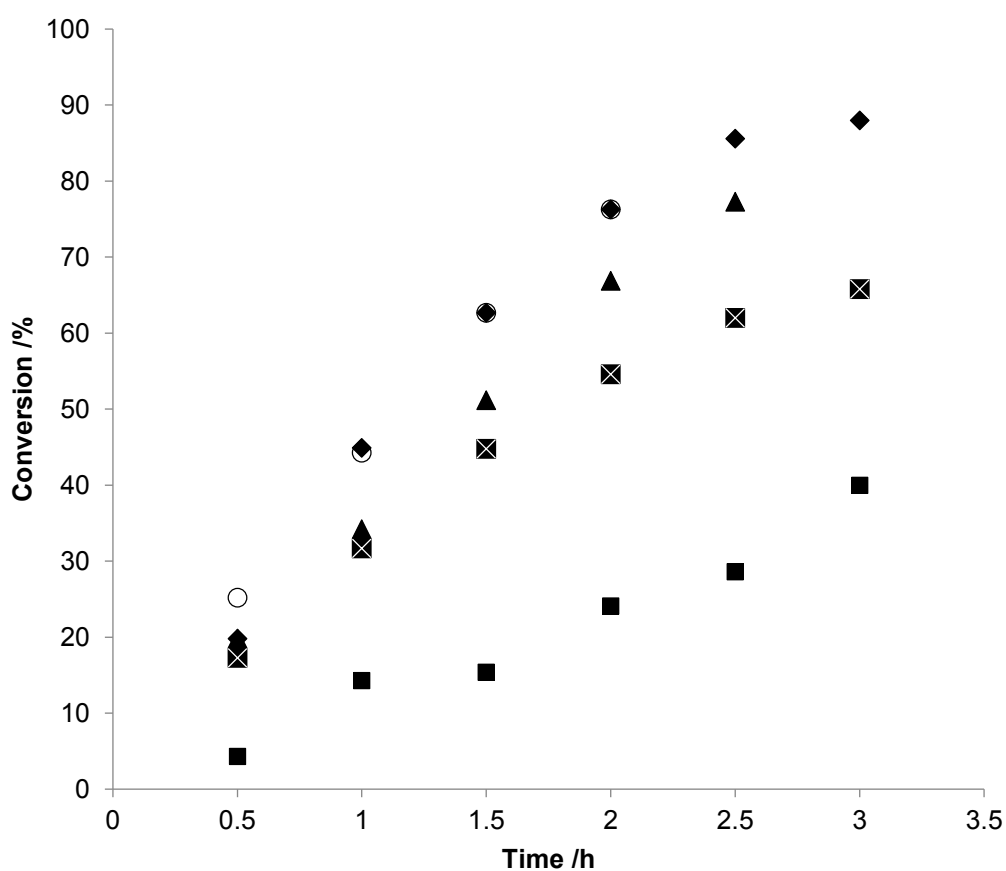
a consequence of limited Au-Pd alloy formation with the Pd existing in a monometallic state, implying that widespread AuPd alloying only occurs when the metals are present in a certain range of ratios.

Figure 3 shows the selectivity's towards toluene and benzaldehyde at 30% isoconversion in order to present a fair comparison of catalytic activity. The monometallic 5wt% Au/TiO<sub>2</sub> is not included as a maximum activity of 27% was achieved with this catalyst, however the remaining data clearly illustrates the extent of synergism occurring for the 2.5 wt%Au-2.5wt%Pd catalyst.



**Figure 3: The selectivity at iso-conversion (30%) towards benzaldehyde and toluene over TiO<sub>2</sub> supported catalysts with varying Au:Pd ratios. Black 5wt%Pd, dark grey 4wt%Pd-1wt%Au, light grey 2.5wt%Au-2.5wt%Pd, white 1wt%Pd-4wt%Au. NB. The 5wt%Au catalyst is not included as it did not reach 30% conversion.**

The Hutchings group have previously extensively characterised the 2.5wt%Au-2.5wt%Pd/TiO<sub>2</sub> catalyst showing that the metal present predominantly exists as large (> 50 nm) particles, with very small bimetallic particles also present.<sup>21</sup> With the intention of trying to improve the metal distribution a series of catalysts in the optimal 1:1 Au:Pd ratio were prepared with total metal loadings varying between 1 and 10 wt%. Figure 4 shows how these catalysts comparatively perform for the oxidation of benzyl alcohol.



**Figure 4: Benzyl alcohol conversion over AuPd/TiO<sub>2</sub> catalysts (1:1 weight Au:Pd) prepared by the physical grinding methodology with varying metal loadings. ♦ 10wt%, ○ 5wt%, ▲ 3wt%, ⊠ 2.5wt%, ■ 1wt%.**

The 5 wt% and 10wt% catalysts clearly afforded the highest levels of benzyl alcohol conversion, with their time-on-line profiles appearing almost identical. This data

indicates that by raising the metal loading from 5wt% to 10wt% no additional increase in catalytic activity is obtained. In order to further investigate the relationship between total metal loading and catalytic activity for the 1:1 Au:Pd catalysts, reaction TOFs at 0.5h were calculated, and are presented in table 2.

**Table 2: The TOF's during the conversion of benzyl alcohol by catalysts prepared by the physical grinding methodology with varying total metal loading and 1:1 Au:Pd (weight) ratio.**

Metal loading (Au:Pd) 1:1 wt ratio	TOF (calculated at 0.5h) (h <sup>-1</sup> )
10	18395
5	42156
3	55031
2.5	57861
1	36087

The data in table 2 appears to corroborate the interpretation of the time-on-line data for the 5wt% and 10wt% catalysts, as significant differences between TOFs calculated at 0.5h are clearly evident with a TOF of 18395 h<sup>-1</sup> for the 10wt% catalyst and a TOF of 42156 h<sup>-1</sup> for the 5wt% catalyst. Table 2 also shows a trend whereby catalyst TOF is observed to increase with decreasing metal loading up until the 2.5wt% catalyst. This demonstrates that even with the 5wt% catalyst a significant proportion of the metal present is not effective for the conversion of benzyl alcohol. The TOF drops substantially for the 1wt% catalyst which may indicate that at such low loadings the metals present are not available in concentrations large enough for alloying to occur.

**Table 3. XPS determined gold and palladium concentrations for catalysts prepared by the physical grinding methodology.**

Catalyst	Pd [conc At%]	Au [conc At%]	Pd:Au ratio
5%Au:5%Pd /TiO <sub>2</sub>	2.94	0.28	10
2.5%Au:2.5%Pd /TiO <sub>2</sub>	1.93	0.21	8.7
1.5%Au:1.5%Pd /TiO <sub>2</sub>	1.34	0.11	11.7
1.25%Au:1.25%Pd /TiO <sub>2</sub>	0.93	0.11	8
0.5%Au:0.5%Pd /TiO <sub>2</sub>	0.29	n/a	n/a

### 3.2.2 X-Ray Photoelectron Spectroscopy (XPS)

AuPd bimetallic catalysts with total (weight %) metal loadings between 1-10 % were subjected to XPS analysis in order to determine surface metal concentrations, the results from which are presented in table 3. For all five catalysts it is clearly apparent that the atomic surface concentrations of gold are significantly lower than the concentrations found within the bulk of the catalyst. The atomic surface concentration of palladium is considerably higher by comparison. This would appear to suggest that whilst gold and palladium acetate precursors were physically ground concomitantly with the TiO<sub>2</sub> support during preparation, the resulting catalyst does not exhibit a morphology in which the two metals are equally distributed, with palladium being dispersed far more effectively than gold. This is an effect that has previously been observed and reported by the Hutchings group. Of interest is, that with regard to the 1 wt% AuPd/TiO<sub>2</sub> catalyst, there was no detection of a signal that could be associated with gold. This would explain the observed drop in TOF as no gold dispersion would ultimately result in the absence of gold:palladium alloy formation.

For the catalysts that did exhibit dispersion of both palladium and gold, there was no identifiable trend as to how the calculated gold:palladium ratios varied with respect to total catalyst metal loading, with ratios between 8.0 and 11.7 having been determined. The presence of a high palladium:gold ratio can be suggestive of formation of bimetallic nano crystal core-shell morphologies, however the gold:palladium ratios calculated here are significantly higher than the discerned ratios of AuPd bimetallic catalysts prepared by either the impregnation or deposition-precipitation morphologies, indicating that these high ratios are a result of improved metal dispersion rather than core-shell formation. This effect was reported in previously published work where imaged from STEM-HAADF analysis failed to provide evidence for the existence of core-shell structures.<sup>21</sup>

**Table 4.**

Catalyst	Metal Phase	Unit Cell volume /Å <sup>3</sup>	Crystallite size /nm	Weight fraction (%)	R value
5%Au:5%Pd /TiO <sub>2</sub>	Au	67.70	51	3.2	2.5 (1.8)
	Pd	59.03	10	5.3	
2.5%Au:2.5%Pd /TiO <sub>2</sub>	Au	67.79	56	1.5	2.7 (1.9)
	Pd	59.08	12	1.6	
1.5%Au:1.5%Pd /TiO <sub>2</sub>	Au	67.85	98	0.7	2.9 (2.0)
	Pd	58.88	11	0.4	
1.25%Au:1.25%Pd /TiO <sub>2</sub>	Au	67.86	144	0.4	2.7 (2.0)
	Pd	58.82	14	0.6	
0.5%Au:0.5%Pd /TiO <sub>2</sub>	Au	67.94	165	0.1	2.9 (2.0)
	Pd	n/a	n/a	n/a	

α Errors: Unit cell volume = ±0.1 Å<sup>3</sup>; Crystallite size = ± 2nm; Weight fraction = 10%

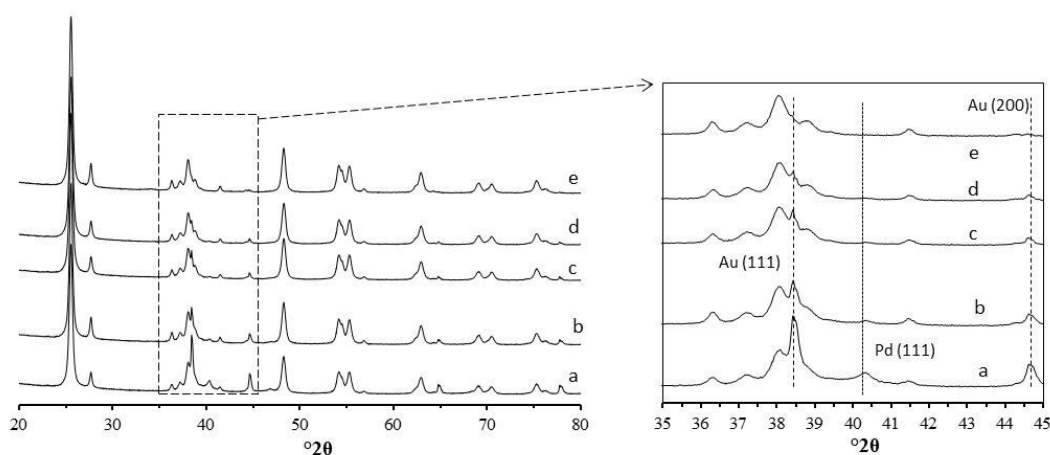


**Figure 5. X-ray diffraction patterns of Au-Pd/TiO<sub>2</sub> bimetallic catalysts prepared by the physical grinding method, in a Au:Pd 1:1 ratio with total metal loadings varying between 1-10 wt%. (a) 10 wt% Au-Pd TiO<sub>2</sub>, (b) 5 wt% Au-Pd TiO<sub>2</sub>, (c) 3 wt% Au-Pd TiO<sub>2</sub>, (d) 2.5 wt% Au-Pd TiO<sub>2</sub>, (e) 1 wt% Au-Pd TiO<sub>2</sub>**

### 3.2.3 X-Ray Diffraction (XRD)

X-ray diffraction patterns (XRD) and refinements are presented in figure 5 and table 4. All of the 1:1 Au:Pd catalysts prepared with various total metal loadings were found to exhibit a cubic phase with a unit cell size matching that of gold. All catalysts, with the exception of the 1wt% catalyst, were also observed to contain cubic palladium. From table 4 a trend can be seen whereby the gold unit cell volume decreases with increasing total metal loading, decreasing by  $0.24 \text{ \AA}^3$  over the loading range. In contrast, the palladium unit cell size was observed to increase by  $0.21 \text{ \AA}^3$  over the weight loading range. These changes in unit cell size may indicate a degree of limited alloying that increases with total metal weight loading. Across the loading range there was however, no observed unit cell sizes corresponding to bulk 1:1 Au:Pd, suggesting that the predominant system is where one element is incorporated into another. For the gold-rich phases a decrease in average crystallite size from 165 nm in the 1wt% catalyst to 51 nm in the 10wt% catalyst was observed, possibly indicative of a greater level of gold dispersion with increased total metal loading.

Conversely, no similar trend of changing crystallite size with varying metal loading can be seen for the palladium-rich phases, with a crystallite size of ~12 nm consistent across the loading range. These observations are consistent with those seen by XPS whereby gold is seen to disperse poorly, and relatively high concentrations of gold are required if significant dispersion is to be achieved. Palladium on the other hand appears to disperse far more effectively, with palladium concentration having less of an effect on the degree of dispersion obtained. It is clear that further increasing the palladium loading has a negligible effect on its relative dispersion, meaning that low palladium loadings can serve to limit wasting of this precious metal, however small quantities of gold appear to be a required in order to facilitate effective dispersion. As a result, the best compromise appears to be catalysts with metal loadings of 1.25wt%Au-1.25wt%Pd/TiO<sub>2</sub>, as gold is present in a concentration sufficient to enable alloy formation and dispersion, and the palladium component is low enough to prevent metal wastage.

### 3.2.4 Glycerol Oxidation

The Hutchings group have previously reported gold palladium catalysts as being efficacious for the oxidation of glycerol, therefore catalysts prepared by the physical mixing methodology were tested alongside analogous catalysts prepared by the impregnation technique. The results of these experiments are displayed in figure 6. In these experiments the amount of catalyst was varied in order to ensure a fixed substrate:metal ratio of 500. Because of this fixed substrate:metal ratio, the TOFs calculated for glycerol oxidation are directly proportional to glycerol concentration.

Figure 6 clearly shows that the catalysts prepared by physical mixing display considerably higher activity than their impregnation counterpart catalysts. Unlike for the benzyl alcohol reaction however, glycerol oxidation is not effected by catalyst metal loading irrespective of whether the catalyst is prepared by physical mixing or

by the impregnation method. The physically mixed catalysts were seen to display a lower selectivity towards  $C_3$  products, however this is probably due to over-oxidation of the desired products as the result of catalytic activity and the reaction conditions used.

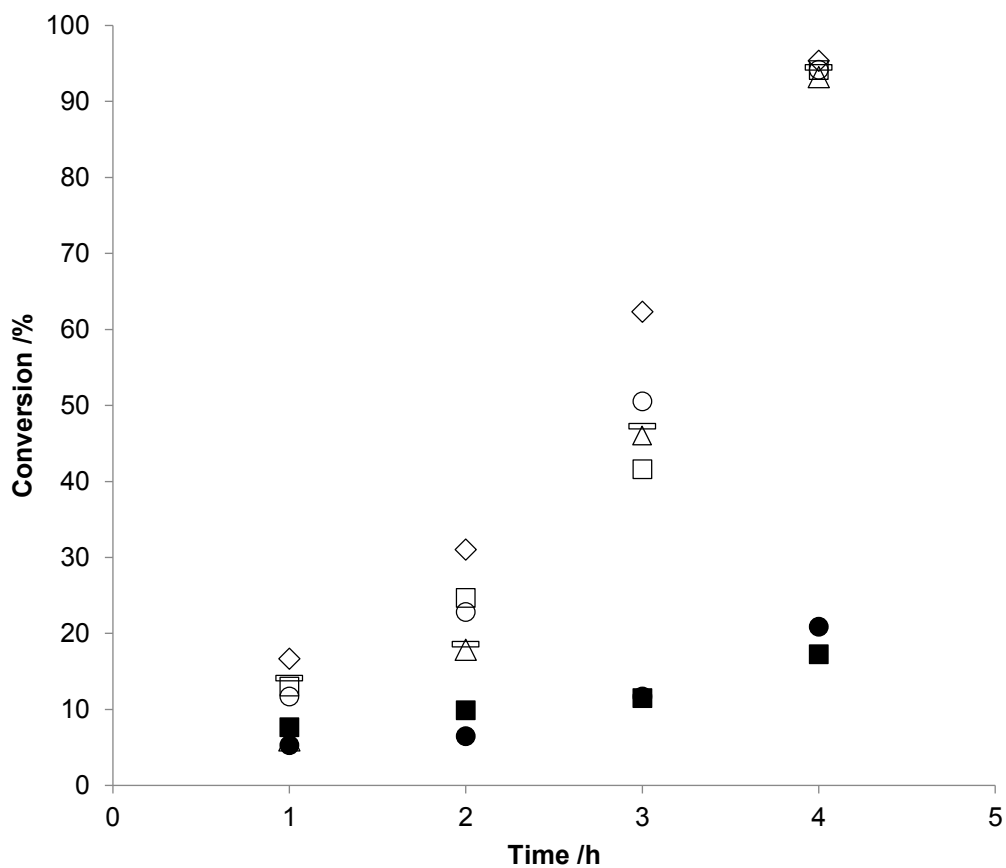


**Figure 6: The oxidation of glycerol by AuPd/TiO<sub>2</sub> catalysts prepared by the physical grinding technique(open symbols); and impregnation methodology (filled symbols) total metal loading: 10%  $\diamond$ , 5%  $\square$ , 3%  $\triangle$  2.5%  $\circ$ , 2%  $—$ .**

### 3.2.5 Hydrogen Peroxide Synthesis

For the direct synthesis of hydrogen peroxide, increased  $\text{H}_2\text{O}_2$  productivity and hydrogenation was observed with increased metal loading across the range of catalysts prepared by physical mixing with weight loadings varying between 1-10 wt% (figure 7). The 10wt% catalyst was an exception to this trend suggesting that further addition of metal does not increase catalytic activity for direct  $\text{H}_2\text{O}_2$  synthesis. In order to investigate this more effectively, the results were calculated with respect to mass of metal rather than as percentage of total catalyst mass (figure 8). The trend generated from this is in agreement with the TOFS calculated for the catalytic oxidation of benzyl alcohol, with 2.5wt% being the optimum metal loading. The data from the catalyst testing indicates increased dispersion of metal, relative to the total metal loading, with decreasing total metal loading. However, for both direct synthesis of  $\text{H}_2\text{O}_2$  and benzyl alcohol oxidation the activity was observed to decrease substantially with the 1wt% catalyst, which suggests that catalyst properties vary with changing total metal loadings. With regard to the 10wt% metal catalyst, the decrease in hydrogenation activity and low activity observed is suggestive of no activity being afforded by the additional metal.

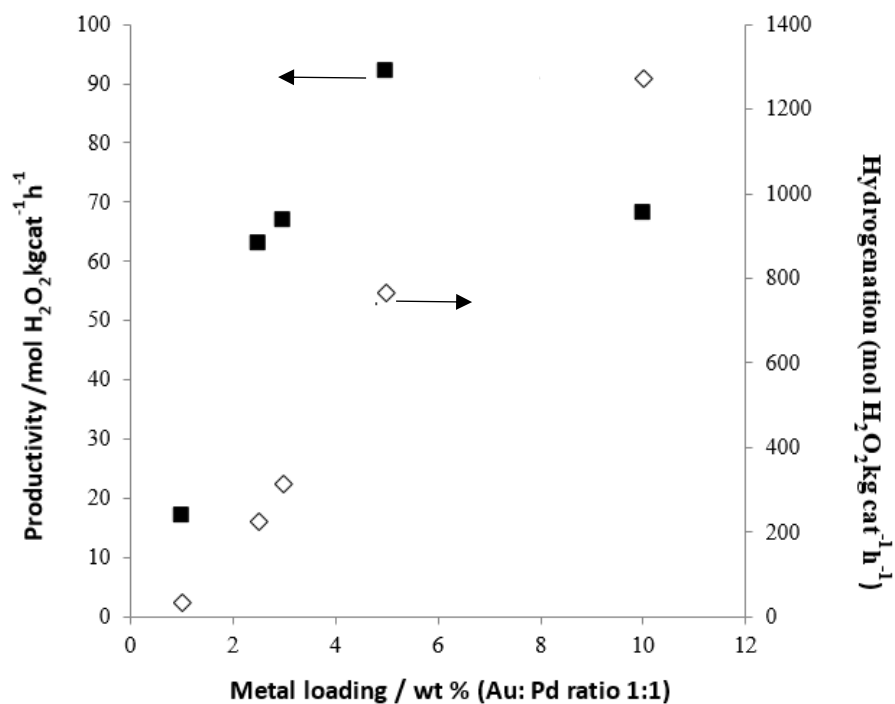


Figure 7: H<sub>2</sub>O<sub>2</sub> hydrogenation and activity data for the 1:1 Au:Pd catalysts with varying total metal loadings expressed as mass of catalyst. ■ Productivity, ◇ hydrogenation.

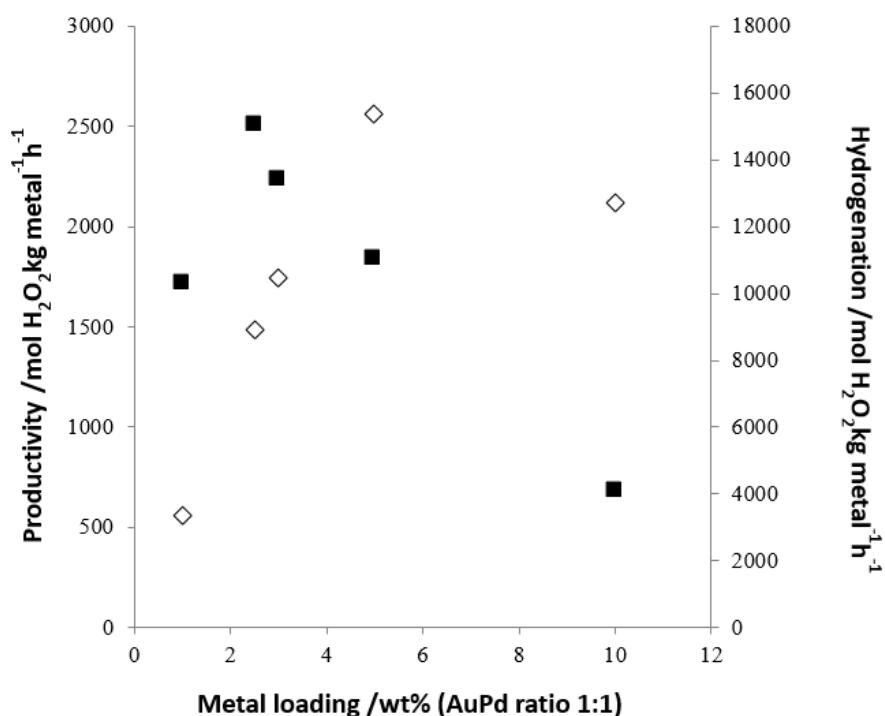


Figure 8: H<sub>2</sub>O<sub>2</sub> hydrogenation and activity data for the 1:1 Au:Pd catalysts with varying total metal loadings expressed as mass of metal. ■ Productivity, ◇ hydrogenation.

### 3.2.6 Oxidation of other alcohols

A series of reactions were performed in order to explore how applicable catalysts prepared by the physical mixing method are to other select oxidation reactions. Previous data demonstrates that the optimal catalyst metal loading for the 1:1 Au:Pd catalyst is 1.25wt%Au-1.25wt%Pd, and therefore this catalyst was chosen for the oxidation of a range of substrates, the resulting TOFs from which are presented in table 5 below.

**Table 5. TOF's for the application of TiO<sub>2</sub> supported Au: Pd (weight) catalysts prepared by the physical grinding methodology for the conversion of select alcohol substrates.**

Alcohol Substrate	TOF (calculated at 0.5h) (h <sup>-1</sup> )
Benzyl Alcohol	25079
Benzyl Alcohol <sup>†</sup>	93875
1-Phenylethanol	26448
1,4-butanediol	52833
Cinnamyl Alcohol <sup>‡</sup>	1149

Reaction conditions: 40 mL substrate; 14 mg 1.25%Au:1.25%Pd/TiO<sub>2</sub> catalyst; 160 °C; 10 bar O<sub>2</sub>

<sup>†</sup>7 mg 2.5%Au:2.5%Pd/TiO<sub>2</sub> catalyst; <sup>‡</sup>40 mL 0.2M aqueous solution, 90 °C.

The TOF data shows that the catalysts prepared by the physical mixing method display high initial activities for a range of substrates for oxidation reactions, with the TOFs calculated for cinnamyl alcohol (1149) and benzyl alcohol oxidation (93875) being higher than TOFS currently reported in the literature over catalysts prepared by either the impregnation, or the deposition-precipitation techniques. This shows that by careful tuning of the catalyst preparation method to produce optimised catalysts, the catalytic activity of gold-palladium catalysts for oxidation reactions can be significantly enhanced.

### 3.3 Conclusions

The physical grinding of metal acetates for the preparation of chloride-free catalysts can be used to produce catalysts that display significantly enhanced activity when compared to analogous catalysts prepared by alternative common preparation techniques. It has been shown that by lowering the total metal weight loading of the catalyst it is possible to achieve higher TOFs, which suggests that with catalysts comprised of higher metal weight loadings a substantial amount of the metal present is in the form of a spectator species separate from, and not contributing to, the activity of active metal particles. When the metal loadings are below a threshold level the gold-palladium synergistic effect is not observed, this is indicative of a lack of formation of the alloy particles to which the high catalytic activity is attributed. This simple catalyst preparation methodology has been successfully applied to a number of other selected oxidation reactions, with the resulting calculated TOFs being equal to, or better than, those achieved with catalysts prepared by other methods.

## 3.4 References

1. P. Landon, P. J. Collier, A. J. Papworth, C. J. Kiely and G. J. Hutchings, *Chem. Commun. (Cambridge, U. K.)*, 2002, 2058-2059.
2. M. Haruta, T. Kobayashi, H. Sano and N. Yamada, *Chem. Lett.*, 1987, 405-408.
3. M. Haruta, N. Yamada, T. Kobayashi and S. Iijima, *J. Catal.*, 1989, **115**, 301-309.
4. S. Biella, L. Prati and M. Rossi, *J. Catal.*, 2002, **206**, 242-247.
5. F. Porta and L. Prati, *J. Catal.*, 2004, **224**, 397-403.
6. A. K. Sinha, S. Seelan, S. Tsubota and M. Haruta, *Angew. Chem., Int. Ed.*, 2004, **43**, 1546-1548.
7. M. D. Hughes, Y.-J. Xu, P. Jenkins, P. McMorn, P. Landon, D. I. Enache, A. F. Carley, G. A. Attard, G. J. Hutchings, F. King, E. H. Stitt, P. Johnston, K. Griffin and C. J. Kiely, *Nature (London, U. K.)*, 2005, **437**, 1132-1135.
8. L. Kesavan, R. Tiruvalam, R. M. H. Ab, S. M. I. bin, D. I. Enache, R. L. Jenkins, N. Dimitratos, J. A. Lopez-Sanchez, S. H. Taylor, D. W. Knight, C. J. Kiely and G. J. Hutchings, *Science (Washington, DC, U. S.)*, 2011, **331**, 195-199.
9. P. J. Miedziak, Q. He, J. K. Edwards, S. H. Taylor, D. W. Knight, B. Tarbit, C. J. Kiely and G. J. Hutchings, *Catal. Today*, 2011, **163**, 47-54.
10. D. I. Enache, J. K. Edwards, P. Landon, B. Solsona-Espriu, A. F. Carley, A. A. Herzing, M. Watanabe, C. J. Kiely, D. W. Knight and G. J. Hutchings, *Science (Washington, DC, U. S.)*, 2006, **311**, 362-365.
11. J. K. Edwards, B. E. Solsona, P. Landon, A. F. Carley, A. Herzing, C. J. Kiely and G. J. Hutchings, *J. Catal.*, 2005, **236**, 69-79.
12. H. S. Oh, J. H. Yang, C. K. Costello, Y. M. Wang, S. R. Bare, H. H. Kung and M. C. Kung, *J. Catal.*, 2002, **210**, 375-386.
13. A. Schulz and M. Hargittai, *Chem.--Eur. J.*, 2001, **7**, 3657-3670.
14. I. Dobrosz-Gomez, I. Kocemba and J. M. Rynkowski, *Appl. Catal., B*, 2009, **88**, 83-97.
15. H. H. Kung, M. C. Kung and C. K. Costello, *J. Catal.*, 2003, **216**, 425-432.
17. L. Delannoy, H. N. El, A. Musi, N. N. L. To, J.-M. Krafft and C. Louis, *J. Phys. Chem. B*, 2006, **110**, 22471-22478.
18. F. Somodi, I. Borbath, M. Hegedus, A. Tompos, I. E. Sajo, A. Szegedi, S. Rojas, F. J. L. Garcia and J. L. Margitfalvi, *Appl. Catal., A*, 2008, **347**, 216-222.
19. W.-C. Li, M. Comotti and F. Schueth, *J. Catal.*, 2006, **237**, 190-196.

20. Y. Lin, K. A. Watson, M. J. Fallbach, S. Ghose, J. G. Smith, D. M. DeLozier, W. Cao, R. E. Crooks and J. W. Connell, *ACS Nano*, 2009, **3**, 871-884.
21. S. A. Kondrat, G. Shaw, S. J. Freakley, Q. He, J. Hampton, J. K. Edwards, P. J. Miedziak, T. E. Davies, A. F. Carley, S. H. Taylor, C. J. Kiely and G. J. Hutchings, *Chem. Sci.*, 2012, **3**, 2965-2971.
22. D. I. Enache, D. Barker, J. K. Edwards, S. H. Taylor, D. W. Knight, A. F. Carley and G. J. Hutchings, *Catalysis Today*, 2007, **122**, 407-411.
23. D. Enache, D. Knight and G. Hutchings, *Catal Lett*, 2005, **103**, 43-52.
24. G. L. Brett, P. J. Miedziak, N. Dimitratos, J. A. Lopez-Sanchez, N. F. Dummer, R. Tiruvalam, C. J. Kiely, D. W. Knight, S. H. Taylor, D. J. Morgan, A. F. Carley and G. J. Hutchings, *Catalysis Science and Technology*, 2012, **2**, 97-104.
25. S. Meenakshisundaram, E. Nowicka, P. J. Miedziak, G. L. Brett, R. L. Jenkins, N. Dimitratos, S. H. Taylor, D. W. Knight, D. Bethell and G. J. Hutchings, *Faraday Discuss.*, 2010, **145**, 341-3

# Chapter 4

## 4. An investigation of the effect of the addition of tin to 5wt% Pd/TiO<sub>2</sub> for the hydrogenation of furfuryl alcohol

### 4.1 Introduction

Furfural, obtained from hydrogenation and dehydrogenation of lignocellulosic xylan, is one of the most important platforms for the manufacture of renewable, value-added, bioderivatives. Of the possible furfural upgrade strategies, hydrogenation and hydrogenolysis are considered to be the most effective methods, and it is through hydrogenation of furfural that furfuryl alcohol (FA) is obtained, with FA being one of the most commercially important furfural-derived products.<sup>1</sup> Furfuryl alcohol can itself undergo subsequent conversion to a number of valorised fuel components, including 1,5-pentanediols,<sup>2</sup> tetrahydrofurfuryl alcohol,<sup>3</sup> and 2-methylfuran (2-MF).<sup>4</sup> Although these FA derivatives do have important potential applications as fuel additives, their synthesis in a green chemistry manner poses a number of challenges.<sup>5</sup>

2-MF can be produced from either furfural or furfuryl alcohol, with initial hydrogenation of furfural to FA required if the former is the substrate, followed by hydrogenolysis of FA. Aside from its potential as a fuel blender, 2-MF has also found use in the production of cysanthemate pesticides, in perfume intermediates, and medical applications in chloroquine lateral chains.<sup>6</sup> The first catalyst reported for the liquid phase conversion of FA was copper chromite in 1931, where a 70% yield of pentanediol was achieved at a reaction temperature of 100 °C under a hydrogen pressure of between 100-150 bar.<sup>2</sup> Chromium-based catalysts have also been used

for 2-MF synthesis,<sup>5a</sup> with Chapter 1 containing a more in-depth discussion of this. THFA production from FA has been demonstrated over nickel catalysts, although the relatively harsh reaction conditions of 180 °C for 3.5 h were required.<sup>5c,7</sup> Nickel, as well as copper, have also been reported as being active for the selective synthesis of 2-MF and furan from FA.<sup>4,6a</sup> Manganese oxide supported platinum, palladium, and ruthenium catalysts have demonstrated high activity for FA conversion in the aqueous phase, requiring hydrogen pressures of between 30 and 60 bar, operating at 120 °C for 4 h.<sup>5c</sup> Supported palladium, rhodium, and platinum catalysts, although active for FA hydrogenation, appear to display lower activity than nickel catalysts even at higher temperatures and pressures.<sup>7b,8</sup>

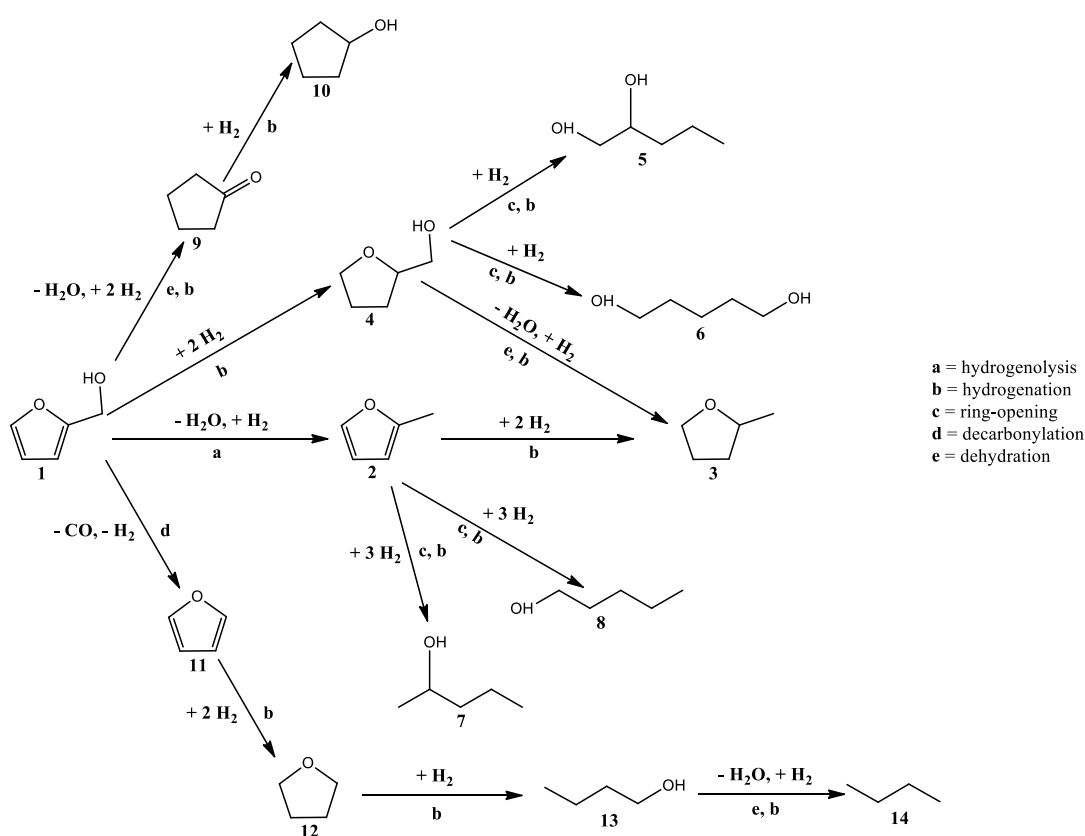
The examples discussed above demonstrate a reliance on relatively high temperatures and pressures to facilitate these selective transformations. As a result, a process that could selectively produce 2-MF from FA under green reaction conditions would be extremely desirable, albeit challenging due to by-product formation. The Hutchings group have recently demonstrated the efficacy of a 5wt% Pd/TiO<sub>2</sub> catalyst prepared by the impregnation method for the selective synthesis of 2-MF from FA at room temperature in 1,2-dichloroethane solvent.<sup>9</sup> The work presented herein begins with a comparison in catalytic activity of this 5wt% Pd/TiO<sub>2</sub> catalyst with an analogous commercially available 5wt% Pd/TiO<sub>2</sub> catalyst in order to provide a benchmark against which the in-house impregnation preparation method can be tested. The commercially available 5wt% Pd/TiO<sub>2</sub> catalyst and the 5wt% Pd/TiO<sub>2</sub> catalyst prepared by the impregnation technique were found to display marked differences in both catalytic activity and selectivity, with the origin of these differences appearing to be linked to the oxidation state of palladium in the two catalysts. Follow-on work focused on investigating the effect of addition of tin to the 5wt% Pd/TiO<sub>2</sub> catalyst for hydrogenation of FA. Catalytic activity was observed to be similar to that of the monometallic Pd catalyst, however more effective hydrogenation

of the furan ring was observed with the bimetallic SnPd catalyst. Furthermore, work has been conducted to explore the effect of reaction solvent, with methanol being found to be an acceptable and environmentally friendly alternative to 1,2-dichloroethane.<sup>17</sup> The reaction was observed to be less selective to 2-MF, with quantitative production of THFA achieved over a bimetallic 5wt% SnPd/TiO<sub>2</sub> catalyst in a Sn:Pd ratio of 1:1. THFA has predominantly found application as a cheap biodegradable solvent with industrial uses, especially within the agricultural industry. THFA synthesis can be achieved through furfural hydrogenation over nickel, and copper chromite catalysts,<sup>2,3</sup> however this is environmentally unfavourable due to the inherent toxicity associated with the production and post-reaction recycling of the copper chromite catalyst.<sup>5b</sup> There is also the potential for the formation of large quantities of furfural condensates which further renders this process unfavourable. Nickel, palladium, ruthenium, and rhodium catalysts, are all frequently used for THFA production from FA, although long reaction times and operating temperatures of 50 °C are required.<sup>3,5c,8</sup> 2-Methyltetrahydrofuran (MTHF), a molecule also reported to have excellent application as a fuel additive, has also been synthesised alongside THFA through variation of hydrogen pressure (1-3 bar) over a SnPd catalyst. The alloying of tin with known hydrogenation metals such as ruthenium,<sup>11</sup> platinum,<sup>12</sup> iron,<sup>13</sup> nickel,<sup>14</sup> rhodium,<sup>15</sup> and palladium,<sup>16</sup> is well established as an efficacious catalyst for the hydrogenation of organic molecules, there are however, no other reports of bimetallic SnPd catalysts for the hydrogenation of furan compounds. This body of work has been conducted in an effort to develop and contribute a green chemistry process utilising a novel catalyst composition for the selective conversion of furfuryl alcohol to valorised organic derivatives.

## 4.2 Results and Discussion

As discussed, the Hutchings group have demonstrated the selective conversion of FA to 2-MF over TiO<sub>2</sub> supported Pd catalysts prepared by the standard

wet impregnation method.<sup>1</sup> In order to build on these results, and to further our understanding of the efficacy of Pd/TiO<sub>2</sub> for the selective hydrogenolysis of FA to valorised fuel additives, a commercially available 5wt% Pd/TiO<sub>2</sub> (designated, Std-Pd/TiO<sub>2</sub>) was tested to provide a standardised level of activity by which the performance of an in-house synthesised 5wt% Pd/TiO<sub>2</sub> (designated, Imp-Pd/TiO<sub>2</sub>) prepared by the impregnation methodology could be compared. These catalysts were investigated for FA hydrogenolysis (**1**, Scheme 1) in 1,2-dichloroethane solvent, under 3 bar H<sub>2</sub> at 25 °C.



**Scheme 1. Reaction pathways for the hydrogenation of Furfuryl alcohol. 1). Furfuryl alcohol; 2). 2-methylfuran; 3). 2-methyltetrahydrofuran; 4). Tetrahydrofurfuryl alcohol; 5). 1,2-pentanediol; 6). 1,5-pentanediol; 7). 2-pentanol; 8). 1-pentanol; 9). Cyclopentanone; 10). Cyclopentanol; 11). Furan; 12). Tetrahydrofuran; 13). Butanol; 14). Butane**

Hydrogenation of the aromatic furan ring without hydrogenolysis would yield tetrahydrofurfuryl alcohol (THFA) (**4**); FA hydrogenolysis would give 2-methylfuran (2-MF) (**2**); which could either ring-open to form 2-pentanol (**7**); or undergo further hydrogenation of the furan ring to form methyltetrahydrofuran (MTHF) (**3**). There are a number of possible products that can be derived from furfuryl alcohol hydrogenation, and the initial focus remained on maximising the yield of the fuel component 2-MF.

#### **4.2.1 The Effect of Reaction Time on the Catalytic Hydrogenolysis of FA**

An initial set of experiments were conducted to investigate how the conversion of FA and the corresponding product yield distribution varied with respect to reaction time. The results of these experiments are displayed graphically in Figure 1 and Figure 2.

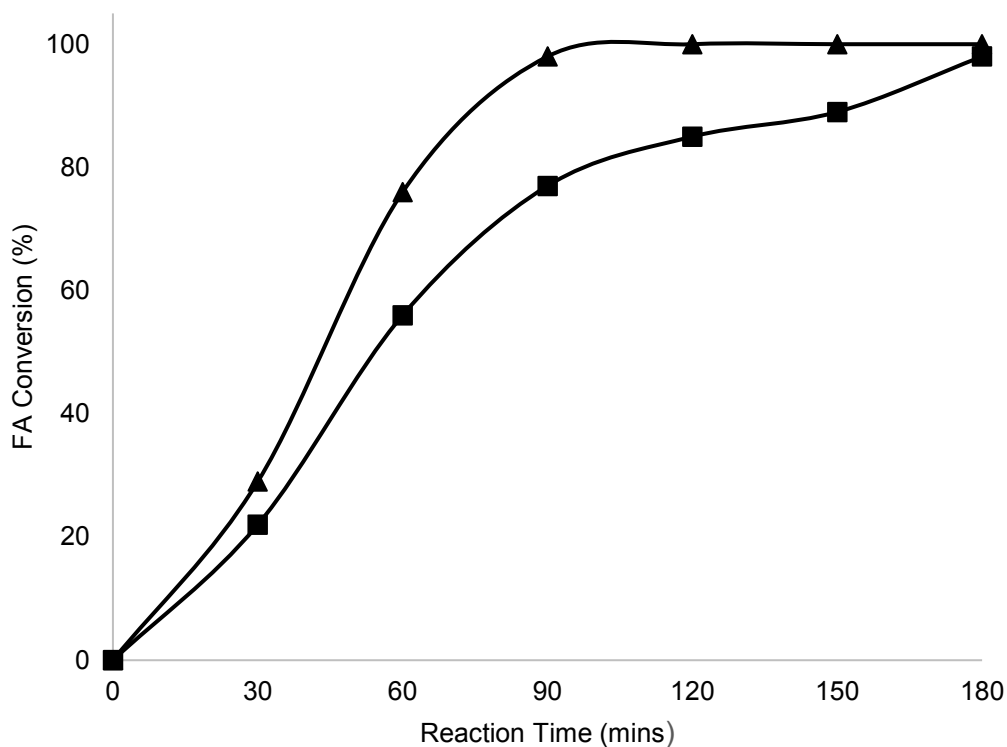


**Figure 1. Time online reaction comparing the activity of Imp-Pd/TiO<sub>2</sub> against Std-Pd/TiO<sub>2</sub> for the conversion of FA., ▲ Imp-Pd/TiO<sub>2</sub>, ■ Std-Pd/TiO<sub>2</sub>**

Figure 1 clearly shows that both Imp-Pd/TiO<sub>2</sub> and Std-Pd/TiO<sub>2</sub> are active for the conversion of FA. Despite both catalysts achieving complete, or almost complete, conversion of FA within 180 mins, Imp-Pd/TiO<sub>2</sub> demonstrated a higher initial rate of activity, reaching 100% conversion at around 90 mins.

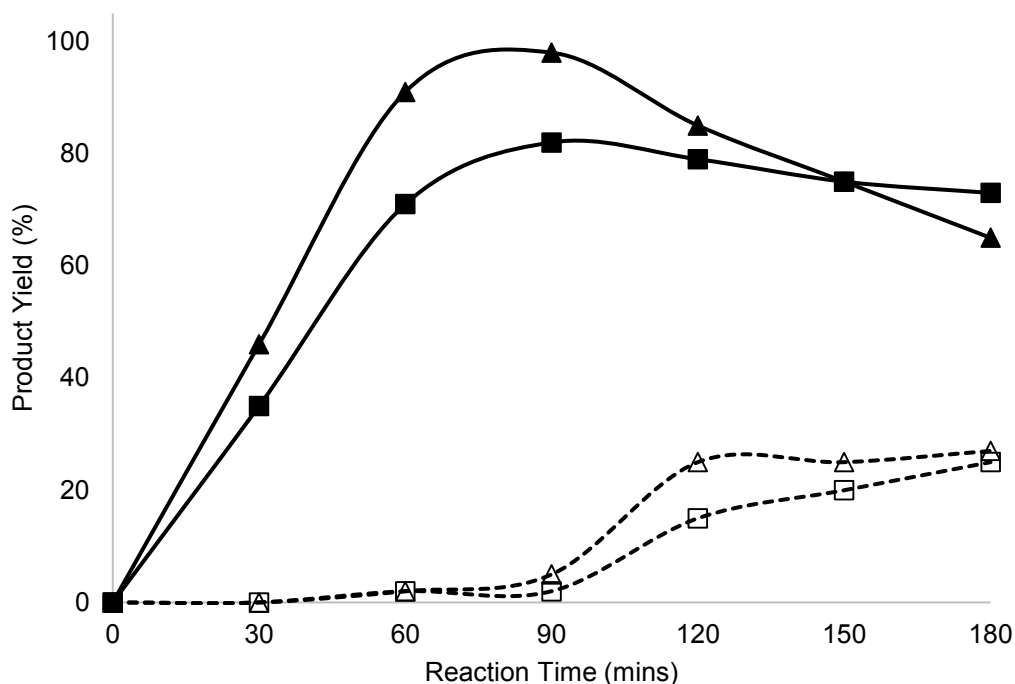


**Figure 2** Time online reaction comparing the activity of Imp-Pd/TiO<sub>2</sub> against Std-Pd/TiO<sub>2</sub> for the production of 2-MF and 2-pentanol. ▲ Imp-Pd/TiO<sub>2</sub> ■ Std-Pd/TiO<sub>2</sub> (solid symbols = 2-MF; Open symbols = 2-pentanol)

Both catalysts display high activity for the production of 2-MF, formed through hydrogenolysis of FA. Imp-Pd/TiO<sub>2</sub> achieved a 2-MF yield of 98% in 90 mins, with the less-active Std-Pd/TiO<sub>2</sub> producing a maximum yield of 82% in the same time. Subsequent hydrogenation of the aromatic ring in 2-MF to produce 2-MTHF was not observed, instead, between 90-180 mins, the yield of 2-MF was seen to decrease in tandem with a corresponding increase in the production of 2-pentanol. This is most likely caused by hydrogenative ring-opening of 2-MF to produce 2-pentanol. Another possible ring-opening product, 1-pentanol, was not detected.

## 4.2.2 X-Ray Diffraction (XRD)

Inspection of the powder X-ray diffraction (XRD) patterns of Imp-Pd/TiO<sub>2</sub> and Std-Pd/TiO<sub>2</sub> presented in figure 3 reveal distinct morphological differences between the two catalysts. Imp-Pd/TiO<sub>2</sub> has a catalyst support composed of both anatase and rutile TiO<sub>2</sub> polymorphs in a 4:1 ratio respectively (ICDD 01-070-7347). This is to be expected considering the catalyst has been synthesised using a commercial source of TiO<sub>2</sub>, Degussa P-25, a powder comprised of crystallites of rutile and anatase TiO<sub>2</sub>. The Std-Pd/TiO<sub>2</sub> catalyst, in comparison, has a support solely composed of anatase TiO<sub>2</sub> (ICDD 01-070-7348).

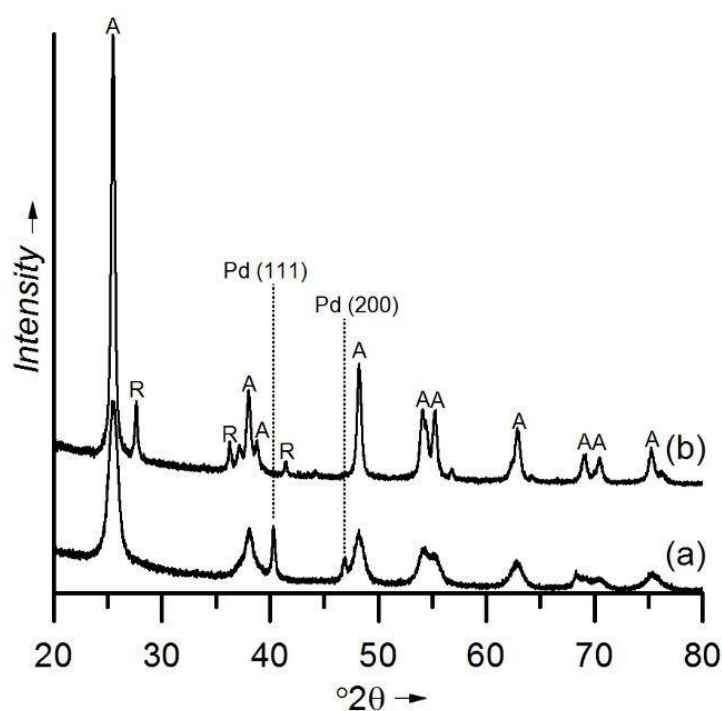


**Figure 3.** XRD patterns of Std-5%Pd/TiO<sub>2</sub> (a) and IM-Pd/TiO<sub>2</sub> (b). (A) denotes the anatase phase, (R) denotes the rutile phase, with (Pd) highlighting the associated cubic metallic reflections.

Another significant notable difference is that within the XRD pattern of Imp-Pd/TiO<sub>2</sub> there are no identifiable reflections corresponding to any Pd phase. This is in direct contrast to the Std-Pd/TiO<sub>2</sub> catalyst, where cubic metallic reflections associated with the Pd unit cell are clearly apparent.

**Table 1. MP-AES data of actual Pd metal loadings of Imp-Pd/TiO<sub>2</sub> and Std-Pd/TiO<sub>2</sub> catalysts compared with theoretical Pd weight loadings.**

Catalyst	Theoretical Loading Pd (wt%)	Actual Loading Pd (wt%)
Imp-Pd/TiO <sub>2</sub>	5.0	4.7
Std-Pd/TiO <sub>2</sub>	5.0	4.8

Both catalysts were subjected to microwave plasma atomic emission spectroscopy (MP-AES) analysis to confirm actual Pd weight percentages, the results of which show that the Pd loadings of Imp-Pd/TiO<sub>2</sub> and Std-Pd/TiO<sub>2</sub> catalysts are comparable, with loadings of 4.7 and 4.8% (weight) respectively. This suggests that the absence of reflections relating to Pd in the XRD pattern of Imp-Pd/TiO<sub>2</sub> must be attributed to a mean crystallite size of Pd below that of the XRD detectable limit (ca. <5 nm). This is markedly different from a calculated mean Pd particle size of 22 nm for the Std-Pd/TiO<sub>2</sub> catalyst, as determined through application of the Scherrer equation. A direct relationship between mean Pd crystallite size and catalytic activity might therefore exist, with the smaller mean Pd particle sizes of Imp-Pd/TiO<sub>2</sub> being responsible for the higher activity observed with this catalyst.

### 4.2.3 Transmission Electron Microscopy

In order to further investigate the disparity in Pd particle sizes between the two catalysts, Imp-Pd/TiO<sub>2</sub> and Std-Pd/TiO<sub>2</sub> were subjected to transmission electron microscopy (TEM) analysis, representative images from which, are presented in figure 4.4 below. In accordance with the XRD analysis, differences in the physical characteristics of each catalyst are clearly discernible. An interesting feature of Std-Pd/TiO<sub>2</sub> in figure 4.4 is the apparent presence of Pd clusters. A provisional measurement of particle size within these clusters indicates a Pd particle size in the region of 2-3 nm, however, due to extensive overlap of particles within the cluster it was not possible to perform a more definitive measurement of particle size distribution. Results obtained from XRD analysis suggest that a large degree of Pd particle agglomeration may be taking place within these clusters. The TEM image in figure 4.4 indicates evidence of cluster formation in Imp-Pd/TiO<sub>2</sub> also, however the Pd particles do appear to be more evenly distributed.

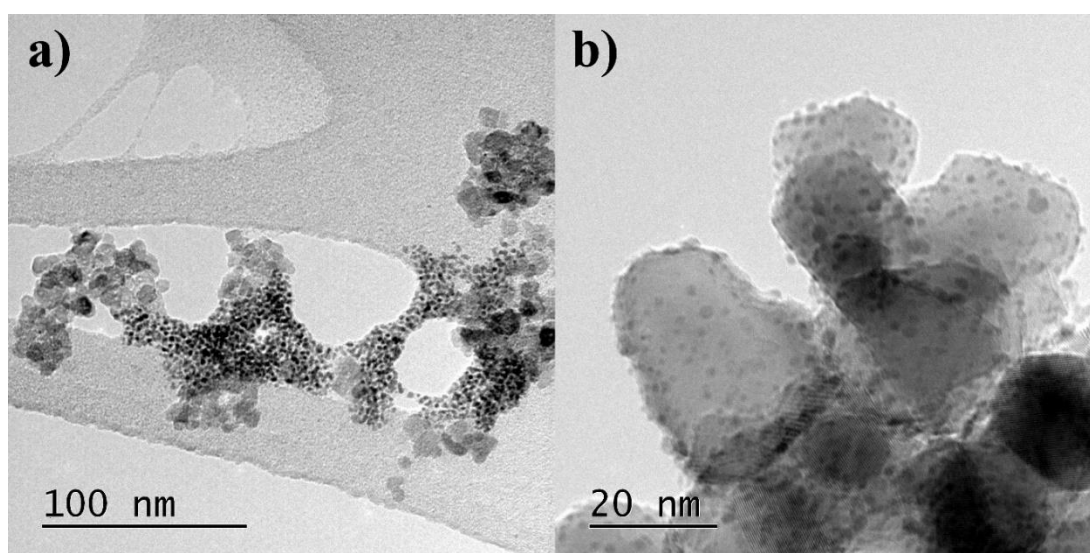
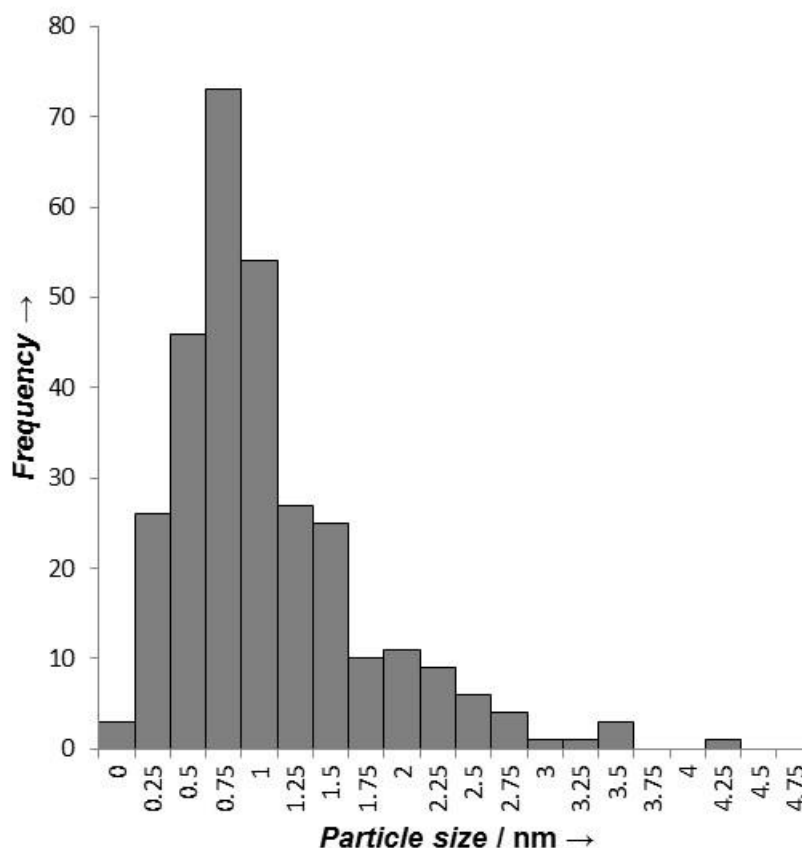


Figure 4. TEM images of the (a). Std-Pd/TiO<sub>2</sub> and (b).Imp-Pd/TiO<sub>2</sub> catalysts.

Figure 5 below displays a representative measurement of particle size distribution for Imp-Pd/TiO<sub>2</sub>, showing an average Pd particle size of 1.18 nm, with a standard deviation of 0.67. The difference in palladium particle size between the two catalysts appears to provide a rational explanation as to the observed differences in activity.



**Figure 5. The palladium particle size distribution for IM-Pd/TiO<sub>2</sub>. (based on 300 particles)**

#### **4.2.4 X-Ray Photoelectron Spectroscopy (XPS)**

Through XPS analysis it was possible to determine differences in the initial oxidation states of Pd species present on the surfaces of Imp-Pd/TiO<sub>2</sub> and Std-Pd/TiO<sub>2</sub>. As can be seen from table 2 the Pd species present in the imp catalyst are exclusively found in the 2+ oxidation state, existing as both oxide (336.8 eV) and

chloride (337.9 eV), with the chloride being the predominant species. In contrast, the Pd (3d) core-level spectra for the Std-Pd/TiO<sub>2</sub> catalyst revealed the presence of three separate Pd environments; nominally a significant proportion of metallic Pd<sup>0</sup> (335.5 eV), alongside Pd<sup>2+</sup> oxide and chloride species. It is possible therefore to draw a correlation between the Pd oxidation state of the Imp-Pd/TiO<sub>2</sub> and Std-Pd/TiO<sub>2</sub> catalysts and their respective selectivities to 2-MF: the presence of oxidised Pd species, as in Imp-Pd/TiO<sub>2</sub>, is necessary for the highly selective conversion of FA to 2-MF; whereas metallic Pd species are responsible for the activation of ring-opening pathways with the concomitant lowering of selectivity towards 2-MF. XPS analysis of the post-reaction used catalysts appears to support this hypothesis where, under the reducing conditions of the reaction, significant proportions of Pd<sup>0</sup> can be observed in both catalysts, which is congruous with a displayed increase in the formation of 2-pentanol through the ring-opening of 2-MF. A Pd/Ti ratio of 0.14 for Imp-Pd/TiO<sub>2</sub> compared with 0.05 for Std-Pd/TiO<sub>2</sub> indicates a greater level of Pd dispersion for Imp-Pd/TiO<sub>2</sub>, further corresponding with the data obtained from XRD and TEM analysis, that suggests that increased initial rates of catalytic activity are a result of higher levels of Pd dispersion.

**Table 2. Quantified XPS results for Imp-Pd/TiO<sub>2</sub> and Std-Pd/TiO<sub>2</sub>.**

Sample	Assignment	Conc. [%At].	Ratio					
			Ti/O	Pd/Sn	Sn/Pd	Pd/Ti	Sn/Ti	Pd:PdO:PdCl
IM-Pd/ TiO <sub>2</sub>	Pd 3d	3.59	0.37			0.14		01:03.3
	O 1s	67.56						
	Ti 2p	24.82						
	Cl 2p	4.03						
Std- 5%Pd/ TiO <sub>2</sub>	Pd 3d	1.48	0.42			0.05		1:0.85:1.11
	O 1s	67.66						
	Ti 2p	28.59						
	Cl 2p	2.27						

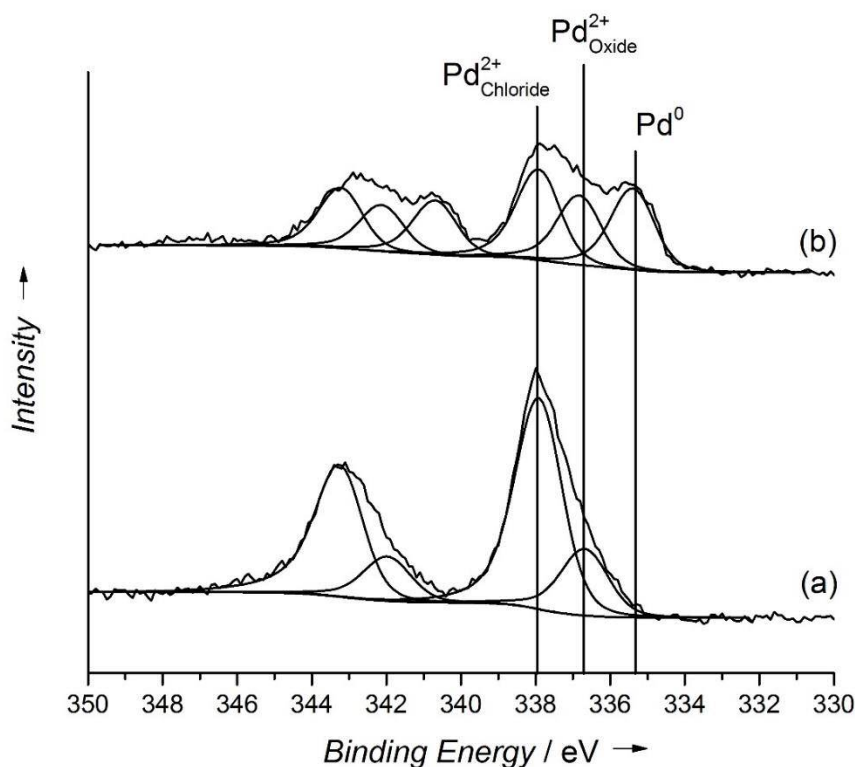


**Figure 6.** XPS curve-fitted Pd(3d) core-level spectra for for the two 5% Pd/TiO<sub>2</sub> catalysts: (a) IM-Pd/TiO<sub>2</sub> and (b) Std-5%Pd/TiO<sub>2</sub>.

#### 4.2.5 Sn-Pd bimetallic catalysts

A number of papers have been published in which the activity of bimetallic Sn-Pd catalysts for hydrogenation and hydrogenolysis reactions have been reported.<sup>10</sup> To investigate the efficacy of a Sn-Pd bimetallic system for the hydrogenation of FA, a 2.5 wt%Sn-2.5 wt%Pd/TiO<sub>2</sub> catalyst was prepared by the impregnation methodology and tested under the reaction conditions previously established for the Imp-Pd/TiO<sub>2</sub> catalyst. A reaction time of 60 mins was selected, as neither the Imp-Pd/TiO<sub>2</sub> nor the Std-Pd/TiO<sub>2</sub> catalyst achieved full conversion in this time, therefore making any differences in activity all the more apparent. As can be seen from table 3, over the course of 60 mins the Pd-Sn bimetallic catalyst is more active for the conversion of FA than either one of the monometallic 5wt% Pd/TiO<sub>2</sub> catalysts, achieving 87% conversion; compared with 76% for Imp-Pd/TiO<sub>2</sub>; and 56% with Std-

Pd/TiO<sub>2</sub>. The bimetallic catalyst was, however, less selective to the hydrogenolysis product 2-MF: with a yield of 57% observed after the same reaction time; compared with 91% for Imp-Pd/TiO<sub>2</sub>; and 71% over the Std-Pd/TiO<sub>2</sub> catalyst. The reaction performed with 2.5 wt%Sn-2.5 wt%Pd/TiO<sub>2</sub> also generated a small amount of the hitherto unseen product MTHF, produced via the subsequent hydrogenation of 2-MF. (see scheme 1) . The ring-opening product, 2-pentanol, was not observed.

**Table 3. FA hydrogenolysis over a 2.5wt%Sn-2.5wt%Pd/TiO<sub>2</sub> catalyst.<sup>[a]</sup>**

T [°C]	Conversion [%]	Yield [%]	
		2-MF	MTHF
25	86.5	57.4	1.3
50	93.6	77.2	0
80	80.8	53.4	0

[a]. Reaction conditions: 1,2-dichloroethane (15mL); 1 bar H<sub>2</sub>; catalyst (0.1g); furfuryl alcohol (1.0g); 60 min.

#### 4.2.5.1 Sn-Pd bimetallic catalysts - The effect of Temperature

Table 3 further shows the effect of temperature on the catalytic hydrogenolysis of FA. Reactions were performed at 50 and 80 °C to explore whether raising reaction temperature could increase MTHF production. Increasing the temperature to 50 °C led to an increase in the level of FA conversion, with a concomitant increase in 2-MF product at a yield greater than that observed for either of the monometallic Pd catalysts. However, under these conditions no MTHF was detected. Further increasing the temperature to 80 °C resulted in an observed decrease in both FA conversion and 2-MF yield, with no observable production of MTHF.

### 4.2.5.2 Sn-Pd bimetallic catalysts - The effect of Pressure

In an attempt to achieve a greater degree of control over the product selectivity, the performance of 2.5 wt%Sn-2.5 wt%Pd/TiO<sub>2</sub> at various hydrogen pressures was investigated, the results of which are displayed in table 4 below. Raising the reaction pressure from 1 bar to 2 bar H<sub>2</sub> only marginally increased the level of conversion, which suggests that under our standard 1 bar H<sub>2</sub> reaction conditions the hydrogen is not mass-transfer limited. Minor differences in 2-MF and MTHF yields were also observed, however this is likely associated with the extent of FA substrate conversion, rather than through the operation of a different reaction pathways at different pressures.

**Table 4. Effect of pressure variation on FA hydrogenolysis over a 2.5wt%Sn-2.5wt%Pd/TiO<sub>2</sub> catalyst.<sup>[a]</sup>**

P H <sub>2</sub> [bar]	Conversion [%]	Yield [%]	
		2-MF	MTHF
1	86.5	57.4	1.3
2	100	44	1.62
3	95	50	1

[a]. Reaction conditions: 1,2-dichloroethane (15mL); catalyst (0.1g); furfuryl alcohol (1.0g); 25 °C; 60 min.

### 4.2.5.3 Sn-Pd bimetallic catalysts - The effect of Solvent

Due to the inherent toxicity and aquatic polluting potential of 1,2-dichloroethane, reactions under standard conditions with 2.5 wt%Sn-2.5 wt%Pd/TiO<sub>2</sub> were further performed in methanol and ethanol; solvents that are more preferable from a green chemistry and environmental perspective. As can be seen from table 5, varying the

solvent did not have a pronounced effect on the level of FA conversion, however the reaction performed in methanol proceeded the furthest, reaching full conversion in the 60 min reaction time. Of considerable interest is the difference in product distribution for the reactions performed in methanol and ethanol, compared with the products observed in 1,2-dichloroethane. In the alcohol solvents, significant production of tetrahydrofurfuryl alcohol (THFA) is observed. This high selectivity to THFA is achieved through a different reaction pathway than that by which 2-MF is formed, as production of THFA requires the selective hydrogenation of the two double bonds within the aromatic heterocyclic furan ring without hydrogenolysis of the –OH functional group. This changing of selectivity to product with solvent variation is not an unprecedented observation, the Hutchings group having previously reported on this effect with regard to oxidation reactions.<sup>19</sup>

**Table 5. Effect of solvent variation on FA hydrogenolysis over a 2.5wt%Sn-2.5wt%Pd/TiO<sub>2</sub> catalyst.<sup>[a]</sup>**

Solvent	Conversion [%]	Yield [%]		
		2-MF	MTHF	THFA
ethanol	92	50	3	43
methanol	100	25	8	52
1,2-dichloroethane	86.5	57.4	1.3	-

[a]. Reaction conditions: 1 bar H<sub>2</sub>; catalyst (0.1g); furfuryl alcohol (1.0g); 25 °C; 60 min.

#### 4.2.5.4 Sn-Pd bimetallic catalysts - The effect of Sn:Pd ratio

Of the monometallic 5 wt% Pd/TiO<sub>2</sub> catalysts tested, Imp-Pd/TiO<sub>2</sub> displayed the highest selectivity towards 2-MF in 1,2-dichloroethane solvent; the Sn-Pd bimetallic catalyst, 2.5 wt%Sn-2.5 wt%Pd/TiO<sub>2</sub>, on the other hand produced THFA in high yield

when the reaction was performed in methanol solvent. Reports from within the Hutchings group have previously detailed how the activity of a catalyst and the respective product selectivity can be modulated with variation of the metal to metal ratio in bimetallic catalysts for the oxidation of benzyl alcohol.<sup>20</sup> Consequently, Sn-Pd bimetallic catalysts with differing ratios of Sn and Pd were synthesised and tested them under the methanolic conditions in an attempt to achieve more control over product selectivity. The Imp-Pd/TiO<sub>2</sub> catalyst was also tested under these conditions so that a more direct comparison of catalyst activity and selectivity could be made.

In a trend similar to as seen with the Sn-Pd bimetallic catalyst, FA conversion with Imp-Pd/TiO<sub>2</sub> is higher in methanol than in 1,2-dichloroethane solvent, reaching 82% conversion in 60 mins compared with 76% in the same time. The selectivity to 2-MF in methanol was, however, significantly lower, reaching a yield of 14% over the course of the reaction compared with 46% in 1,2-dichloroethane, highlighting once again that solvent choice can have a significant effect on product selectivity.

Continuing with methanol as the solvent, of the three Sn-Pd bimetallic catalysts tested, the more palladium-rich 1.0 wt%Sn-4.0 wt%Pd/TiO<sub>2</sub> (Sn/Pd = 1:4) was observed to form THFA as the major product, achieving a yield of 52% in 60 min. The 2.5 wt%Sn-2.5 wt%Pd/TiO<sub>2</sub> (Sn/Pd = 1:1) catalyst produced THFA in the same yield as the Sn/Pd = 1:4 catalyst, however they differed considerably in their selectivity towards other products, as can be seen in table 6 below.

**Table 6. Effect of varying metal loading for catalytic FA hydrogenolysis.<sup>[a]</sup>**

Catalyst /TiO <sub>2</sub>	Conversion [%]	Yield [%]		
		2-MF	MTHF	THFA
IM- 5%Pd	81.7	14.3	1.5	69.4
Sn/Pd =4:1	75	12	0	23
Sn/Pd =1:4	85	0	25	52
Sn/Pd =2.5:2.5	100	25	8	52

[a]. Reaction conditions: methanol (15mL) 1 bar H<sub>2</sub>; catalyst (0.1g); furfuryl alcohol (1.0g); 25 °C; 60 min.

Table 6 shows that for the Sn-Pd bimetallic catalysts significant quantities of 2-MF can be produced when tin and palladium are present in a 1:1 ratio, however if the metal ratio is shifted so that palladium becomes the predominant component, 2-MF is no longer observed, with formation of the sequential hydrogenation product MTHF evident. This observation is in agreement with the data presented on the monometallic Pd catalyst, as this was the most active of all the catalysts tested in this body of work. The addition of small amounts of tin may act by preventing the ring-opening pathway discussed previously, thus allowing for further hydrogenation to take place. The catalyst in which tin was the most prevalent metal (4.0 wt%Sn-1.0 wt%Pd/TiO<sub>2</sub>) gave the lowest yield of THFA along with no detectable quantities of MTHF. This catalyst does appear to activate the hydrogenolysis pathway however, as 2-MF production is observed.

#### 4.2.5.5 X-ray photoelectron spectroscopy

The Sn-Pd bimetallic catalysts were subjected to XPS for further investigation, with the Pd(3d) and Sn(3d) core-levels determined for the catalysts with different metal loading ratios being shown in figure 5. The tin core level rarely shifts between the +2 and +4 oxidation states, however application of the modified Auger parameter (919.2 eV) suggests that the tin present is in the form of SnO<sub>2</sub>. The palladium was observed

to exist mostly as PdO (337 eV), regardless of the Sn:Pd ratio, with small quantities of metallic Pd (335.5 eV) also present (table 7). The relative concentrations of palladium species were observed to change with variation of metal ratio, for example at low palladium concentrations i.e. with the 4.0 wt%Sn-1.0 wt%Pd/TiO<sub>2</sub> catalyst, Pd<sup>0</sup> is significant proportion of the palladium species present, whereas at higher palladium concentrations the predominant palladium species is Pd<sup>2+</sup>. For both the 2.5 wt%Sn-2.5 wt%Pd/TiO<sub>2</sub> and the 1.0 wt%Sn-4.0 wt%Pd/TiO<sub>2</sub> catalysts the observed Pd:Sn ratios are very similar, indicating that a substantial amount of palladium within the 2.5 wt%Sn-2.5 wt%Pd/TiO<sub>2</sub> catalyst must be occluded in SnO<sub>2</sub>. In contrast, the Pd:Sn ratio is significantly lower for the 4.0 wt%Sn-1.0 wt%Pd/TiO<sub>2</sub> catalyst, which may be indicative of low palladium dispersion on tin. This could possibly explain why a different reaction pathway was observed, with reactants being restricted in their ability to access the palladium active sites.

**Table 7. Quantified XPS results for SnPd/TiO<sub>2</sub> catalysts with varying metal loadings.**

Sample	Assignment	Conc. [%At]	Ratio					
			Ti/O	Pd/Sn	Sn/Pd	Pd/Ti	Sn/Ti	Pd:PdO:PdCl
2.5:2.5 SnPd/TiO <sub>2</sub>	Pd 3d	1.58						
	O 1s	67.05						
	Sn 3d 5/2	1.91	0.42	0.83	1.21	0.06	0.07	04:09.1
	Ti 2p	28.2						
	Cl 2p	1.26						
1:4 SnPd/TiO <sub>2</sub>	Pd 3d	1.14						
	O 1s	67.87						
	Sn 3d 5/2	1.26	0.43	0.9	1.11	0.04	0.04	03:07.1
	Ti 2p	29.04						
	Cl 2p	0.68						
4:1 SnPd/TiO <sub>2</sub>	Pd 3d	0.33						
	O 1s	67.79	0.44	0.17	5.82	0.01	0.06	

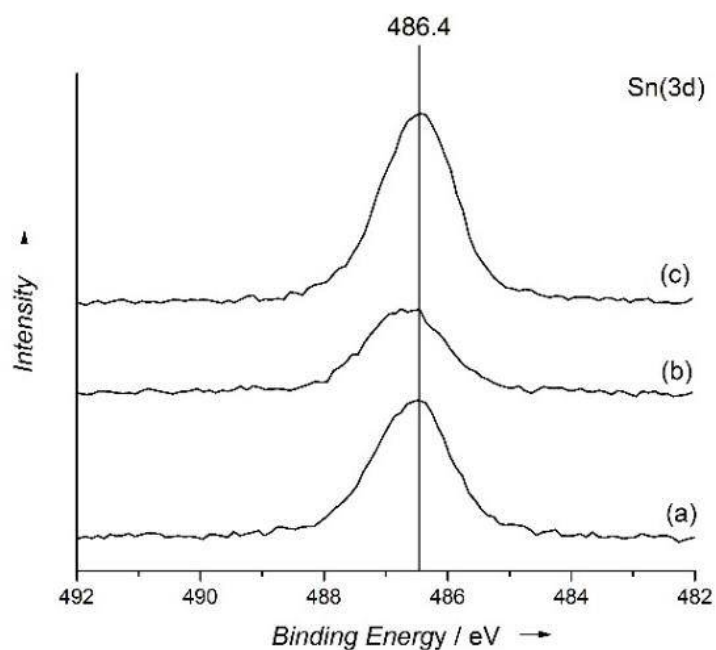
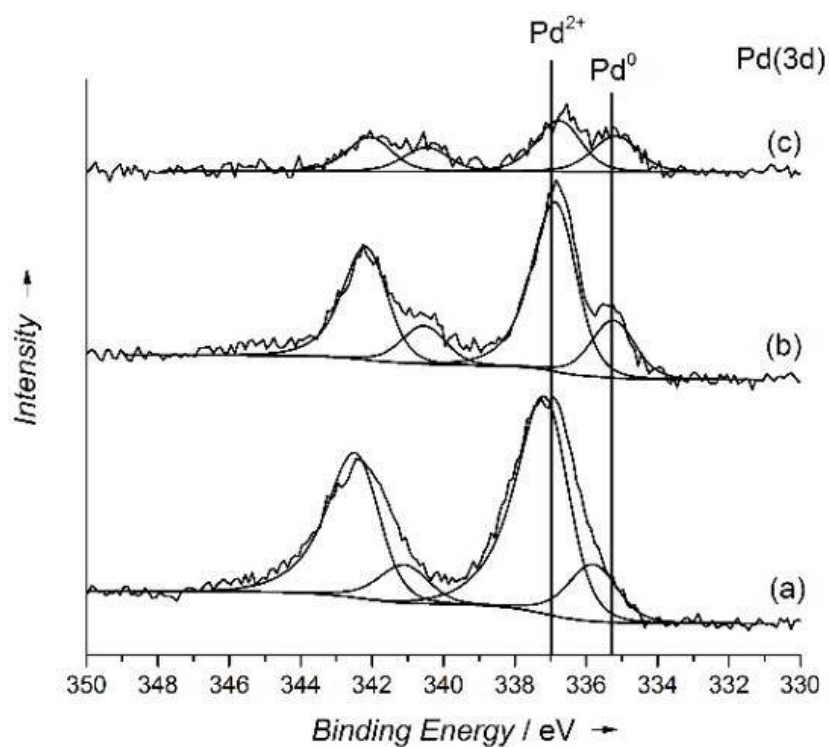


**Figure 7. XPS spectra showing the Pd(3d) and Sn(3d) core levels for SnPd/TiO<sub>2</sub> catalysts with varying metal ratios where a). 2.5wt%Sn-2.5wt%Pd; b). 1.0wt%Sn-4.0wt%Pd; and c). 4.0wt%Sn-1.0wt%Pd.**

### 4.2.5.6 X-ray diffraction

XRD analysis, as seen in figure 6, reveals a reflection at  $2\theta = 33.9^\circ$  that grows systematically with increasing tin content. This reflection corresponds to the  $\text{SnO}_2$  plane (101), and therefore appears to corroborate the analysis determined by XPS. No palladium reflections were observed in any of the SnPd bimetallic catalysts.

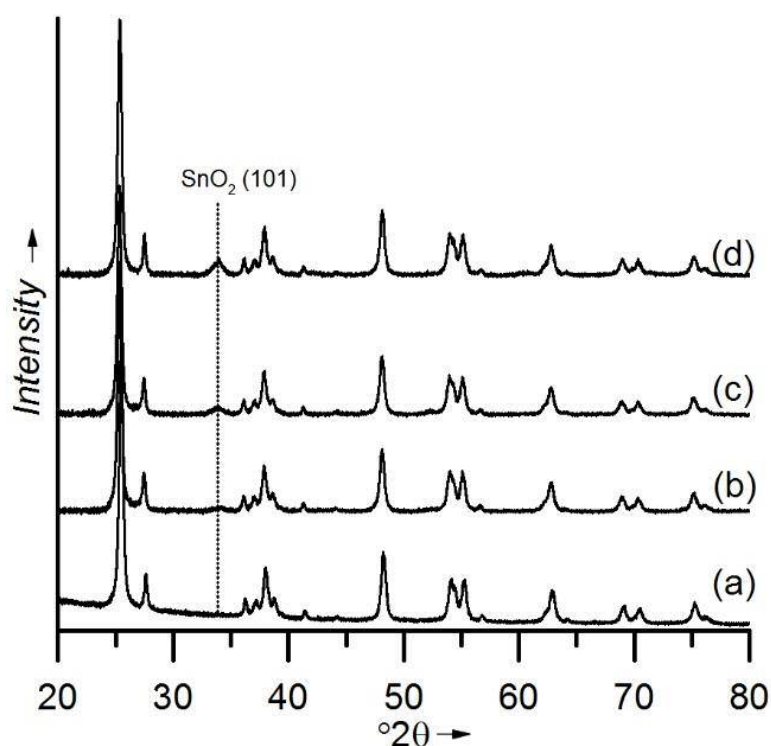


**Figure 8.** XRD patterns of 5.0wt%Pd/TiO<sub>2</sub> and 5.0wt%SnPd/TiO<sub>2</sub> with varying metal loadings (a) 5wt% Pd/TiO<sub>2</sub>; (b) 1.0wt%-4.0wt%SnPd/TiO<sub>2</sub>; (c) 2.5wt%Sn-2.5wt%Pd/TiO<sub>2</sub>; 4.0wt%Sn-1.0wt%Pd/TiO<sub>2</sub>

### 4.2.5.7 Transmission electron microscopy

The Sn-Pd catalysts were also subjected to TEM analysis, the images from which can be found in figure 7 below. Small particles in the region of ~2-3 nm were seen on all three catalysts, with higher magnification also demonstrating the presence of even smaller ~0.5 nm particles. Catalysts prepared by the impregnation methodology have

been shown to display bimodal particle size distributions previously.<sup>21</sup> Due to the particles being at the detection limit of this spectroscopic technique, it was not possible to perform a statistically relevant analysis of particle size distribution.

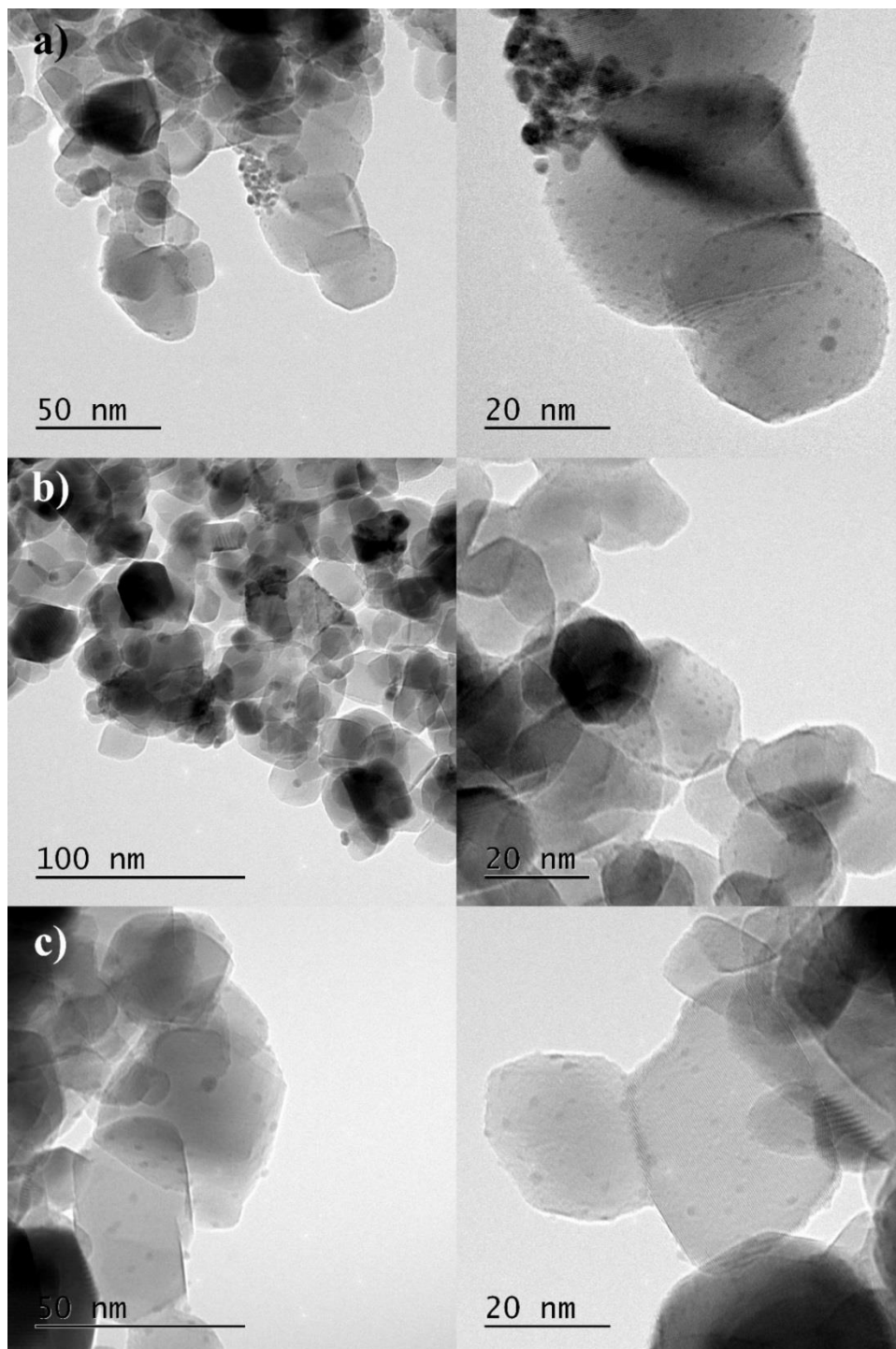


**Figure 9.** TEM images of (a). 2.5wt%Sn-2.5wt%Pd/TiO<sub>2</sub>; (b). 1.0wt%-4.0wt%SnPd/TiO<sub>2</sub>; and (c). 4.0wt%Sn-1.0wt%Pd/TiO<sub>2</sub>

## 4.3 Conclusions

This body of work has demonstrated that 5wt%Pd/TiO<sub>2</sub> catalysts prepared by the impregnation method can be highly active for the selective hydrogenolysis of furfuryl alcohol substrate to 2-methylfuran, a highly desirable product with biofuel blending applications, at room temperature and under low hydrogen pressures.

Through the addition and weight loading variation of a secondary metal, namely tin, it has been shown that the reaction pathway can be driven away from hydrogenolysis and more towards furan ring hydrogenation, resulting in the selective production of tetrahydrofurfuryl alcohol, and methyltetrahydrofuran ring-saturated products.

## 4.4 References

1. A. Corma, *Chem. Rev.* **2014**, *114*, 1545-1546.
2. H. Adkins, R. Connor, *J. Am. Chem. Soc.* **1931**, *53*, 1091-1095.
3. A. P. Dunlop, H. Schegulla, Quaker Oats Co. , **1958**.
4. S. Sitthisa, W. An, D. E. Resasco, *J. Catal.* **2011**, *284*, 90-101.
5. a). I. Ahmed, Pure Energy Corporation, USA . **2002**, p. 41 pp; b). A. Corma, S. Iborra, A. Velty, *Chem. Rev. (Washington, DC, U. S.)* **2007**, *107*, 2411-2502; c). B. Zhang, Y. Zhu, G. Ding, H. Zheng, Y. Li, *Green Chem.* **2012**, *14*, 3402-3409.
6. a). Y.-L. Zhu, H.-W. Xiang, Y.-W. Li, H. Jiao, G.-S. Wu, B. Zhong, G.-Q. Guo, *New Journal of Chemistry* **2003**, *27*, 208-210; b).G. Li, N. Li, S. Li, A. Wang, Y. Cong, X. Wang, T. Zhang, *Chemical Communications* **2013**, *49*, 5727-5729.
7. a).B. Zhang, Y. Zhu, G. Ding, H. Zheng, Y. Li, *Green Chem.* **2012**, *14*, 3402-3409; b). X. Chen, W. Sun, N. Xiao, Y. Yan, S. Liu, *Chem. Eng. J. (Amsterdam, Neth.)* **2007**, *126*, 5-11; c). Z. Zhang, K. Dong, Z. K. Zhao, *ChemSusChem* **2011**, *4*, 112-118.
8. S. Sitthisa, W. An, D. E. Resasco, *J. Catal.* **2011**, *284*, 90-101.
9. Y.-L. Zhu, H.-W. Xiang, Y.-W. Li, H. Jiao, G.-S. Wu, B. Zhong, G.-Q. Guo, *New J. Chem.* **2003**, *27*, 208-210.
10. a). Z. Zhang, K. Dong, Z. Zhao, *ChemSusChem* **2011**, *4*, 112-118; b). N. Merat, C. Godawa, A. Gaset, *J. Chem. Technol. Biotechnol.* **1990**, *48*, 145-159.
11. S. Iqbal, X. Liu, O. F. Aldosari, P. J. Miedziak, J. K. Edwards, G. L. Brett, A. Akram, G. M. King, T. E. Davies, D. J. Morgan, D. K. Knight, G. J. Hutchings, *Catal. Sci. Technol.* **2014**, *4*, 2280-2286.
12. N. Merat, C. Godawa, A. Gaset, *J. Chem. Technol. Biotechnol.* **1990**, *48*, 145-159.
13. T. Wabnitz, D. Breuninger, J. Heimann, R. Backes, R. Pinkos, BASF SE, Germany., **2009**, p. 18 pp.
14. a).A. C. Crucean, N. Teodorut, Chimigaz Srl, Rom. . **2015**, p. 6pp; b).S. Akiyama, T. Kakio, S. Indou, R. Oikawa, K. Ugou, R. Hiraki, M. Sano, T. Suzuki, T. Miyake, *J. Jpn. Pet. Inst.* **2014**, *57*, 216-224; c).J.-M. Lee, P. P. Upare, J.-S. Chang, Y. K. Hwang, J. H. Lee, D. W. Hwang, D.-Y. Hong, S. H. Lee, M.-G. Jeong, Y. D. Kim, Y.-U. Kwon, *ChemSusChem* **2014**, *7*, 2998-3001.

15. a). Y. Xu, S.-f. Cao, C.-l. Ning, Y.-g. Li, H.-l. Xu, C.-l. Zhang, *Fudan Xuebao, Ziran Kexueban* **2014**, *53*, 236-241; b). A. P. Tathod, P. L. Dhepe, *Bioresour. Technol.* **2015**, *178*, 36-44; c). A. P. Tathod, P. L. Dhepe, *Green Chem.* **2014**, *16*, 4944-4954; d). A.-R. Rautio, P. Maki-Arvela, A. Aho, K. Eranen, K. Kordas, *Catal. Today* **2015**, *241*, 170-178; e). E. Esmaeili, A. M. Rashidi, A. A. Khodadadi, Y. Mortazavi, M. Rashidzadeh, *Fuel Process. Technol.* **2014**, *120*, 113-122.
16. J. Ren, J. Wang, D. Zhao, Z. Liu, China Petroleum & Chemical Corp., Peop. Rep. China; Shanghai Research Institute of Petrochemical Engineering, SINOPEC . **2014**, p. 10pp.
17. a). R. Rodiansono, T. Hara, N. Ichikuni, S. Shimazu, *Bull. Chem. React. Eng. Catal.* **2014**, *9*, 53-59; b). T. Deng, H. Liu, *J. Mol. Catal. A: Chem.* **2014**, *388-389*, 66-73.
18. S. Furukawa, A. Yokoyama, T. Komatsu, *ACS Catal.* **2014**, *4*, 3581-3585.
19. a). O. G. Salnikov, K. V. Kovtunov, D. A. Barskiy, A. K. Khudorozhkov, E. A. Inozemtseva, I. P. Prosvirin, V. I. Bukhtiyarov, I. V. Koptuyug, *ACS Catal.* **2014**, *4*, 2022-2028; b). E. P. A. Rocha, F. B. Passos, F. C. Peixoto, *Ind. Eng. Chem. Res.* **2014**, *53*, 8726-8734; c). J. Zhao, X. Xu, X. Li, J. Wang, *Catal. Commun.* **2014**, *43*, 102-106.
20. J. Xi, D. Ding, Y. Shao, X. Liu, G. Lu, Y. Wang, *ACS Sustainable Chem. Eng.* **2014**, *2*, 2355-2362.
21. R. I. Bickley, T. Gonzalez-Carreno, J. S. Lees, L. Palmisano, R. J. D. Tilley, *Journal of Solid State Chemistry* **1991**, *92*, 178-190.
22. M. D. Hughes, Y. J. Xu, P. Jenkins, P. McMorn, P. Landon, D. I. Enache, A. F. Carley, G. A. Attard, G. J. Hutchings, F. King, E. H. Stitt, P. Johnston, K. Griffin, C. J. Kiely, *Nature* **2005**, *437*, 1132-1135.
23. J. Pritchard, L. Kesavan, M. Piccinini, Q. He, R. Tiruvalam, N. Dimitratos, J. A. Lopez-Sanchez, A. F. Carley, J. K. Edwards, C. J. Kiely, G. J. Hutchings, *Langmuir* **2010**, *26*, 16568-16577.

# Chapter 5

## 5. Palladium and Ruthenium heterogeneous catalysts for the hydrogenation of furfural

### 5.1. Introduction

Furfural, produced by the hydrolysis and dehydration of lignocellulosic xylan, offers a comprehensive platform from which a wide range of biofuel components and other valorised organic molecules can be derived. A number of copper-based catalysts have been utilised for the liquid phase hydrogenation of furfural, for example Dongxia et al. reported the selective conversion of furfural to FA over a copper chromite catalyst operating at 180 °C under a hydrogen pressure of between 69-104 bar.<sup>1</sup> Hydrogenation of furfural to 2-MF, MTHF, and FA has also been reported over oxide supported copper catalysts such as Cu/TiO<sub>2</sub>,<sup>2</sup> Cu/SiO<sub>2</sub>,<sup>3-5</sup> Cu/Cr,<sup>6</sup> Cu/Fe,<sup>7,8</sup> Cu/Pd,<sup>9,10</sup> Cu/Zn/Al,<sup>11</sup> and Cu/Ni/Mg/Al.<sup>12</sup> Metal oxide supported Ru,<sup>13,14</sup> Ni,<sup>15</sup> and Fe<sup>15-17</sup> have also been shown to be active for furfural hydrogenation.

Most of the examples listed above require relatively harsh conditions with respect to reaction temperatures and pressures in order for activity to be observed. The chemoselective hydrogenation of a carbonyl group in the proximity of a double bond or an aromatic ring is a particularly challenging problem, since C=C hydrogenation is thermodynamically more favourable than C=O hydrogenation by approximately 35 kJ/mol.<sup>18</sup> Successful reduction of multi-unsaturated aldehydes and ketones is of industrial interest as their respective unsaturated alcohols have applications in pharmacology, food processing, and as fragrances.<sup>19</sup> Homogeneous catalysts can, in principle, be employed in the selective hydrogenation of these compounds; however heterogeneous catalysts present the advantage of being easier to separate and reuse, and are potentially more environmentally friendly.<sup>19</sup> Platinum

and ruthenium heterogeneous catalysts have been demonstrated as being efficacious for such transformations; nevertheless, the availability, reduced cost, and comparative properties of ruthenium has resulted in the almost complete disuse of platinum for such reactions.

A number of bimetallic ruthenium catalysts have been employed for chemoselective hydrogenation reactions, including RuSn/TiO<sub>2</sub>,<sup>20</sup> RuFe/C,<sup>21,22</sup> RuCe/C,<sup>23</sup> RuCr/SiO<sub>2</sub>,<sup>24</sup> RuSn/SiO<sub>2</sub>,<sup>25</sup> and RuSn/Al<sub>2</sub>O<sub>3</sub>.<sup>26</sup> When compared to the activity displayed by a monometallic ruthenium catalyst, addition of Fe and Cr served to decrease catalyst activity,<sup>20,21</sup> whereas in contrast the activity of a bimetallic RuSn/TiO<sub>2</sub> catalyst employed for citral hydrogenation activity was observed to proceed through a maximum with increasing tin content.

RuPd bimetallic catalysts have previously been shown to be active and selective for furfural hydrogenation,<sup>27</sup> herein the reaction parameters have been widened to further explore their efficacy.

Carbon supported ruthenium catalysts have been shown to active for the catalytic transfer hydrogenation of furfural in the liquid phase.<sup>28</sup> 95% conversion of the furfural substrate with a 2-methyluran yield of 61% was reported for the liquid phase reaction performed at 180 °C in 2-propanol solvent, over the course of 10 hours. A commercially available 5wt% Ru/C has been investigated herein for activity for furfural hydrogenation in methanol.

## 5.2 Results and Discussion

Previous work conducted by the Hutchings group has focused on exploring a range of organic solvents in order to find the most efficient solvent for furfural hydrogenation under the mild reaction conditions of 25 °C and 3 bar H<sub>2</sub> for the selective production

of FA and 2-MF.<sup>29</sup> A solvent is usually selected for its ability to dissolve high concentrations of H<sub>2</sub>, thereby increasing the rate of hydrogenation compared to a solvent with a lower concentration of dissolved H<sub>2</sub>.<sup>27</sup> High catalytic activity has been achieved in both methanol and toluene, however selectivity differences between the two solvents were clearly evident, with methanol enabling relatively high selectivity to THFA as well as to large quantities of side products, whilst toluene also displayed high selectivity to THFA, and 2-MF too.<sup>29</sup>

In contrast to FA hydrogenation performed in 1,2-dichloroethane where full conversion to 2-MF was observed, reactions performed in 1,2-dichloroethane for furfural hydrogenation were shown to produce a mixture of products with low yields of desired products. In order to investigate this reaction further, Pd/TiO<sub>2</sub> catalysts were prepared with varying weight loadings by the impregnation method and tested for furfural hydrogenation along with a commercially available 5wt% Pd/TiO<sub>2</sub> catalyst, which was added to provide a benchmark for the in-house prepared catalysts. The results from these experiments are displayed in table 1.

**Table 1. Pd/TiO<sub>2</sub> catalysts with varying weight loadings for furfural hydrogenation in 1,2-dichloroethane**

Catalyst	Conv. [%]	Yield [%]					
		FA	2-MF	MTHF	THFA	1,5-PeD	1,2-PeD
1.0 wt % Pd/TiO <sub>2</sub>	98.7	5.5	34.9	0	7.5	0	0
2.5 wt % Pd/TiO <sub>2</sub>	99.2	14.0	63.8	1.6	11.0	0	0
5.0 wt % Pd/TiO <sub>2</sub> (Impreg.)	100	0	67.4	4.1	0	0	0
5.0 wt % Pd/TiO <sub>2</sub> (commercial)	100	0	91.0	1.4	2.1	0	0

Reaction conditions: 1.0g Furfural; 0.1 catalyst; 15 mL solvent; 25 °C, 3 bar H<sub>2</sub>, 1000 rpm stirring, 1 h.

Pd/TiO<sub>2</sub> catalysts prepared by the impregnation method with varying weight loadings have previously been characterised by the Hutchings group,<sup>27</sup> with palladium particle

size being seen to be very low (< 2 nm), with little variation in particle size distribution across the loading range. Due to this uniformity in particle size distribution, the observed increase in catalytic activity can be attributed to an increasing number of metal active sites as the weight loading of the catalyst is increased.

The results depicted above suggest that 1,2-dichloroethane can be a suitable solvent for furfural hydrogenation, with selective production of 2-MF clearly evident. No further work was carried out on the 1,2-dichloroethane solvent from this point on, due to a shift in focus towards investigating furfural hydrogenation in a less environmentally-toxic alternative.

With a palladium loading of 5wt% being the most active for furfural hydrogenation in 1,2-dichloroethane, the 5.0wt% Pd/TiO<sub>2</sub> catalyst prepared by the impregnation technique (Imp-Pd/TiO<sub>2</sub>), and the commercially available 5.0wt% Pd/TiO<sub>2</sub> catalyst (Std-Pd/TiO<sub>2</sub>) were taken forward to see whether the selectivity to desired products could be increased when the furfural hydrogenation reaction is performed in methanol. A time-on-line reaction was conducted with both catalysts, the results from which can be seen in table 2 below.

**Table 2. Time-on-line reaction investigating the activity of Imp-Pd/TiO<sub>2</sub> and Std-Pd/TiO<sub>2</sub> for the catalytic hydrogenation of furfural in methanol.**

T (mins)	Catalyst	Conv. [%]	Yield [%]					
			FA	2-MF	MTHF	THFA	1,5-PeD	1,2-PeD
60	IMP-5.0wt% Pd/ TiO <sub>2</sub>	96.1	0	0	0.4	11.3	12.5	0
120	IMP-5.0wt% Pd/ TiO <sub>2</sub>	97.9	0	0	2.3	11.3	12.8	0
180	IMP-5.0wt% Pd/ TiO <sub>2</sub>	98.0	0	0	2.7	12.1	13.6	0
60	STD-5.0wt% Pd/ TiO <sub>2</sub>	92.4	18.4	7	0	18.4	7.6	34.9
120	STD-5.0wt% Pd/ TiO <sub>2</sub>	92.7	14	1.6	0	2.7	2.4	60.4
180	STD-5.0wt% Pd/ TiO <sub>2</sub>	94.3	13.2	1.5	0	2.4	2.9	60.9

Reaction conditions: 1.0g Furfural; 0.1 catalyst; 15 mL solvent; 25 °C, 3 bar H<sub>2</sub>, 1000 rpm stirring, 1 h.

The catalyst prepared by the impregnation method does appear to be marginally more active than the commercially available catalyst, however there was an extremely high number of side products formed, with < 30% of products formed being desirable. Whilst MTHF, 1,5-pentanediol (1,5-PeD), and 1,2-pentanediol (1,2-PeD) were observed, no detectable quantities of FA or 2-MF could be seen, which could suggest that either all FA and 2-MF produced subsequently underwent further reaction, or an alternative reaction pathway is in use, with hydrogenation of furfural's furan ring to produce tetrahydrofurfural with subsequent hydrogenolysis to tetrahydrofurfuryl alcohol. Tetrahydrofurfuryl alcohol could then undergo ring opening to produce either 1,2-PeD or 1,5-PeD, or it could undergo hydrogenolysis whilst retaining the integrity of the furan ring to produce MTHF.

Catalytic activity was slightly lower with the Std-Pd/TiO<sub>2</sub> catalyst, however in this case both FA and 2-MF could be seen. Whilst no MTHF could be detected, THFA, 1,5-PeD, and relatively high selectivity to 1,2-PeD was observed. A THFA yield of 18.4% could be seen after the first 60 mins, decreasing to 2.7% 60 mins later. This was accompanied by a concomitant increase in 1,2-PeD yield from 34.9 to 60.4% in the same time span, suggesting 1,2-PeD is being formed through THFA ring opening.

Both Imp-Pd/TiO<sub>2</sub> and Std-Pd/TiO<sub>2</sub> have previously been characterised,<sup>30</sup> with a marked difference in mean palladium particle size evident for the two catalysts. The Imp-Pd/TiO<sub>2</sub> was seen to be comprised of smaller palladium crystallite sizes, whereas Std-Pd/TiO<sub>2</sub> was determined to have a mean crystallite size of 22 nm.<sup>30</sup> It is these differences in particle size that could account for the significant differences in catalytic activity seen above.

### 5.2.1 Ru-Pd/TiO<sub>2</sub> catalysts for furfural hydrogenation

The data presented above clearly shows that 5wt%Pd/TiO<sub>2</sub> is a highly active catalyst for furfural hydrogenation in methanol, with good selectivity to 1,2-PeD being possible. However, the formation of large quantities of unwanted side products is a concern. In the previous chapter it was shown that selectivity patterns for FA hydrogenation can be improved through the addition of a second metal (Sn) to a 5wt%Pd/TiO<sub>2</sub> catalyst prepared by the impregnation method. Alteration of the metal ratio in bimetallic catalysts can also have a marked effect on the reaction profile, as has been demonstrated for hexenol and benzyl alcohol oxidation reactions. As ruthenium has been researched quite extensively for the hydrogenation of furanic compounds, it was selected as the secondary metal for the preparation of bimetallic RuPd/TiO<sub>2</sub> catalysts.

Bimetallic catalysts with Ru:Pd ratios of 2.5wt%Ru-2.5wt%Pd/TiO<sub>2</sub>; 1.0%Ru-4.0wt%Pd/TiO<sub>2</sub>; and 0.5wt%Ru-4.5wt%Pd/TiO<sub>2</sub> were prepared and tested for furfural hydrogenation in methanol, the results for which can be seen in table 3. Palladium has been shown to be the active component in bimetallic RuPd/TiO<sub>2</sub> catalysts for furfural hydrogenation in octane; increasing the ruthenium composition so that it became the predominant metal was seen to decrease catalytic activity, with it being hypothesised that the substrate could no longer reach the palladium active sites in this case.<sup>27</sup> As a result of this, and this being an investigation into the modification of palladium activity for furfural hydrogenation, no catalysts were prepared with ruthenium as the predominant metal component.

**Table 3. 5wt% RuPd/TiO<sub>2</sub> catalysts with varying metal ratios for furfural hydrogenation in methanol.**

Catalyst	Conv. [%]	Yield [%]				
		FA	2-MF	MTHF	1,2-PeDiol	Others
2.5wt%Ru-2.5wt%Pd /TiO <sub>2</sub>	95	19.1	33.3	0	4.1	43.5
1.0wt%Ru-4.0wt%Pd /TiO <sub>2</sub>	98	7.7	52.3	2.5	3.5	34
0.5wt%Ru-4.5wt%Pd /TiO <sub>2</sub>	100	0	63.9	2.6	4.5	29

Reaction conditions: 1.0g Furfural; 0.1 catalyst; 15 mL solvent; 25 °C, 3 bar H<sub>2</sub>, 1000 rpm stirring, 1 h

As can be seen from the data above, catalytic activity although high for all three catalysts, increases with increasing palladium concentration. With the 1:1 Ru:Pd catalyst displaying the lowest level of conversion, it also displayed the highest yields of FA and unwanted side products. As the palladium concentration increases, FA yield drops substantially and 2-MF yield rises significantly. Comparing the activity of the 0.5wt%Ru-4.5wt%Pd/TiO<sub>2</sub> catalyst with the 5wt%Pd/TiO<sub>2</sub> catalyst in table 2, it can be seen that the addition of a small quantity of ruthenium has a marked effect on catalytic activity and selectivity to 2-MF. This small amount of ruthenium may be acting by preventing subsequent unwanted hydrogenation reactions from taking place, an effect that has been demonstrated before, where palladium, being designated as the active species, is isolated and diluted by the presence of ruthenium.<sup>27</sup>

### 5.2.2 XRD Analysis

The Hutchings group have previously characterised impregnation-prepared RuPd/TiO<sub>2</sub> catalysts of varying metal weight loadings by XRD.<sup>27</sup> No significant difference between the catalysts could be determined, with all major visible reflections being attributed to either homogeneous dispersion of the metals across the TiO<sub>2</sub> surface, or the formation of palladium and ruthenium particles (oxide or metallic), with a particle size below that of the limit of detection.<sup>27</sup>

### 5.2.3 TEM Analysis

In order to further understand the differences in catalytic activity for the 5wt% RuPd/TiO<sub>2</sub> catalysts with varying metal ratios, the Hutchings group subjected the catalysts to TEM, where the 1.0wt%Ru-4.0wt%Pd/TiO<sub>2</sub> and the 0.5wt%Ru-4.5wt%Pd/TiO<sub>2</sub> catalysts were observed to have very small average particle sizes of 1.1 nm, and 1.3 nm respectively.<sup>27</sup> These average particle sizes are larger than those found in the 5wt% Pd/TiO<sub>2</sub> catalyst tested in table 2, however due to clearly different selectivity profiles being exhibited between the monometallic and bimetallic catalysts it is likely that catalyst composition has a more marked effect on determining reaction pathway than does particle size.<sup>27</sup> The 2.5wt%Ru-2.5wt%Pd/TiO<sub>2</sub> catalyst was shown to be comprised of particles with a smaller than average particle size, although there was evidence of the presence of some slightly larger particles also.<sup>27</sup>

### 5.2.4 TPR Analysis

TPR measurements of the RuPd/TiO<sub>2</sub> catalysts discussed above have been performed by the Hutchings group to determine the reducibility of the metal oxide species. The 1.0wt%Ru-4.0wt%Pd/TiO<sub>2</sub> and the 0.5wt%Ru-4.5wt%Pd/TiO<sub>2</sub> catalysts were observed to emit trapped hydrogen (Pd β hydride species) at just below 100 °C, suggesting that these catalysts can adsorb hydrogen on to their surfaces at sub

ambient temperatures, and then subsequently release it at temperatures exceeding 90 °C.<sup>27</sup> This behaviour was not observed for the 2.5wt%Ru-2.5wt%Pd/TiO<sub>2</sub> catalyst.

### 5.2.5 XPS analysis

XPS analysis performed by the Hutchings group revealed the presence of two ruthenium species in a 1:1 ratio with binding energies of 280.1 and 280.8 eV on a monometallic 5wt% Ru/TiO<sub>2</sub> catalyst, attributed to Ru(0) and RuO<sub>2</sub> respectively, indicating coverage of metallic ruthenium by an oxide layer.<sup>27</sup> An O (1s) shoulder at 529 eV was also reported, further supporting the evidence for presence of RuO<sub>2</sub>.<sup>27</sup> Bimetallic catalysts with high palladium loadings, such as 1.0wt%Ru-4.0wt%Pd/TiO<sub>2</sub> and the 0.5wt%Ru-4.5wt%Pd/TiO<sub>2</sub> catalysts were reported also contain Ru in the two oxidation states described, however a shift to a higher binding energy was seen for the Ru (3d) signals, which was attributed to a particle size effect.<sup>27</sup> The Ru(0):Ru(IV) ratio was observed to remain constant at 1:1.<sup>27</sup>

### Effect of Pressure

In order to further explore the efficacy of bimetallic 2.5wt%Ru-2.5wt%Pd/TiO<sub>2</sub>, 1.0wt%Ru-4.0wt%Pd/TiO<sub>2</sub> and 0.5wt%Ru-4.5wt%Pd/TiO<sub>2</sub> catalysts for furfural hydrogenation, and to investigate whether selectivity to desired products can be improved with variation of reaction parameters, the 5wt%RuPd/TiO<sub>2</sub> catalysts were tested for furfural conversion at hydrogen pressures of 10 bar; 20 bar; and 30 bar. The results of these experiments are provided in tables 4; 5; and 6 respectively, with the resulting trends to desired products being presented in figures 1; 2; and 3, further below.

**Table 4. 5wt% RuPd/TiO<sub>2</sub> catalysts with varying metal ratios for furfural hydrogenation in methanol at 10 bar H<sub>2</sub>.**

Catalyst	Conv. [%]	Yield [%]				
		FA	2-MF	MTHF	1,2-PeDiol	Others
2.5wt%Ru-2.5wt%Pd /TiO <sub>2</sub>	98	9.5	20.9	3.4	3.4	62.8
1.0wt%Ru-4.0wt%Pd /TiO <sub>2</sub>	100	0	14.8	5	15.3	64.9
0.5wt%Ru-4.5wt%Pd /TiO <sub>2</sub>	99	0	19.8	9.4	15.4	55.4

Reaction conditions: 1.0g Furfural; 0.1 catalyst; 15 mL solvent; 25 °C, 10 bar H<sub>2</sub>, 1000 rpm stirring, 1 h

**Table 5. 5wt% RuPd/TiO<sub>2</sub> catalysts with varying metal ratios for furfural hydrogenation in methanol at 20 bar H<sub>2</sub>.**

Catalyst	Conv. [%]	Yield [%]				
		FA	2-MF	MTHF	1,2-PeDiol	Others
2.5wt%Ru-2.5wt%Pd /TiO <sub>2</sub>	99	0	27.4	7.1	11.5	54
1.0wt%Ru-4.0wt%Pd /TiO <sub>2</sub>	100	1.8	7.8	7.1	23.8	59.5
0.5wt%Ru-4.5wt%Pd /TiO <sub>2</sub>	100	0	8.1	11	23.4	57.5

Reaction conditions: 1.0g Furfural; 0.1 catalyst; 15 mL solvent; 25 °C, 20 bar H<sub>2</sub>, 1000 rpm stirring, 1 h

**Table 6. 5wt% RuPd/TiO<sub>2</sub> catalysts with varying metal ratios for furfural hydrogenation in methanol at 30 bar H<sub>2</sub>.**

Catalyst	Conv. [%]	Yield [%]				
		FA	2-MF	MTHF	1,2-PeDiol	Others
2.5wt%Ru-2.5wt%Pd /TiO <sub>2</sub>	100	1.4	8	3.7	9.1	77.8
1.0wt%Ru-4.0wt%Pd /TiO <sub>2</sub>	100	0	5.6	9.5	14.5	70.4
0.5wt%Ru-4.5wt%Pd /TiO <sub>2</sub>	100	0	6.9	9.7	20.1	63.3

Reaction conditions: 1.0g Furfural; 0.1 catalyst; 15 mL solvent; 25 °C, 30 bar H<sub>2</sub>, 1000 rpm stirring, 1 h

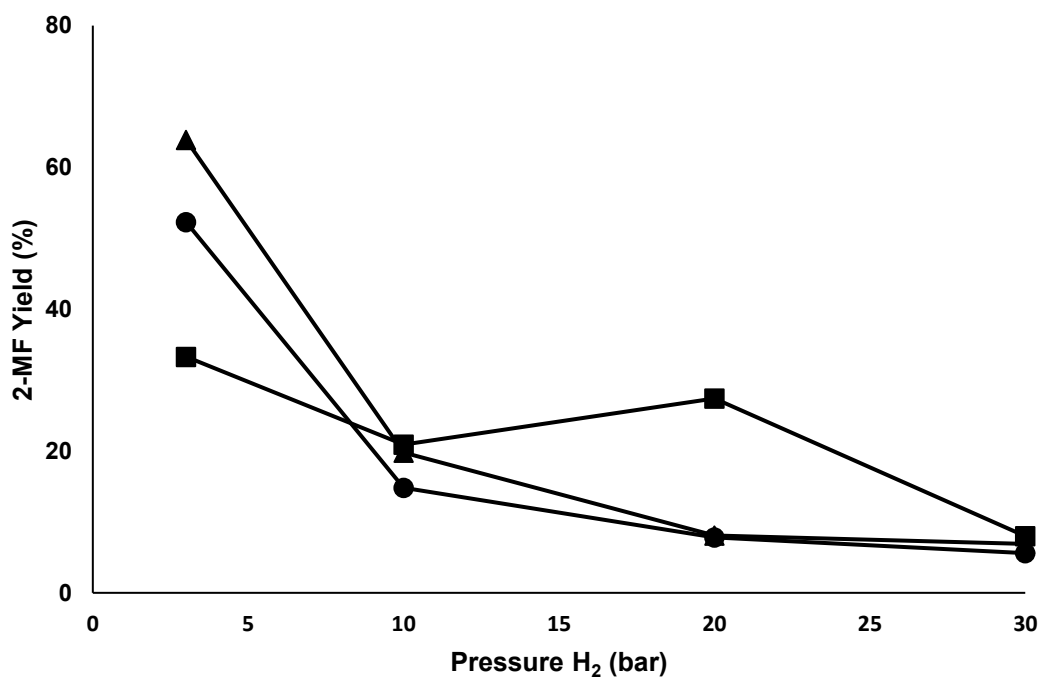


**Figure 1. 2-methylfuran yield (%) as a function of reaction pressure produced from furfural hydrogenation over RuPd/TiO<sub>2</sub> catalysts with varying metal loadings in methanol at room temperature. ▲0.5wt%Ru-4.5wt%Pd/TiO<sub>2</sub> ●1.0wt%Ru-4.0wt%Pd/TiO<sub>2</sub> ■ 2.5wt%Ru-2.5wt%Pd/TiO<sub>2</sub>**

As can be seen from figure 1 above, increasing the reaction pressure above 3 bar  $H_2$  is unfavourable for the production of 2-methylfuran. The quantity of unwanted side products increases with increasing pressure, indicating that reaction pathways other than the hydrogenolysis pathway are more favourable at higher pressures. Whilst hydrogenolysis reactions are occurring to a limited degree at higher pressures, a greater percentage of them are concomitantly followed by hydrogenation of the furan ring to generate the methyltetrahydrofuran product than is observed to occur at lower  $H_2$  pressure (figure 2).

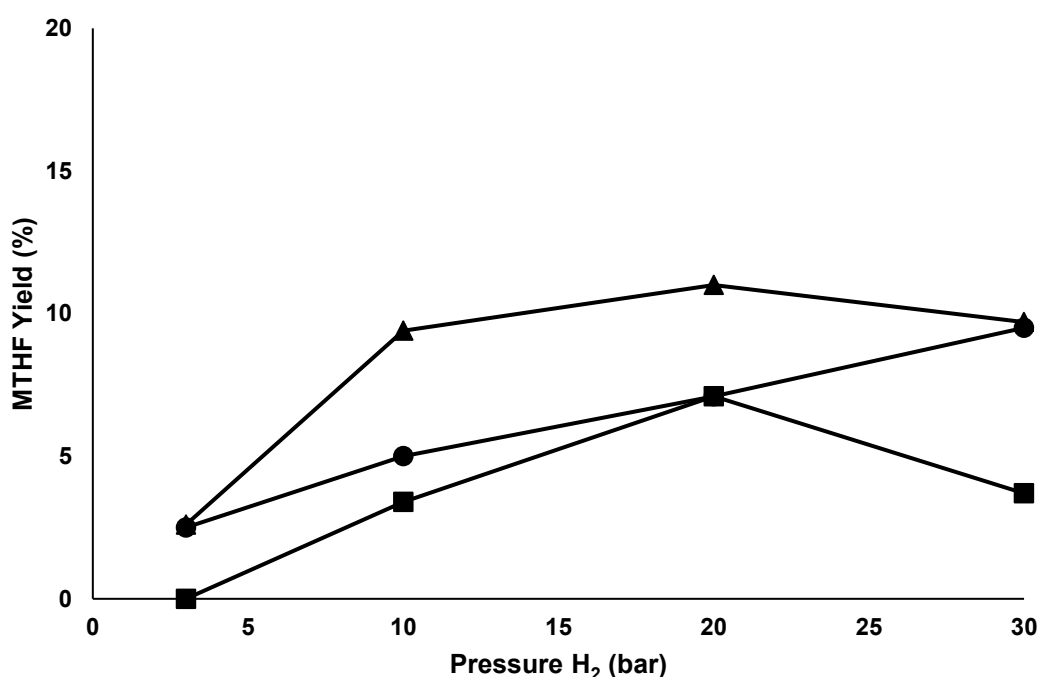


**Figure 2. Methyltetrahydrofuran yield (%) as a function of reaction pressure produced from furfural hydrogenation over RuPd/TiO<sub>2</sub> catalysts with varying metal loadings in methanol at room temperature. ▲ 0.5wt%Ru-4.5wt%Pd/TiO<sub>2</sub> ● 1.0wt%Ru-4.0wt%Pd/TiO<sub>2</sub> ■ 2.5wt%Ru-2.5wt%Pd/TiO<sub>2</sub>**

For all three bimetallic catalysts, 1,2-PeD production was observed to increase with increasing pressure up until 20 bar H<sub>2</sub>, with the two catalysts comprised of higher concentrations of palladium displaying almost identical activity up until this point (figure 3). Above this pressure, 1,2-PeD production is seen to decrease for all three catalysts, with the most significant drop in yield of this desired product being seen with the 1.0wt%Ru-4.0wt%Pd/TiO<sub>2</sub> catalyst. These decreases in activity correlate with an increase in production of side products, suggesting that a number of competing reaction pathways become more favourable at higher pressures.

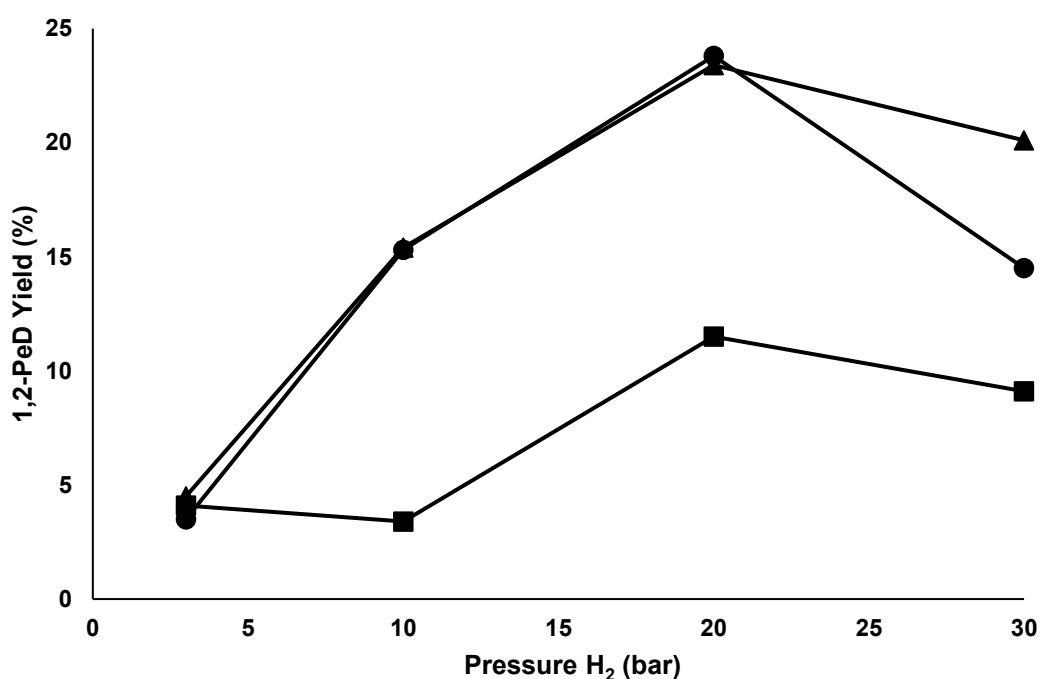


**Figure 3. 1,2-pentanediol yield (%) as a function of reaction pressure produced from furfural hydrogenation over RuPd/TiO<sub>2</sub> catalysts with varying metal loadings in methanol at room temperature. ▲ 0.5wt%Ru-4.5wt%Pd/TiO<sub>2</sub>**

**● 1.0wt%Ru-4.0wt%Pd/TiO<sub>2</sub> ■ 2.5wt%Ru-2.5wt%Pd/TiO<sub>2</sub>**

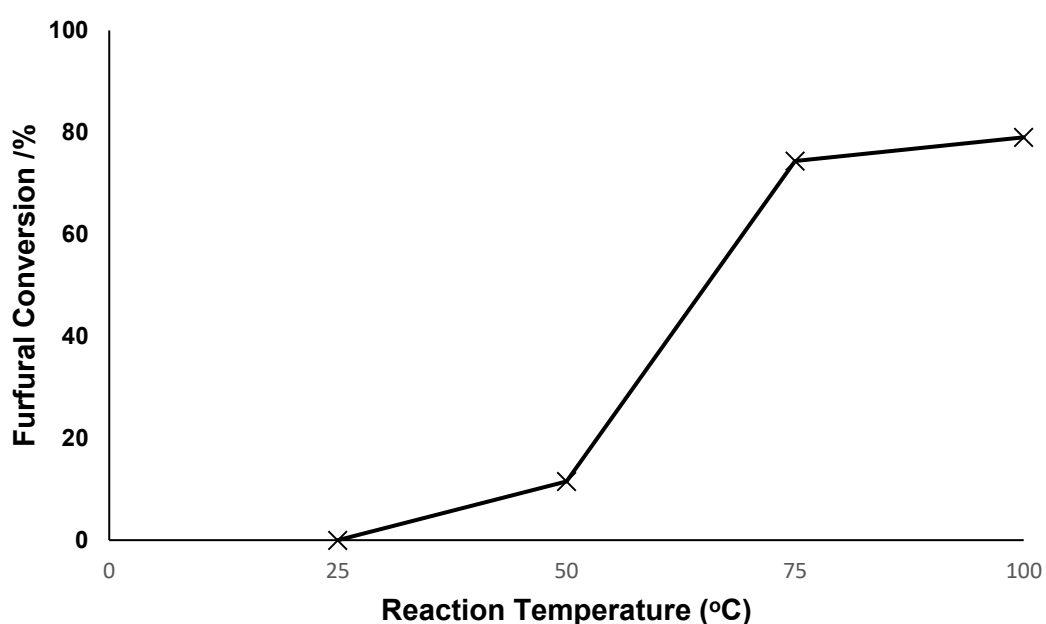
Unfortunately, due to time constraints, no work was undertaken to further explore the activity of the 5wt% RuPd/TiO<sub>2</sub> catalysts with further variations in reaction

parameters. This could certainly form the basis of a future body of work, where furfural conversion as a function of reaction temperature could be an interesting starting point.

### 5wt% Ru/C Catalyst for Furfural Hydrogenation

A commercially available 5wt% Ru/C catalyst has been investigated herein for furfural conversion in methanol at temperatures of up to 100 °C, and hydrogen pressures up to 50 bar. A number of reactions were performed in various solvents at temperatures between 25-100 °C at hydrogen pressures between 1-3 bar, however no conversion was observed under any circumstances. The reactions presented below are therefore performed at pressures between 10 and 50 bar H<sub>2</sub>, where quantitative conversion of furfural could be recorded.

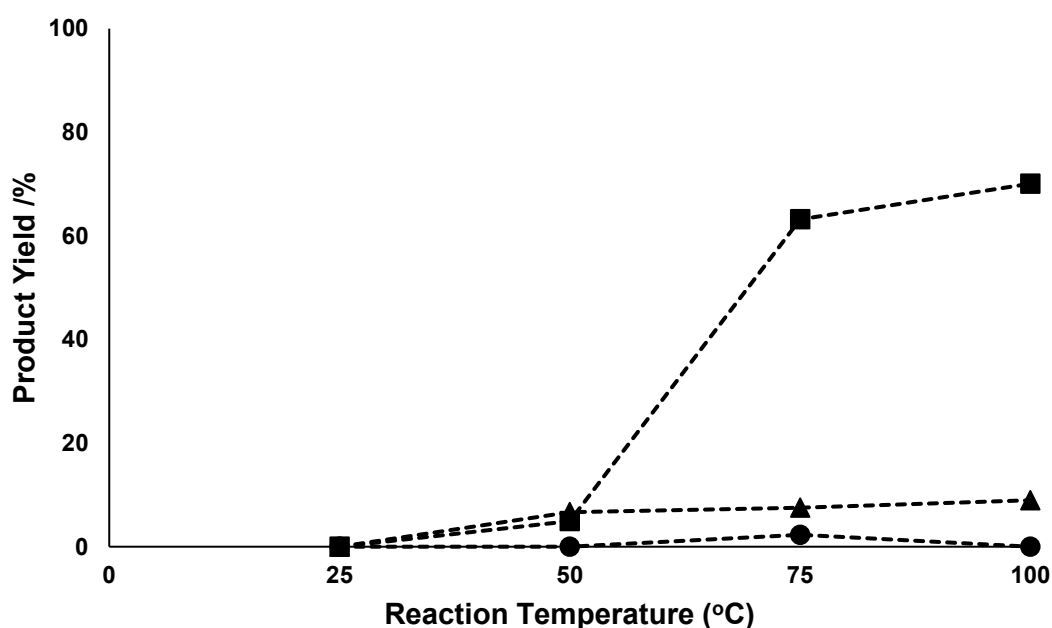
#### Ru/C 10 bar H<sub>2</sub>



**Figure 5. Conversion of furfural with respect to reaction temperature at 10 bar H<sub>2</sub> (reaction conditions)**

Figure 5 shows how conversion of furfural substrate varies with respect to reaction temperature at 10 bar H<sub>2</sub> (reaction conditions). At 25 °C no observable conversion of

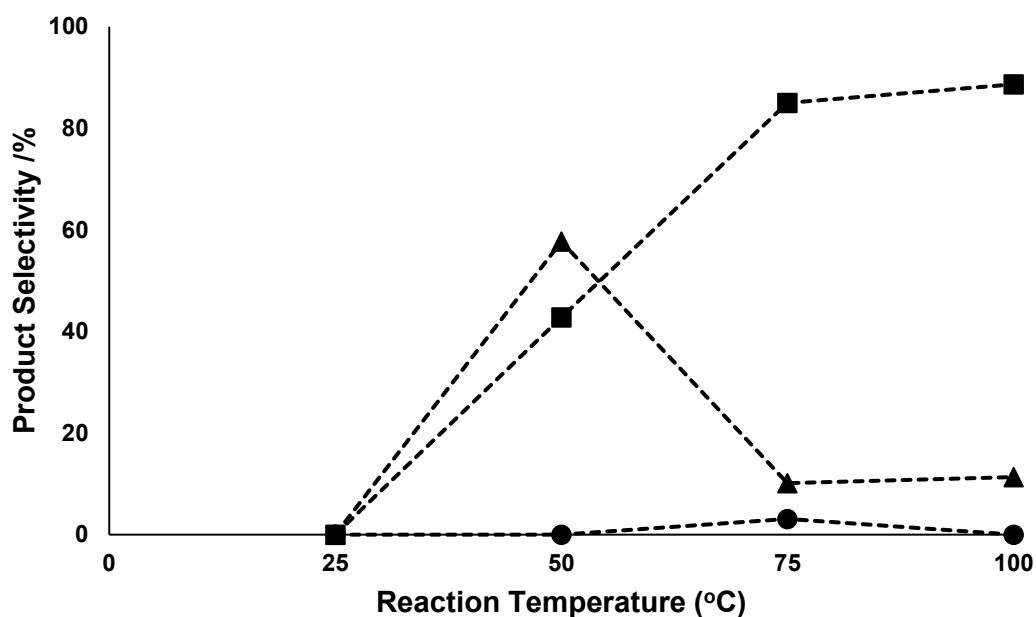
furfural occurred during the course of the 1 hour reaction, however conversion is noticeably evident when the reaction temperature is set at 50 °C, with approximately 12% of the starting material being converted to product. With a reaction temperature of 75 °C a significant increase in furfural conversion was achieved, with 74 % of the substrate undergoing reaction. Furfural conversion was increased to 79 % by further raising the reaction temperature to 100 °C.



**Figure 6. Yield (%) of reaction products: ▲ furfuryl alcohol; ■ 1,2-pentanediol; and ● 2-methylfuran, for the hydrogenation of furfural with respect to temperature at 10 bar H<sub>2</sub> (reaction conditions)**

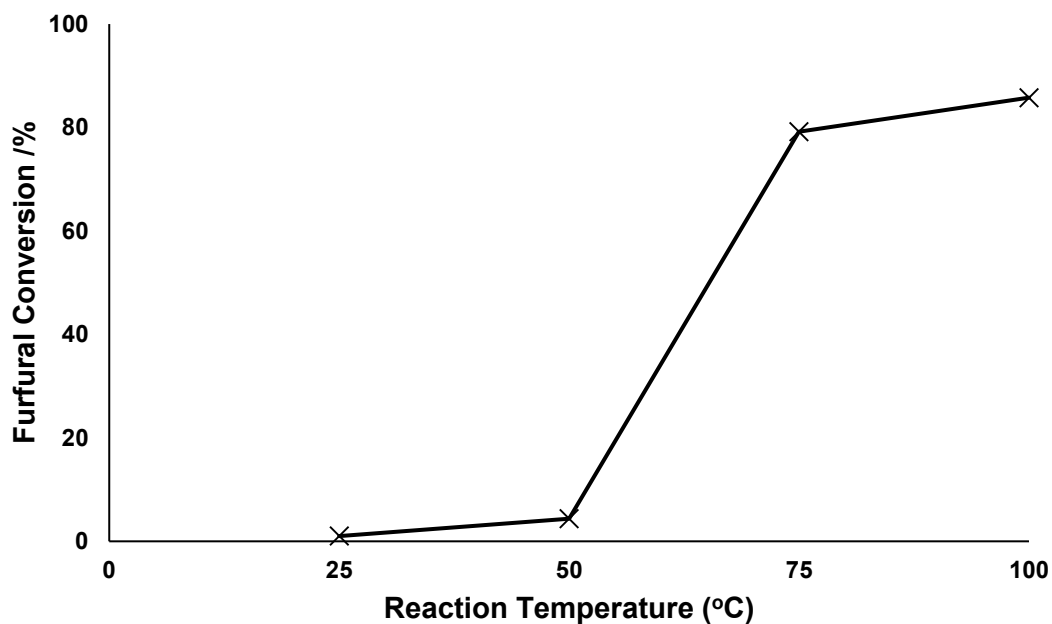
Figure 6 shows the yield and distribution of products obtained at different reaction temperatures at 10 bar H<sub>2</sub> corresponding with the respective levels of conversion of furfural substrate as displayed in figure 5, at (reaction conditions). At a reaction temperature of 25 °C no products were observed after 1 hour due to the substrate not undergoing reaction, however at 50 °C the reaction products FA, and 1,2-PeD were obtained at yields of 6.6 and 4.9 % respectively. When the reaction was performed at

75°C the FA yield increased to 7.5 %, with the yield of 1,2-PeDI rising significantly to 63 %. A small amount of 2-MF (~ 2.0 %) was also produced under these conditions.



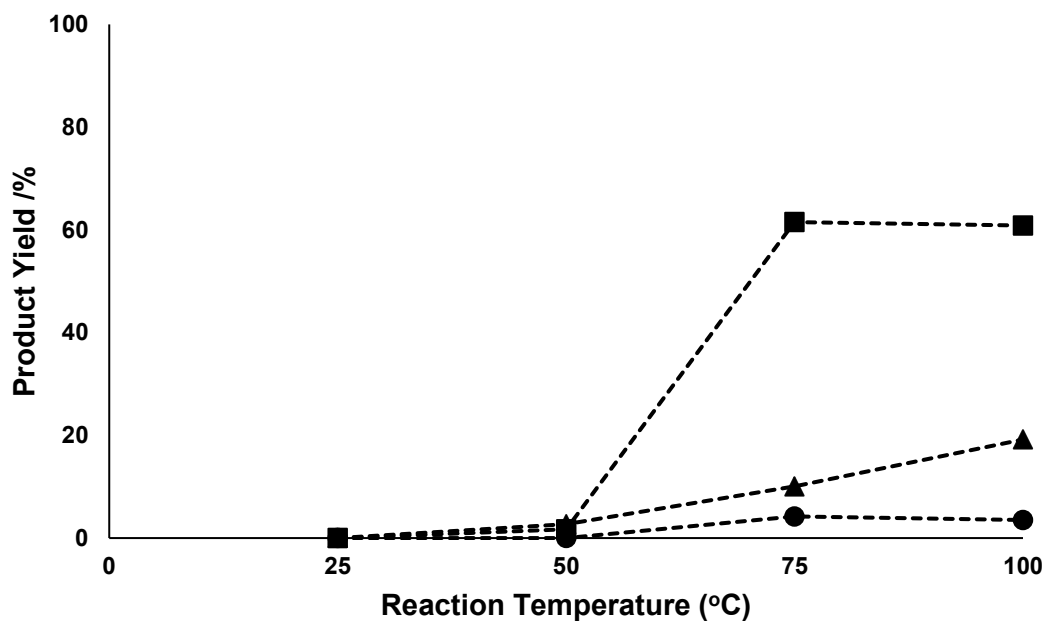
**Figure 7. selectivity (%) to the reaction products: ▲ furfuryl alcohol; ■ 1,2-pentanediol; and ● 2-methylfuran, for the hydrogenation of furfural with respect to temperature at 10 bar H<sub>2</sub> (reaction conditions)**

With no substrate conversion at 25 °C, an increase in reaction temperature to 50 °C was seen to afford a product selectivity towards FA of 57%, and 1,2-PeD of 43%. Selectivity towards FA dropped and levelled off at higher temperatures, with selectivity towards 1,2-PeD increasing. Small quantities of 2-MF were only seen at 75 °C.

**20 bar H<sub>2</sub>**

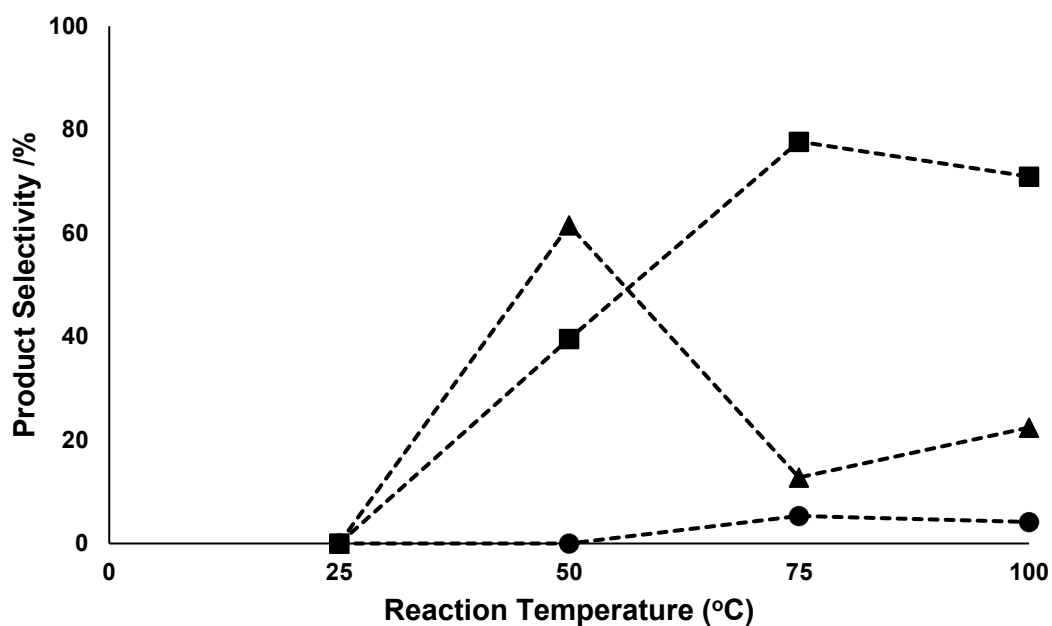
**Figure 8. Conversion of furfural with respect to reaction temperature at 20 bar H<sub>2</sub> (reaction conditions)**

Very low catalytic activity was observed at a reaction temperature of 25 °C under 20 bar H<sub>2</sub> with only 1% furfural conversion occurring over the course of the reaction. Conversion was seen to increase substantially over temperatures of 50 °C, with around 80% conversion seen at 75 °C. Conversion increased marginally with a further reaction temperature increase of 25 °C.



**Figure 9. Yield (%) of reaction products: ▲ furfuryl alcohol; ■ 1,2-pentanediol; and ● 2-methylfuran, for the hydrogenation of furfural with respect to temperature at 20 bar H<sub>2</sub> (reaction conditions)**

With very low product FA and 2-MF yields at 50 °C, a reaction temperature of 75 °C afforded a 60% yield of 1,2-PeD, and approximately 10% Fa, and 3% 2-MF. At 100 °C no further increase in 1,2-PeD or 2-MF could be detected, however FA yield was seen to rise to 20%.

30 bar H<sub>2</sub>

**Figure 10. selectivity (%) to the reaction products: ▲ furfuryl alcohol; ■ 1,2-pentanediol; and ● 2-methylfuran, for the hydrogenation of furfural with respect to temperature at 20 bar H<sub>2</sub> (reaction conditions)**

As can be seen from figure 10 above, selectivity to 1,2-PeD increased with increasing temperature between 25-75 °C, dropping off between 75 and 100°C. Selectivity to 2-MF was around 5% over 50 °C, with FA product selectivity decreasing sharply between 50 and 75°C before rising slightly at 100 °C.

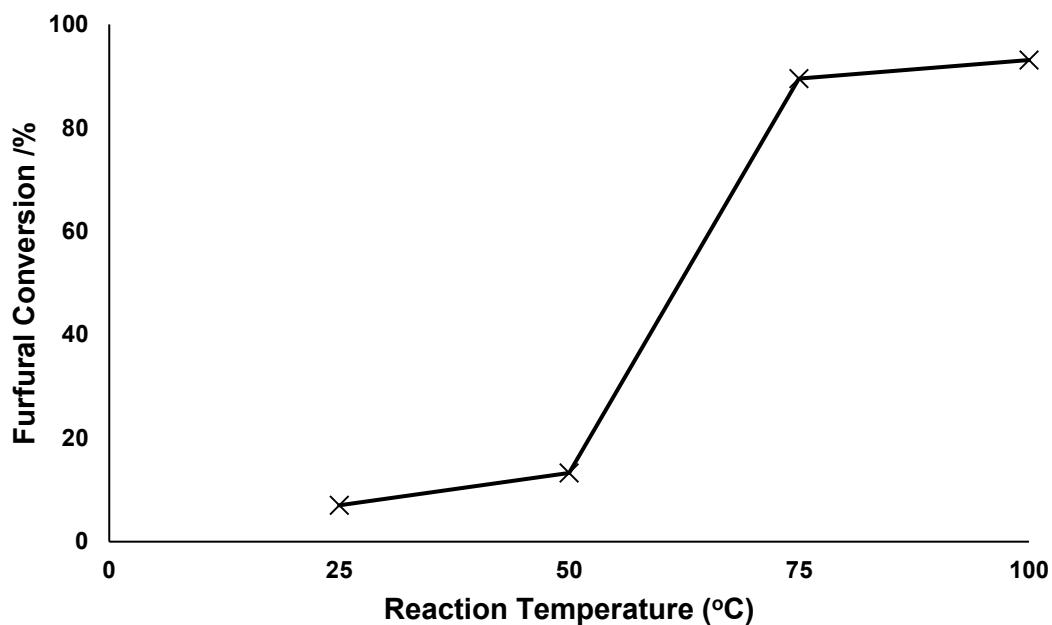


**Figure 11. Conversion of furfural with respect to reaction temperature at 30 bar H<sub>2</sub> (reaction conditions)**

At 30 bar H<sub>2</sub> conversion of furfural (7%) can be seen for the first time at the lowest reaction temperature of 25 °C. 13% conversion is observed at 50 °C, and significantly increases to almost 90% at 75°C. A further increase in temperature only marginally increases conversion above 90%.

Product yield of all three desired products was seen to increase between 25 and 50 °C, with yield of 1,2-PeD and FA increasing sharply at 75 °C and levelling off at 100 °C. This is shown in figure 12

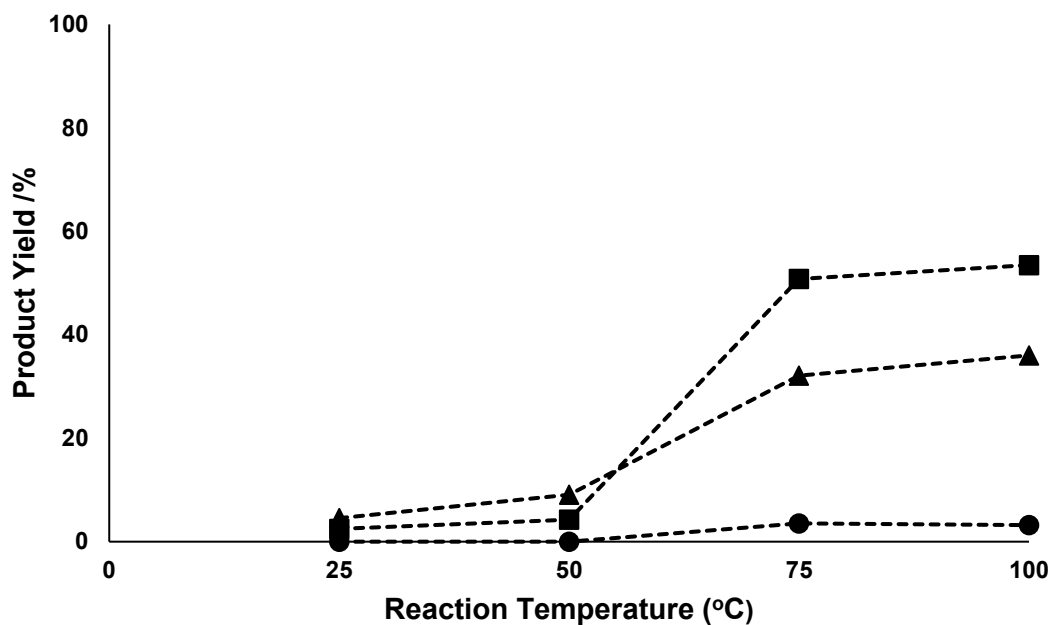


Figure 12. Yield (%) of reaction products: ▲ furfuryl alcohol; ■ 1,2-pentanediol; and ● 2-methylfuran, for the hydrogenation of furfural with respect to temperature at 30 bar H<sub>2</sub> (reaction conditions)

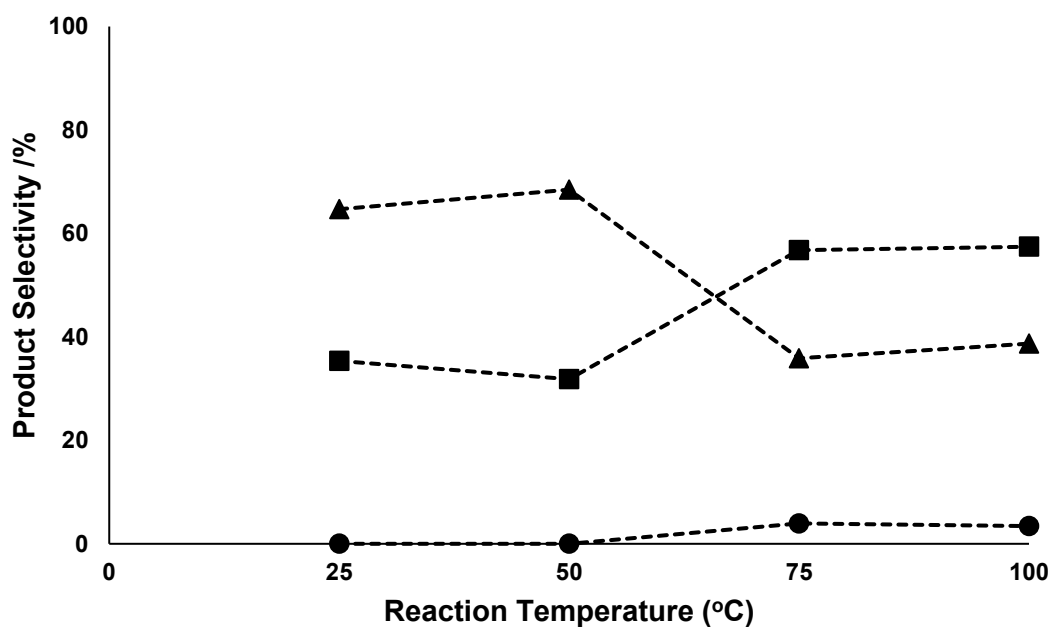
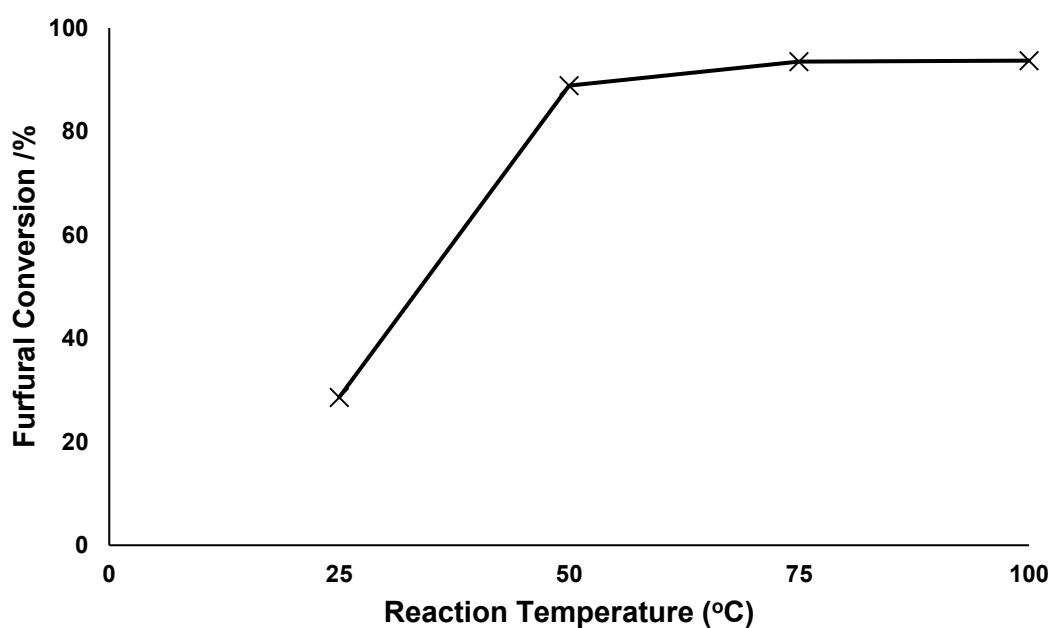


Figure 13. selectivity (%) to the reaction products: ▲ furfuryl alcohol; ■ 1,2-pentanediol; and ● 2-methylfuran, for the hydrogenation of furfural with respect to temperature at 30 bar H<sub>2</sub> (reaction conditions)

The selectivity (%) to the desired products FA, 1,2-PeD, and 2-MF for 5wt%Ru/C catalysed furfural hydrogenation can be seen in figure 13, selectivity to FA is around 65% at 25 and 50 °C, decreasing to around 30% at 75 and 100 °C, whilst selectivity to 1,2-PeD appears to behave almost inversely to that of FA. Selectivity to 2-MF is relatively low across the temperature range.



**Figure 14. Conversion of furfural with respect to reaction temperature at 40 bar H<sub>2</sub> (reaction conditions)**

At 40 bar H<sub>2</sub> a 29% furfural conversion is observed at reaction temperature of 25 °C, 89% at 50 °C, and 93 at 75 °C. Further increasing the temperature above 75 °C does not afford an increase in substrate conversion.

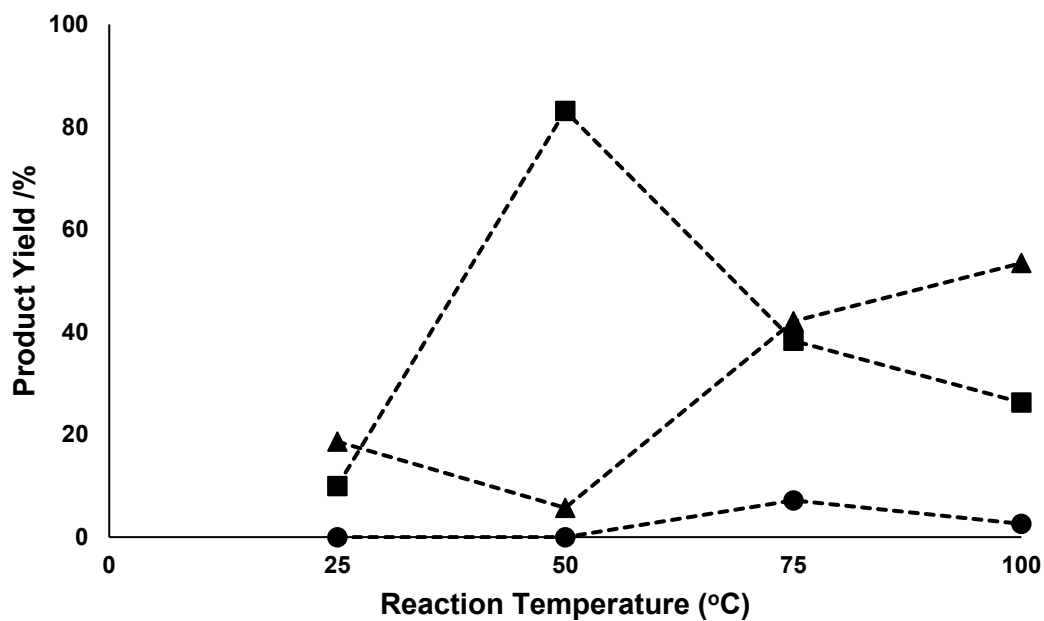


**Figure 15. Yield (%) of reaction products: ▲ furfuryl alcohol; ■ 1,2-pentanediol; and ● 2-methylfuran, for the hydrogenation of furfural with respect to temperature at 40 bar H<sub>2</sub> (reaction conditions)**

As can be seen from figure 15, at 40 bar H<sub>2</sub> the greatest product yield observed is that of 1,2-PeD which is formed almost exclusively (83%) at 50 °C. Increasing the temperature serves to decrease 1,2-PeD yield whilst concomitantly increasing the yield of furfuryl alcohol.

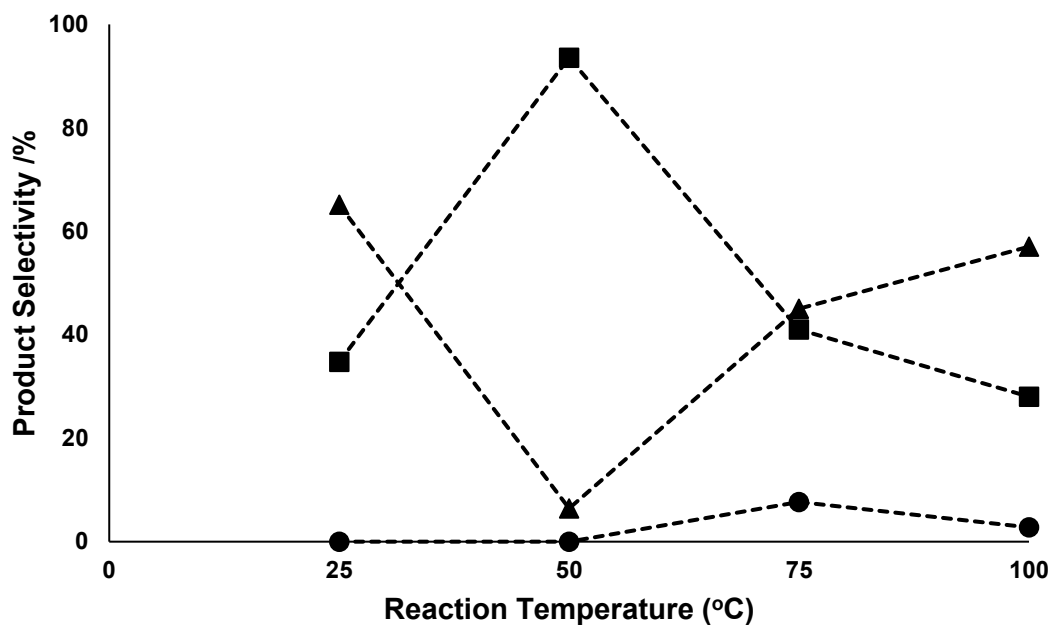


**Figure 16. selectivity (%) to the reaction products: ▲ furfuryl alcohol; ■ 1,2-pentenediol; and ● 2-methylfuran, for the hydrogenation of furfural with respect to temperature at 40 bar H<sub>2</sub> (reaction conditions)**

Selectivity to FA (65%) is highest at 25 °C and lowest (6%) at 50 °C with almost the opposite trend observed for 1,2-PeD, with 35% selectivity to 1,2-PeD at 25 °C and 94% selectivity at 50 °C. At above 75 °C selectivity to 1,2-PeD drops dramatically, whilst selectivity towards FA increases. The highest selectivity to 2-MF (8%) can be seen at 75 °C.

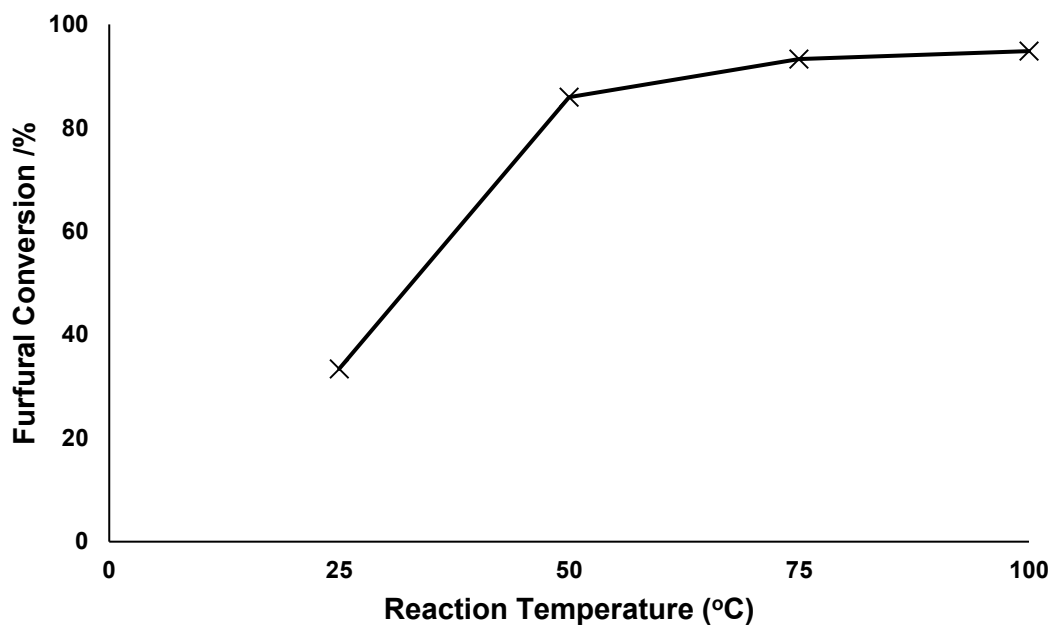


**Figure 17. Conversion of furfural with respect to reaction temperature at 50 bar H<sub>2</sub> (reaction conditions)**

At 50 bar H<sub>2</sub> a 33% furfural conversion is observed at reaction temperature of 25 °C, 86% at 50 °C, and 93 at 75 °C. Further increasing the temperature above 75 °C only increases the conversion by a marginal 1%.

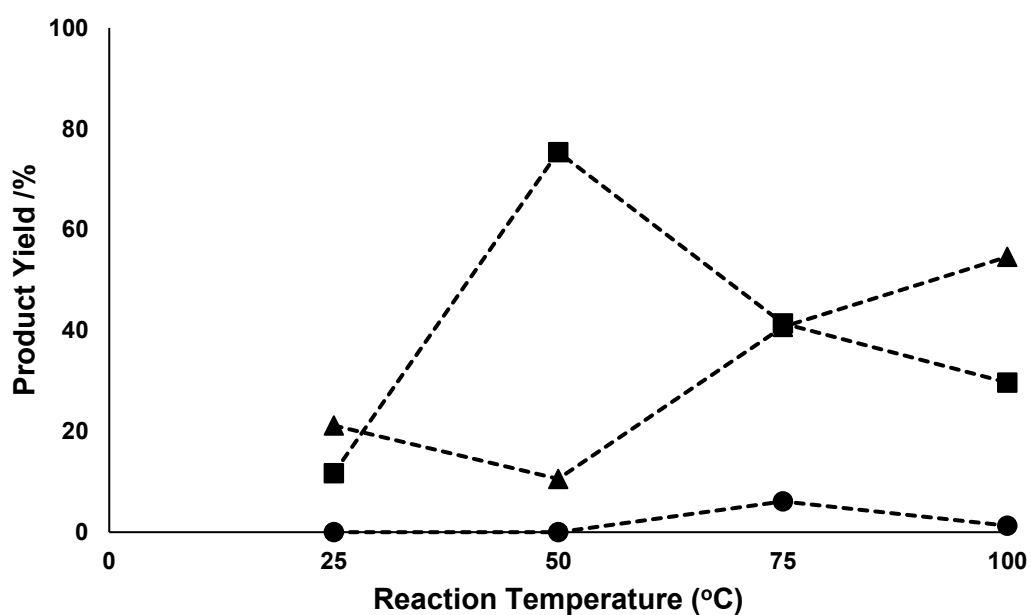


**Figure 18. Yield (%) of reaction products: ▲ furfuryl alcohol; ■ 1,2-pentanediol; and ● 2-methylfuran, for the hydrogenation of furfural with respect to temperature at 50 bar H<sub>2</sub> (reaction conditions)**

At 25 °C both FA and 1,2-PeD are produced at 50 bar H<sub>2</sub>, with product yields of 21% and 12% respectively. FA yield is seen to decrease slightly as the reaction temperature is increased to 50 °C, whereas 1,2-PeD yield increases dramatically to 75%. Increasing the reaction temperature further increases production of FA whilst concomitantly lowering the production of 1,2-PeD. A product yield of 6% 2-MF can be seen at 75 °C.

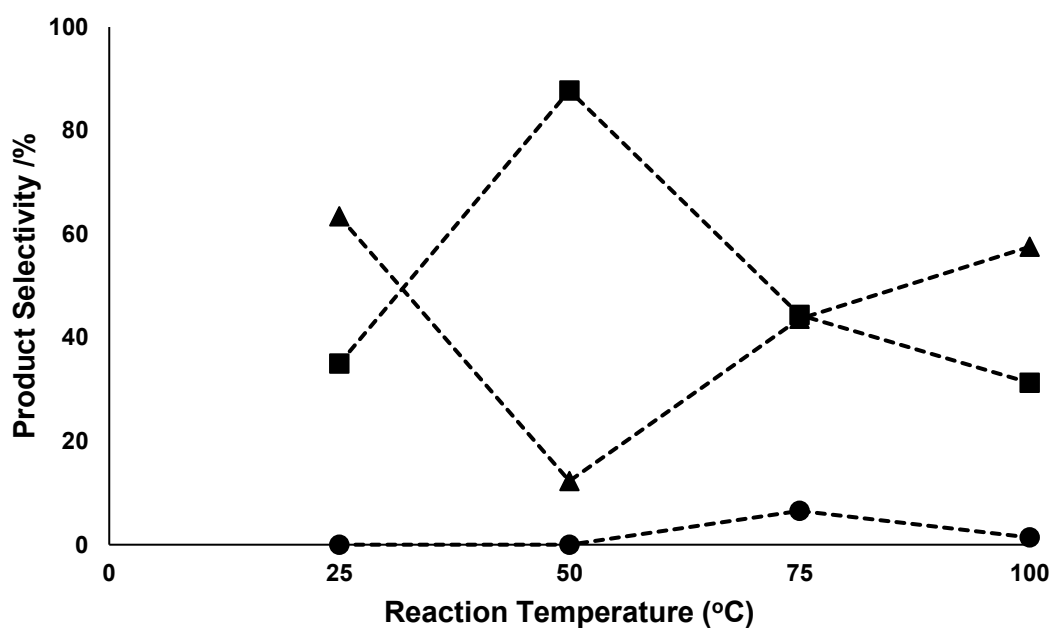


**Figure 19. selectivity (%) to the reaction products: ▲ furfuryl alcohol; ■ 1,2-pentanediol; and ● 2-methylfuran, for the hydrogenation of furfural with respect to temperature at 50 bar H<sub>2</sub> (reaction conditions)**

Selectivity to FA is relatively high (63%) at 25 °C, but drops substantially to 12% when the reaction temperature is raised to 50 °C. Above this temperature, selectivity to FA

increases further, reaching 58% at 100 °C. Selectivity to 1,2-PeD is observed to be 35% at the lowest reaction temperature, rises significantly to 88% at 50 °C, before dropping dramatically with increasing temperature, reaching 31% at 100°C. A selectivity of 6.5% to 2-MF can be seen at 75 °C.

### 5.3 Discussion

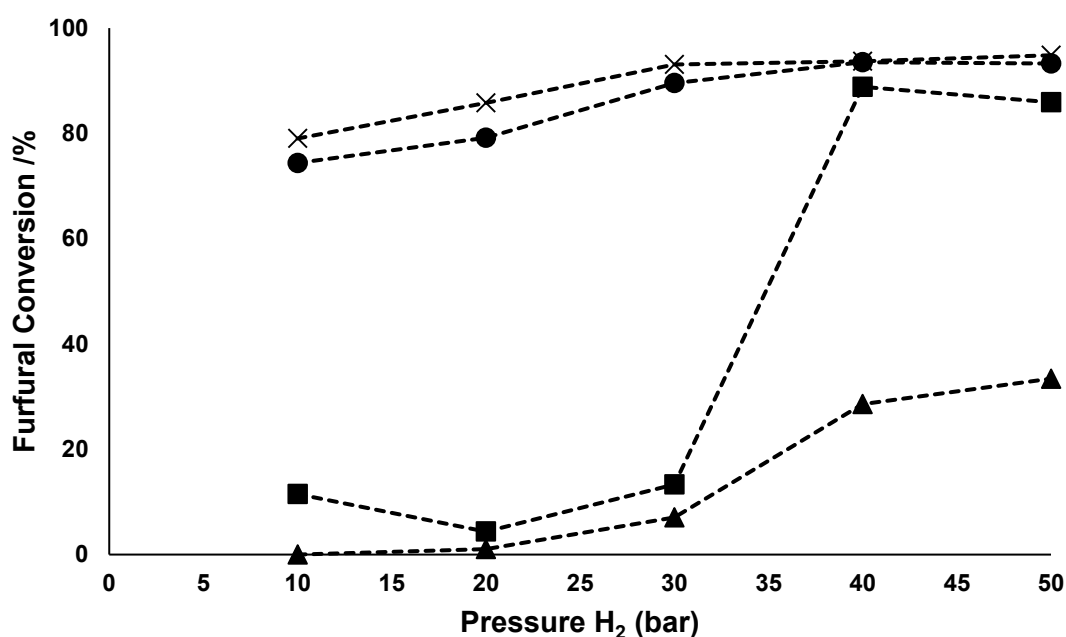


**Figure 20. Furfural conversion as a function of hydrogen pressure (bar) at different temperatures. ▲ 25 °C; ■ 50 °C; ● 75 °C; X 100 °C**

As can be seen from figure 20 above, furfural hydrogenation increases with temperature, however the extent to which conversion is moderated by temperature changes dramatically with reaction pressure. At temperatures of 75 and 100 °C, increasing pressure incrementally doesn't appear to alter the level of furfural conversion too substantially. At lower temperatures however, a significant rise in furfural conversion is observed for the reaction performed at 50 °C when the pressure

is increased from 30 to 40 bar  $H_2$ . From figure 21 below, it can be seen that under these conditions the reaction pathway to 1,2-PeD is operating with very high selectivity, meaning that ring-opening is extremely favourable under these conditions, with the hydrogenolysis pathway being largely avoided. This shows that selectivity to a desired product can be tuned by control of the reaction temperature and pressure.

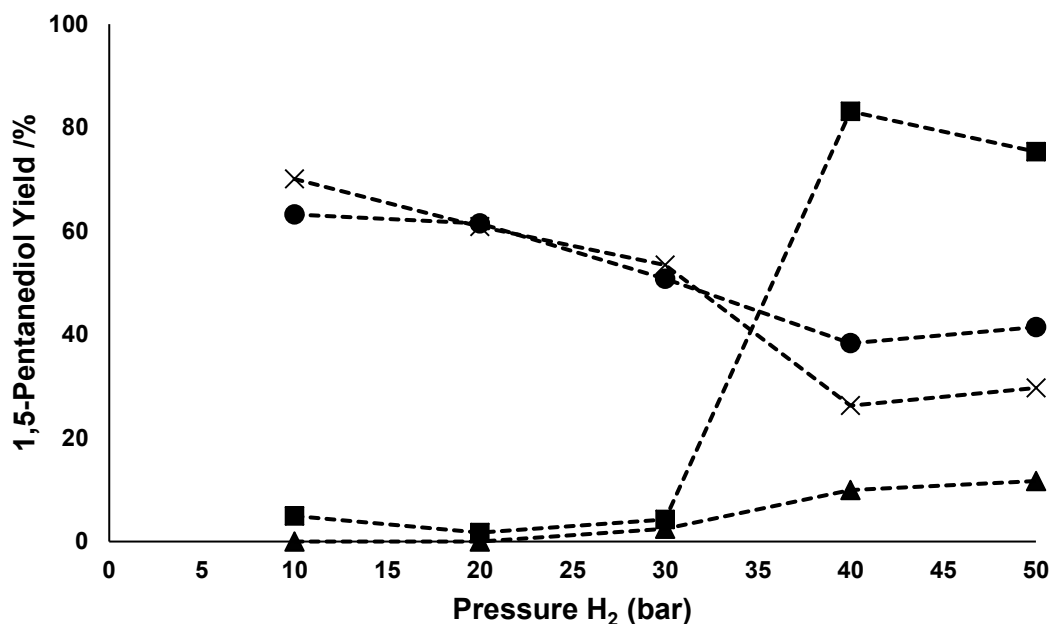


**Figure 21. 1,2-Pentanediol yield (%) as a function of hydrogen pressure (bar) at different temperatures. ▲ 25 °C; ■ 50 °C; ● 75 °C; X 100 °C**

Generally it can be seen that for a given hydrogen pressure between 10 and 30 bar, temperatures of 75 °C and above are more favourable for production of 1,2-PeD. At pressures of 40 and 50 bar, moderate temperatures of 50 and 75 °C are more favourable for 1,2-PeD synthesis than the outlying reaction temperatures of 25 and 100 °C

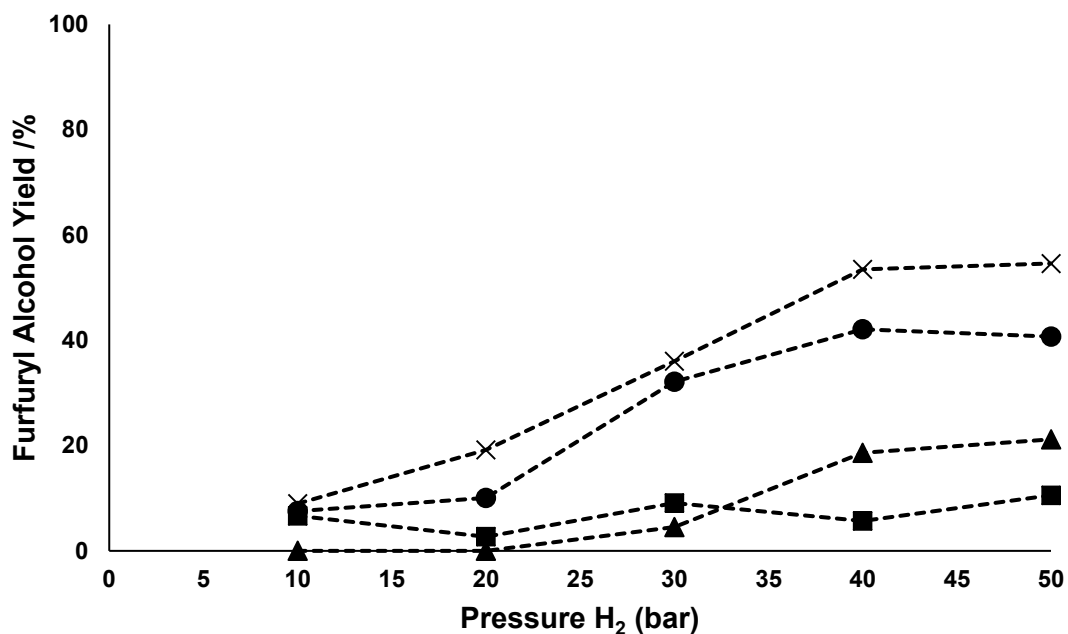


**Figure 22. Furfuryl alcohol yield (%) as a function of hydrogen pressure (bar) at different temperatures. ▲ 25 °C; ■ 50 °C; ● 75 °C; X 100 °C**

Furfuryl alcohol synthesis was observed to increase with increasing pressure, with production of this desired product more favourable at higher temperatures and higher pressures. This suggests that under these conditions, the reaction pathway that facilitates hydrogenolysis of the furfural substrate becomes generally more favourable than at lower temperatures and pressures.

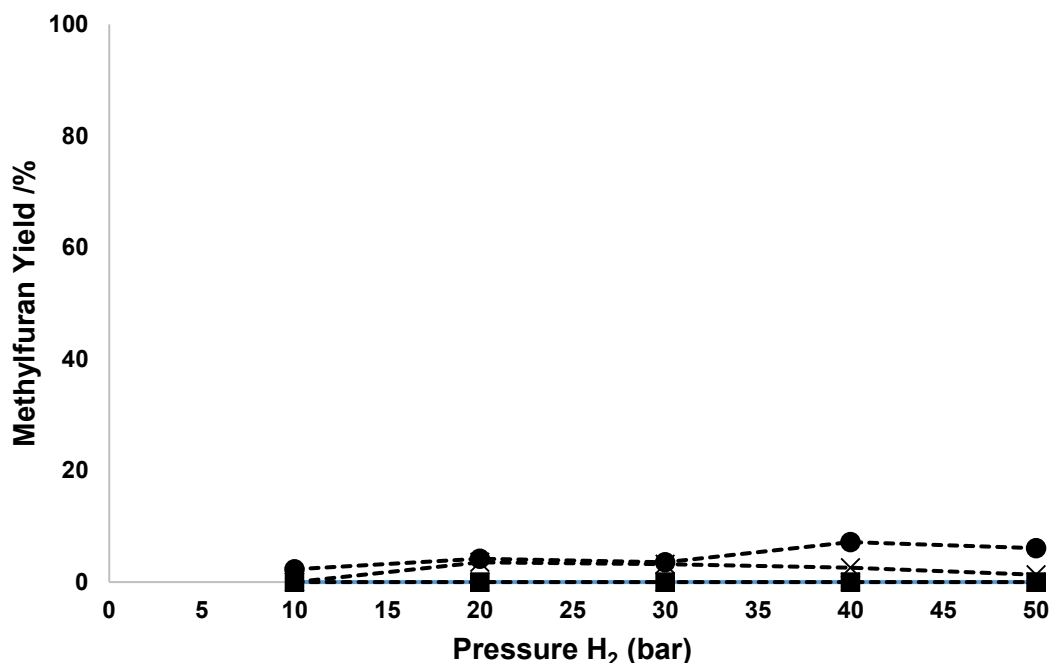


**Figure 22. 2-methylfuran (%) as a function of hydrogen pressure (bar) at different temperatures. ▲ 25 °C; ■ 50 °C; ● 75 °C; X 100 °C**

2-Methylfuran production is low across all reaction parameters tested, however it is most favourable at 75 °C with 40 bar H<sub>2</sub> pressure (figure 22).

In order to shed light on the origin of the catalytic activities described above it would be helpful to characterise the Ru/C catalyst tested. The same commercially available 5wt% Ru/C catalyst presented here has previously been extensively characterised by the Hutchings group for the hydrogenation of lactic acid, where it was reported that treatment under the reaction conditions facilitated the changing of ruthenium from raft-like morphologies to the desired nanoparticle morphologies which were required for catalytic activity.<sup>31</sup> It would be of interest to explore the conversion of furfural over the 5wt% Ru/C catalyst as function of time and to conduct corresponding investigations into the morphology of the catalyst to explore the changing structure of the catalyst in the furfural system and to relate physical changes to observed

differences in selectivity. Unfortunately, due to time constraints, this has not been performed in this body of work.

## 5.4 Conclusions

Research has been conducted into the efficacy of monometallic palladium catalysts, bimetallic palladium catalysts modified with ruthenium, and a carbon supported monometallic ruthenium catalyst for the hydrogenation of furfural. Through variation of the metal ratio for the bimetallic catalyst it was shown that addition of small quantities of ruthenium can improve the selectivity towards 2-MF when compared to the monometallic 5wt% Pd/TiO<sub>2</sub>. Increasing the pressure was seen to decrease selectivity towards desired products and increase the amount of unwanted side products formed. By raising the temperature and pressure, the selectivity pattern to desired products was observed to vary dramatically, showing that full exploration of the reaction space is important in order to properly map product selectivities.

## 5.5 References

1. D. Liu, D. Zemlyanov, T. Wu, R. J. Lobo-Lapidus, J. A. Dumesic, J. T. Miller and C. L. Marshall, *J. Catal.*, 2013, 299, 336–345.
2. H. Zhang, C. Canlas, A. Jeremy Kropf, J. W. Elam, J. A. Dumesic and C. L. Marshall, *J. Catal.*, 2015, 326, 172–181.
3. D. Vargas-Hernandez, J. M. Rubio-Caballero, J. SantamariaGonzalez, R. Moreno-Tost, J. M. Merida-Robles, M. A. Perez Cruz, A. Jimenez-Lopez, R. Hernandez-Huesca and P. MairelesTorres, *J. Mol. Catal. A: Chem.*, 2014, 383–384, 106–113.
4. M. M. Villaverde, N. M. Bertero, T. F. Garetto and A. J. Marchi, *Catal. Today*, 2013, 213, 87–92.
5. Z. Li, G. Wang and W. Li, *Adv. Mater. Res.*, 2012, 599, 27–31.
6. J. G. M. Bremner and R. K. F. Keeys, *J. Chem. Soc.*, 1947, 1068–1080.
7. Y.-L. Zhu, H.-W. Xiang, Y.-W. Li, H. Jiao, G.-S. Wu, B. Zhong and G.-Q. Guo, *New J. Chem.*, 2003, 27, 208–210.
8. J. Lessard, J.-F. Morin, J.-F. Wehrung, D. Magnin and E. Chornet, *Top. Catal.*, 2010, 53, 1231–1234.
9. F. Dong, Y. Zhu, G. Ding, J. Cui, X. Li and Y. Li, *ChemSusChem*, 2015, 8, 1534–1537.
10. K. Fulajtarova, T. Sotak, M. Hronec, I. Vavra, E. Dobrocka and M. Omastova, *Appl. Catal., A*, 2015, 502, 78–85.

11. Y. Wang, M. Zhou, T. Wang and G. Xiao, *Catal. Lett.*, 2015, 145, 1557–1565.
12. C. Xu, L. Zheng, D. Deng, J. Liu and S. Liu, *Catal. Commun.*, 2011, 12, 996–999.
13. P. Panagiotopoulou, N. Martin and D. G. Vlachos, *ChemSusChem*, 2015, 8, 2046–2054.
14. M. J. Gilkey, P. Panagiotopoulou, A. V. Mironenko, G. R. Jenness, D. G. Vlachos and B. Xu, *ACS Catal.*, 2015, 5, 3988–3994.
15. S. Sitthisa, W. An and D. E. Resasco, *J. Catal.*, 2011, 284, 90–101.
16. Z. Li, S. Kelkar, C. H. Lam, K. Luczek, J. E. Jackson, D. J. Miller and C. M. Saffron, *Electrochim. Acta*, 2012, 64, 87–93.
17. H.-Y. Zheng, Y.-L. Zhu, B.-T. Teng, Z.-Q. Bai, C.-H. Zhang, H.-W. Xiang and Y.-W. Li, *J. Mol. Catal. A: Chem.*, 2006, 246, 18–23.
18. C. Mohr, P. Claus, *Sci. Progress* 2001, 84, 311.
19. P. Mäki-Arvela, J. Hájek, T. Salmi, and D. Yu. Murzin, *Appl. Catal., A*, 2005, 292, 1-49.
20. A.M. Silva, O.A.A. Santos, M.J. Mendes, E. Jordaño, M.A. Fraga, *Appl. Catal. A*, 2003 241, 155.
21. B. Bachiller-Baeza, A. Guerrero-Ruiz, P. Wang, I. Rodríguez-Ramos, *J. Catal.* 2001, 204, 450.
22. T. Gerlach, H.-G. Gobbel, F. Funke, K. Ebel, E. Schwab, S. Unverricht, R. Korner, L. Lobree, US 01149310, 2003
23. M.A. Keane, *J. Mol. Catal. A: Chem.* 1997, 118, 261

24. M. Casagrande, L. Storaro, A. Talon, M. Lenarda, R. Frattini, E. Rodríguez-Castellón, P. Maireles-Torres, *J. Mol. Catal. A: Chem.* 2002, 118, 133.
25. J. Hašek, N. Kumar, T. Salmi, D.Yu. Murzin, *Ind. Eng. Chem. Res.* 2003, 42, 295
26. M. Kuzma, L. Červený, *Res. Chem. Intermed.* 2000, 26, 347
27. O.F. Aldosari, S. Iqbal, P.J. Miedziak, G.L. Brett, D.R. Jones, X.Liu, J.K. Edwards, D.J. Morgan, D.K. Knight, and G.J. Hutchings. *Catal. Sci. Technol.*, 2016, 6, 234
28. P. Panagiotopoulou, D.G. Vlachos. *Appl. Catal. A*, 2014, 480, 17.
29. S. Iqbal, X. Liu, O.F. Aldosari, P.J. Miedziak, J.K. Edwards, G.L. Brett, A. Akram, G.M. King, T.E. Davies, D.J. Morgan, D.K. Knight, and G.J. Hutchings, *Catal. Sci. Technol.*, 2014, 4, 2280.
30. G.M. King, S. Iqbal, P.J. Miedziak, G.L. Brett, S.A. Kondrat, B.R. Yeo, X. Liu, J.K. Edwards, D.J. Morgan, D.K. Knight, and G.J. Hutchings, *ChemCatChem*, 2015, 7, 2122.
31. S. Iqbal, S.A. Kondrat, D.R. Jones, D.C. Schoenmakers, J.K. Edwards, L. Lu, B.R. Yeo, P.P. Wells, E.K. Gibson, D.J. Morgan, C.J. Kiely, and Graham J. Hutchings, *ACS Catal.* 2015, 5, 5047.

## 6. Conclusions and Future Work

The aims and objectives of the work presented in this thesis were to: investigate and optimise the catalytic parameters of titania supported gold:palladium catalysts; and to prepare and investigate the activity of heterogeneous catalysts for the selective hydrogenation of lignocellulosic furfural, and furfuryl alcohol substrates into value added products.

Through the physical grinding of gold and palladium metal acetate precursors it was shown that chloride free catalysts could be produced. Furthermore, these catalysts were shown to display significantly enhanced activity when compared to analogous catalysts prepared by alternative methods for the oxidation of benzyl alcohol and glycerol substrates, and for the direct synthesis of hydrogen peroxide. By lowering the total metal weight loading to an optimised level, high TOFs could be achieved which suggests that catalysts comprised of higher metal weight loadings may have a substantial proportion of metal being present in non-active, spectator states.

It has been demonstrated that 5wt%Pd/TiO<sub>2</sub> catalysts prepared by the impregnation method can be highly active for the selective hydrogenolysis of furfuryl alcohol substrate to 2-methylfuran, a highly desirable product with biofuel blending applications, at room temperature and under low hydrogen pressures. By comparison with an analogous, benchmarking, commercially available catalyst it was elucidated that mean palladium particle size can have a marked difference on the selectivity pattern of Pd/TiO<sub>2</sub> catalysts, with particles below the level of XRD detection (*ca.* < 5 nm) being responsible for the observed increased activity. Modification of 5wt%Pd/TiO<sub>2</sub> catalysts by addition of tin in varying ratios was shown to alter the selectivity pattern to products, with reaction pathways favouring the production of the ring-saturated products tetrahydrofurfuryl alcohol, and methyltetrahydrofuran being observed at low tin ratios. Differences in catalyst activity were observed with varying

tin loadings, as relative concentrations of palladium species were seen to be effected. It was postulated that hindering of access of reactants to palladium sites by tin species resulted in different reaction pathways being available.

Experimental work has been conducted into exploring the efficacy of 5wt% monometallic palladium catalysts, bimetallic palladium catalysts modified with ruthenium, and a carbon supported monometallic ruthenium catalyst for furfural hydrogenation. Via variation of the metal ratio for the RuPd catalyst it was shown that addition of small quantities of ruthenium can improve the selectivity towards 2-methylfuran compared to the activity observed for the ruthenium-free monometallic 5wt% Pd/TiO<sub>2</sub>. Raising the pressure was seen to significantly lower the selectivity towards desired products and increase the amount of unwanted side products formed. By raising the temperature and pressure, the selectivity profile to desired products was seen to vary dramatically, showing that full exploration of the reaction space is crucial in order to properly map the production of products with varying reaction conditions.

With regard to the catalysts prepared by the physical grinding methodology, it would be interesting if future research could be conducted to explore as to whether a planetary ball mill could be employed to accurately replicate the manual physical grinding technique to produce highly active AuPd/TiO<sub>2</sub> catalysts. If successful this could pave the way for alternative solvent-free commercial catalyst production methods. The preparation parameters would have to be investigated in detail as gold (III)acetate decomposes exothermically. Also of interest would be to incrementally dope Cl<sup>-</sup> ions into the chloride-free physically ground catalysts by way of palladium (II)chloride. This would allow for the further investigation into the effect of halogen contamination on selected reactions.

With regard to furfural and furfuryl alcohol substrates, there is huge scope for further work, in particular, directed at trying to selectively produce the ring-saturated product methyltetrahydrofuran (MTHF). Current production methods employ copper chromite catalysts operating at high temperatures and pressures. If a heterogeneous catalysis could be discovered that could produce the biofuel component MTHF selectively under green conditions this would be of huge interest.

It would also be of interest to use the work presented herein as a base for the preparation and testing of catalysts for the hydrogenation of furfural's sister molecule, hydroxymethylfurfural (HMF). HMF can be selectively hydrogenated to the product 2,5-dimethylfuran (DMF), a liquid derivative that has huge biofuel applications, having a greater energy content than bioethanol.